University of Szeged

Faculty of Pharmacy

**Department of Pharmacodynamics and Biopharmacy
& Department of Pharmacognosy**

PhD Thesis

**Investigation of antitumor properties of semi-synthetic flavonoid
derivatives on gynecological cancer cell lines**

Ahmed Dhahir Latif, DVM

Supervisors:

István Zupkó, PhD, DSc

Attila Hunyadi, PhD

Szeged, Hungary

2020

DEDICATION

I would like to dedicate this thesis to my family:

My parents: Father and Mother

My Brothers and Sisters

My loving Wife and Children

SCIENTIFIC PUBLICATION RELATED TO THE SUBJECTS OF THE THESIS

I.   Latif AD, Jenei T, Podolski-Renić A, Kuo C, Vágvölgyi M, Girst G, Zupkó I, Develi S, Ulukaya E, Wang H, Pešić M, Csámpai A, Hunyadi A: Protoflavone-chalcone hybrids exhibit enhanced antitumor action through modulating redox balance, depolarizing mitochondrial membrane and inhibiting ATR-dependent signaling. *Antioxidants* **09**:519 (2020).

(IF$_{2019}$: 5.014; Clinical biochemistry - Q1)

II.   Latif AD, Gonda T, Vágvölgyi M, Kúsz N, Kulmány Á, Ocsovszki I, Zomborszki ZP, Zupkó I, Hunyadi A: Synthesis and *in vitro* antitumor activity of naringenin oxime and oxime ether derivatives. *Int J Mol Sci* **20:** 2184 (2019).

(IF$_{2019}$: 4.556; Organic chemistry - Q1)

ADDITIONAL PUBLICATIONS

Keglevich A, Dányi L, Rieder A, Horváth D, Szigetvári Á, Dékány M, Szántay C, Latif AD, Hunyadi A, Zupkó I, Keglevich P, Hazai L: Synthesis and cytotoxic activity of new vindoline derivatives coupled to natural and synthetic pharmacophores. *Molecules* **25**: 1010 (2020).

(IF$_{2019}$: 3.267; Pharmaceutical science - Q1)

LIST OF ABBREVIATIONS

ATR	Ataxia telangiectasia and Rad3-related protein
Caspase-3	Cysteine-aspartic proteases-3
Chk1 & Chk2	Checkpoint kinase 1 and 2
DDR	DNA damage response
DMSO	Dimethyl sulfoxide
DNA	Deoxyribonucleic acid
DPPH	1,1′-diphenyl-2-picrylhydrazyl
EMEM	Eagle's minimum essential medium
ER+	Estrogen receptor-positive
FBS	Fetal bovine serum
Fl	Flavonoid
HPV	Human Papilloma Virus
IC_{50}	Half maximal inhibitory concentration
MDR	Multi-drug resistance
MTT	([3-(4,5-Dimethylthiazol-2-yl)-2,5-diphenyltetrazolium bromide])
NEAA	Non-essential amino acids
NG	Naringenin
NGOX	Naringenin oximes
ORAC	Oxygen radical absorbance capacity
PI	Propidium iodide
PrFl	Protoflavones
RNS	Reactive nitrogen species
ROS	Reactive oxygen species
RS	Replication stress
SDS	Sodium dodecyl sulfate
SEM	Standard error of the mean
TNBC	Triple-negative breast cancer
XO	Xanthine-oxidase

TABLE OF CONTENTS

1   INTRODUCTION

1.1   Epidemiology of cancer

Cancer is considered one of the most dangerous diseases that threaten human health and is the second leading cause of death worldwide. Recent statistics reported by the World Health Organization (WHO) indicated that cancer was responsible for an estimated 9.6 million patient deaths in 2018, and this number will increase to 15 million by 2030 [1]. Independently of gender and age, Asia accounted for the highest cancer incidence and mortality with 43.6% and 49.6%, respectively, followed by Europe with 25.0% and 22.0% [2]. Breast cancer is the most prevalent diagnosed cancer among females, corresponding to 25% of the cases, and the second leading cause of cancer death, while cervical cancer ranks fourth for both incidence and mortality among women around the world [3,4]. In Europe it was estimated that cancer incidence increased with 3.9 million new cases, and 1.9 million deaths reported during 2018. Among different types of cancer, female breast cancer ranked as the first and common type of cancer with 523,000 detected cases, followed by colorectal, lung, and prostate cancer [5]. Moreover, high cancer burden is characteristic of Central and Eastern European countries, including Hungary [6].

In Hungary both breast and cervical cancers are prevalent malignancies in women that may lead to deaths [7,8]. Among Hungarian women 74,920 and 18,610 breast and cervical cancer deaths have been recorded, respectively, during the period 1979-2013, with mortality rates of 12.19 and 10.29 per 100,000 persons per year [9].

In Iraq, according to the latest Iraqi Cancer Registry, breast cancer was the most prevalent type among the registered malignant neoplasms affecting the community, considered as the first cause of cancer death with a mortality rate of 23.6% among Iraqi women during 2016 [10,11].

Breast cancer is commonly classified into subtypes based on the presence or absence of human epidermal growth factor-2 (HER2), estrogen receptors (ER), and progesterone receptors (PR). Subtypes positive for these receptors more often respond to adequate hormonal therapy [12]. Triple-negative breast cancer (TNBC) on the other hand, globally accounting for 15-20% of all diagnosed breast cancers, is one of the most aggressive and challenging subtypes representing a malignancy which is treated only with conventional chemotherapeutic drugs due to the lack of targets for hormonal therapy [13,14].

Human cervical cancer is currently one of the crucial global health problems and a leading cause of mortality in women during their reproductive years. A substantial portion of the cases is related to human papillomavirus (HPV) infection [15]. Chrysostomou *et al.* (2018) and Goodman (2015) proved that HPV variants 16 and 18 are highly associated with carcinogenesis, and HPV-16 and -18 are responsible for approximately 20% and 50% of cervical cancer cases, respectively [16,17].

1.2 Natural products

Chemotherapy is one of the best therapeutic strategies to treat cancer disease but adverse effects and acquired drug resistance may lead to failure for standard therapy [18]. There is still an urgent requirement to develop novel effective, reliable and safe anticancer agents for the treatment of a wide range of cancerous disorders [19]. Traditionally, attention has been concentrated on the use of natural products and their semi-synthetic derivatives to treat human diseases, including cancer [20]. Plants are substantial sources of natural compounds which can be used as models for design and synthesis of innovative drugs [21]. Hence, in modern therapeutics, more than 50% of medicines prescribed worldwide are based on natural products or their derivatives [22].

Phytochemicals (plant-derived compounds) play an essential role in drug development and discovery. Based on their wide range of bioactivities, low cost, and chemical diversity, they are generally considered an essential factor in anticancer drug research [23,24]. Structures of natural products are useful scaffolds for chemical diversification and this property makes them an optimal source for novel compounds in drug discovery [25]. Phytochemicals are regarded as an essential source of anticancer agents that have substantial antiangiogenic, antimetastatic, antiproliferative, and proapoptotic effects in both animal and cell-based models [14,26]. The discovery of active new derivatives through modification of the natural product structure is a promising approach for the development of innovative first-in-class anticancer drugs [27]. Actually, over 75% of current anticancer drugs introduced between 1981 and 2008 had been discovered either directly from natural products or developed based on their semi-synthesis derivatives (e.g. vinblastine, vincristine, paclitaxel, camptothecin, and topotecan) [28,29]. Several plant species and their derivatives exerted strong antiproliferative and proapoptotic effects in different types of cancer cell lines [30–33]. Additionally, the plants which contain high amounts of flavonoids in their structure are accepted in traditional medicine as chemotherapeutic and chemopreventive agents in some countries [34].

1.2.1 Flavonoids

Polyphenols are considered one of the largest classes of phytochemicals, which are classified into two principal categories: non-flavonoids and flavonoids (Fls). Non-flavonoids are divided into main subclasses including phenolic acids (cinnamic acid derivatives, benzoic acid derivatives) and stilbenoids [35]. On the other hand, based on their chemical structure characterized by two (A and B) phenyl rings connected by a heterocyclic C ring and depending on the position of the phenyl rings, the functional groups, the arrangement of hydroxyl groups and the presence or the absence of unsaturation in the C ring, flavonoids are classified into different subgroups which include: flavonols, flavones, flavanones, isoflavones, chalcones, and anthocyanidins [36,37].

Flavonoids, in particular, are considered the largest class of polyphenolic secondary metabolites that are widely distributed in nature and play a prominent role in plant physiology. In addition to protecting the plants from different stresses, they also act as detoxifying and defensive agents [38]. Despite many controversial views regarding the current lack of clinical results, Fls and other phytochemical metabolites continue to have a promising value in cancer research. Most of the new clinical studies on plant secondary metabolites and their derivatives have been applied towards drug discovery and combating cancer [39]. During the last few decades, many studies showed that isolated and synthesized Fl analogs exerted different pharmacological activities such as antibacterial, antiviral, anti-inflammatory, antioxidant, and antitumor effects against a broad range of human cancer cell lines [23,40,41]. Fls and their synthetic analogs have appeared as hopeful agents for the treatment and prevention of breast cancers [42]. Rodriguez *et al*. (2018) mentioned that Fls isolated from the leaves of *Chromolaena tacotana* caused excellent antioxidant and antiproliferative activity on the breast MDA-MB-231 cancer cells [43]. Additionally, it was investigated that treatment with fisetin induces growth inhibition and apoptosis in TNBC (MDA-MB-231 and MDA-MB-468) and ER+ (MCF-7) breast cancers [44]. Yao *et al.* (2012) synthesized two flavone analogs and discussed their potent antiproliferative activities in two types of breast cancer cells, MDA-MB-231 and MCF-7 [24]. Different kinds of Fls isolated from the stems and roots of *Crotalaria bracteata* showed good cytotoxicity against MCF-7 cancer cell lines [45]. Six Fls isolated from propolis induced apoptosis, cytotoxic and antioxidant effects in both MDA-MB-231 human breast and colon cancer HCT-116 cells [46].

Moreover, the cytotoxic activity of 42 different Fls on the MCF7-SC human breast cancer stem-like cell line described the relationship between Fl structure and its cytotoxicity [47]. Furthermore, their cytotoxicity was evaluated against cervical, ovarian, pancreatic, and prostate cancer [48,49]. Treatment of HPV16 or HPV18 positive human cervical cancer with

dietary Fls, including naringenin, naringin, and hesperetin, can lead to concentration- and time-dependent inhibition of cell proliferation through the improvement of apoptosis and the induction of cell cycle arrest [50]. Nugraha *et al.* (2017) showed that Fls derived from *Eriocaulon cinereum* extraction suppressed the growth of HeLa cells with good IC_{50} value [51]. While hesperetin exhibits apoptotic action against SiHa cervical cancer cells [52], the anticancer activities of 26 flavanone derivatives on colorectal cancer cells (HCT116) were reported to block G1 cell cycle progression and inhibit the clonogenicity of cells [53]. Four Fls, namely naringenin, quercetin, chrysin, and vinculin, which were isolated from the rhizome of *Docynia delavayi,* exerted high anti-tumor activity on human cervical adenocarcinoma cell (HeLa), human hematomas cell (HepG2), and esophageal carcinoma cell (EC109) [54]. Flavanone isolated from *Chromolaena leivensis* (Hieron) effectively inhibited the cell growth in the breast MDA-MB-231, cervix SiHa, prostate PC3, colon HT-29, and lung A549 cancer cells, with exhibited cell cycle arrest in lung cells [55]. Liu *et al.* (2015) examined the anticancer efficacy of different types of Fls against various types of leukemia cells, including human leukemia (HL-60) cell line, and found that Fl compounds exhibited good cytotoxic activity against leukemia [56]. Antioxidation, antiproliferation, antiangiogenesis, and apoptosis induction are considered as the main mechanisms behind the anticancer effects of Fls [31,57]. Besides, Fl derivatives can cause cancer cell apoptosis through a caspase-dependent pathway [58]. Furthermore, they can be affected by free radical scavenging activity [59] or protection of the tissues from damage caused by Reactive Oxygen Species (ROS) through the block formation of ROS [60]. Several studies have reported that Fls are essential natural antioxidants, which are mostly associated with the treatment of various diseases and disorders, including cancer, and also, some Fls can behave as both anticancer agents and antioxidants [61,62].

1.2.1.1 Naringenin

Naringenin (NG), which belongs to the flavanone subclass, is considered as one of the greatest abundant dietary Fls predominantly present in grape, citrus fruits, and tomato. It displays several beneficial pharmacological activities on human health, including cardioprotective, anti-inflammatory, antiviral, antioxidant, and anticarcinogenic effects [63,64]. Rebello *et al.* (2020) proved the safety of naringenin in healthy adult humans after the consumption of a single oral dose up to 900 mg [65].

Recently, several *in vivo* and *in vitro* studies demonstrated that NG could effectively inhibit cell proliferation and migration, induced apoptosis, and suppressed cell cycle in several types of human cancer cells, including hepatocellular carcinoma, prostate, pancreas, colon, bladder, cervical, uterine, breast cancer and leukemia [36,66–73]. In an *in vivo*

experimental study Sabarinathan *et al.* (2011) found that, NG has potent antioxidant and antiproliferative effects against cerebrally implanted glioma cells in rats [74]. Besides, NG was shown to exhibit anti-oxidant effects and to alleviate cerebral edema in cases of ischaemic stroke [75]. Also, Arul *et al.* (2013) reported *in vitro* that NG had antiproliferative and apoptotic effects on the human hepatocellular carcinoma (HepG2) cell lines through induction of the cell cycle arrest and activation of caspase-3 [76]. Naringenin exhibited cytotoxic effects in the MDA-MB-231 cells characterized by growth inhibition, cell cycle was arrested in the sub G, G1, and G2 phases besides the apoptotic effects represented by the elevation of both caspase-3 and caspase-9 activities [77,78]. However, the anticancer activity of NG is not strong enough to apply clinically. The use of natural NG as a cancer chemotherapeutic or chemopreventive agent requires the development of NG derivatives that can prompt cytotoxicity at low concentrations [79]. Therefore, based on the chemical structure of NG, several research groups have made attempts to design and synthesize new NG derivatives to improve their biological properties [66,71,80,81]. A lot of NG derivatives were synthesized by the modification of phenolic groups by alkylation and esterification to produce new molecules with potent cytotoxic effects against human colon cancer cells [71]. Lee *et al.* (2003) conducted an *in vivo* study to evaluate the anti-atherogenic effects of naringenin semi-synthetic modifications in high-cholesterol fed rabbits [82]. Recently it has been indicated that 4′- and 7-O-methylated naringenin derivative decreased the epileptic seizures in mouse and zebrafish models [83].

On the other hand, the modification of naringenin at the keto group also provided interesting pharmacological compounds like thiosemicarbazone derivatives, which displayed significant DNA binding properties and antioxidative impacts [84]. Liu *et al*. (2017) produced NG derivatives with a tertiary amino side chain that enhanced the antiproliferative activities of NG against four different human cancer cells: lung (A549), breast (MCF-7), colon (HCT116), and cervical (HeLa) [66]. Besides, the triacetyl derivative of flavanone recorded a high induction of antiproliferative and degradation activity of DNA in MCF-7 cancer cells [85]. Furthermore, Zaim *et al.* (2018) found that the synthesized naringenin-cyclic-aminoethyl derivatives were potent cytotoxic agents and caused mitochondrial apoptosis in the human breast and cervix cancer [86].

Oximes are essential compounds used as chemical building blocks for the synthesis of pharmaceuticals and agrochemicals [87]. Oximes and oxime ethers are important intermediates that have medium to excellent cytotoxicity against cancer cells [88]. The oxime functional group quickly bonds with relevant organic groups such as cyano, nitro, amino, and carbonyl groups that can serve as a convenient protective group [89]. Turkkan *et al.* (2012) and Potaniac *et al*. (2014) synthesized and characterized the naringenin *E*-oxime (NGOX)

derivative and noted that antioxidant and scavenging reactive oxygen species (ROS) activity was significantly higher than NG itself [90,91]. Recently, Kocyigit *et al.* (2016) investigated that both NG and its oxime analogs have good antioxidants with protecting cell activity against oxidative damage induced by hydrogen peroxide [92].

Furthermore, *in vivo,* NGOX relieved the side effects (nephrotoxicity, hepatotoxicity, and genotoxicity) induced in rats after treatment with cisplatin [93]. On the other hand, as compared to their respective parent compounds, the modification of NGOX derivatives was observed to improve significantly in cytotoxicity against different types of cancer cells, and they are considered promising leads for the development of cytotoxic agents [94–97]. However, even though numerous attempts to synthesize and evaluate the pharmacological activity of NGOX have been described in several articles [90–92], only a limited number of oxime ether derivatives have been studied in the literature [98].

1.2.1.2 Protoflavones

Protoflavones (PrFl) represent a rare particular class of natural Fls with an unusual non-aromatic B-ring. Such compounds most typically occur in fern species (e.g., *Thelypteris* and *Pseudophegopterys sp.*) [99]. Several studies mentioned the isolation and/or semi-synthetic preparation of new natural PrFl, recording promising bioactivity against different cancer cells both *in vitro* and *in vivo* [100–103]. Hunyadi *et al.* (2011) developed a one-step semisynthetic method to prepare protoapigenone (for chemical structure, see Fig. 1, blue fragment of compound **9**) directly from its 4′-hydroxyflavone analog, apigenin, and showed that a 1′-*O*-alkyl substituent may increase cytotoxic activity on some human cancer cell lines [104]. The treatment with PrFl derivatives significantly suppressed viability and growth of human breast (MDA-MB-231 and MCF-7), lung (A549), liver (HepG2, and Hep3B), ovarian (MDAH-2774 and SKOV3), colon (HT-29), pancreas (PANC-1) and cervical (HeLa) cancer cell lines, with low and in some cases sub-micromolar IC_{50} values [99,105–108]. PrFls were demonstrated to trigger apoptosis by activating caspase-3 and increase the apoptotic subG1 cell population, besides suppressing the S, G2/M phase in the treated cancer cells [106,109]. Further, Wang *et al.* (2012) demonstrated that protoapigenone inhibited the ataxia-telangiectasia and Rad3-related protein (ATR)-mediated activation of checkpoint kinase-1 (Chk-1), which is a critical component of replication-associated DNA damage response (DDR) [102]. Along with the ataxia-telangiectasia mutated kinase (ATM), this pathway is an attractive novel antitumor target with several related ongoing clinical trials [110–112].

2   SPECIFIC AIMS OF THE STUDY

The present PhD work aimed to study the antitumor potential of a set of new flavonoid derivatives, some (naringenin oxime derivatives) to be prepared and characterized within the scope of this work, and others (protoflavone-chalchone hybrid compounds) prepared and characterized by collaborators. Gynecological (cervical and breast) cancer cell lines were selected to evaluate the compounds' *in vitro* antitumor activity, and we also aimed to evaluate possible mechanism of action for selected compounds. The specific aims were the following.

- Design and synthesis of naringenin oxime and oxime ether derivatives. A straightforward chemical strategy was chosen to prepare nitrogen-containing flavonoid analogs, and we also aimed to possibly isolate by-products of the reactions when performing the preparative chromatographic purification of the compounds.

- Determination of the *in vitro* antiproliferative activity of the synthesized naringenin oxime derivatives on human gynecological cancer cell lines.

- Investigation of the possible mechanism of action of the most active naringenin derivatives through the antioxidant and proapoptotic properties by determining cell cycle analysis and caspase-3 activity.

- Examination of the antioxidant activity of the synthesized naringenin oxime derivatives based on their efficiency to scavenge diphenyl-2-picrylhydrazyl, oxygen radical absorbance capacity and xanthine oxidase inhibitory assays.

- Evaluation of the antiproliferative activity of protoflavone-chalcone hybrid compounds on gynecological cell lines.

- Evaluation of the cell cycle and caspase-3 activity of gynecological cells upon treatment with protoflavone derivatives. This work was aimed as participation in an international collaboration study on the possible mechanism of action of these compounds.

- Evaluation of the pharmacological benefit of coupling protoflavones and chalcones into hybrid compounds, by performing experimental and virtual combination studies on their relevant fragments.

3 MATERIALS AND METHODS

3.1 Chemicals

3.1.1 Synthesis of naringenin oximes and oxime ether derivatives

Naringenin (purity: 98%), used as a starting material, was purchased from Indofine Chemical Company Inc. (Hillsborough, NJ, USA). Ethanol 96% was obtained from Molar Chemicals Ltd. (Halásztelek, Hungary). All other reagents were purchased from Sigma-Aldrich (St. Louis, MO, USA). Normal phase thin-layer chromatography (TLC) (Silica gel 60F$_{254}$, E. Merck, Darmstadt, Germany) was used to monitor the reaction progress. Purification was carried out by flash chromatography on a CombiFlash Rf+ Lumen Instrument (Teledyne Isco, Lincoln, NE, USA) with integrated UV-Vis, photodiode-array (PDA) and evaporative light-scattering (ELS) detection, and using commercially available pre-filled columns (Teledyne Isco, Lincoln, NE, USA) for normal-phase separations in a detection range of 210–366 nm. Naringenin oximes and oxime ethers were characterized by using NMR and MS. ^{1}H (500.1 MHz) and ^{13}C (125.6 MHz) NMR spectra and recorded on a Bruker Avance DRX-500 spectrometer (Bruker, Billerica, MA, USA).

Naringenin oximes and oxime ethers derivatives (**1-8**) were synthesized and characterized as published before [90]. Briefly, naringenin (1.00 g) was dissolved in 100 mL of EtOH, then 3 equiv. (0.77 g) of hydroxylamine hydrochloride and 3-equiv (0.62 g) of KOH were added. The reaction mixture was refluxed for 48 h, and then the solvent was evaporated under vacuum. The residue was re-dissolved in water (100 mL) and the aqueous phase was extracted with EtOAc (3 × 100 mL). The organic phase was combined, dried over Na$_2$SO$_4$, and evaporated to dryness. Compounds were purified by flash chromatography on silica with a solvent system of n-hexane—EtOAc—formic acid (15:4:0.25, v/v/v).

Naringenin oxime ethers were synthesized as follows. An aliquot of 100 mg of naringenin was dissolved in 15 mL of pyridine, then three-equivalents of the corresponding alkyl or aryloxyhydroxylamine hydrochloride was added, and the mixture was refluxed for 48–96 h. Completion of the reaction was decided based on continuous TLC monitoring. When starting material was not detectable any more, the solvent was evaporated under vacuum. After that, 50 mL of water was added to the residue, and solvent-solvent extraction was performed with EtOAc (3 × 50 mL). Then the combined organic phase was dried over Na$_2$SO$_4$, filtered, and evaporated to dryness. Each crude mixture was purified with flash chromatography on polyamide with a solvent system of CH$_2$Cl$_2$–MeOH (9.9:0.1, v/v).

3.1.2 Protoflavone derivatives obtained from collaborators

Using protoapigenone 1′-*O*-propargyl ether (**9**) [99], four new hybrid compounds (**10a-d**) were prepared at the Institute of Chemistry (University of Eötvös Loránd, Budapest, Hungary) and the Institute of Pharmacognosy, University of Szeged, Szeged, Hungary. Each of these compounds joined two fragments, a protoflavone and a chalchone or ferrocene (**11a-d**) through a triazol function (Figure 1).
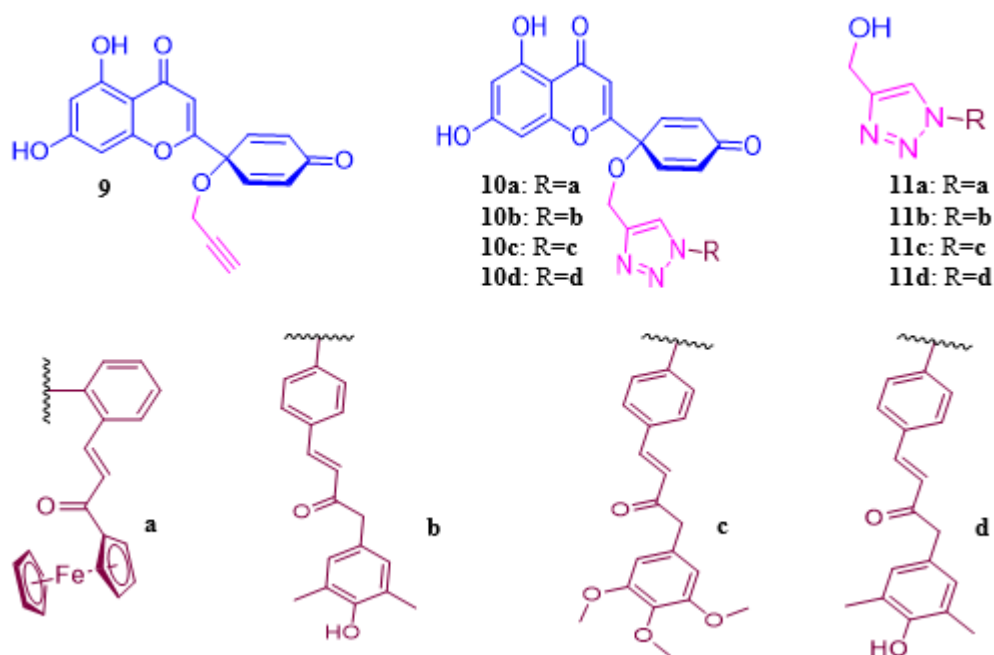
Figure 1. Chemical structure of protoapigenone 1′-*O*-propargyl ether (**9**) and the protoflavone-chalcone hybrids with triazole linkers (**10a-d**). The hydroxymethyl derivatives (**11a-d**) corresponding to the chalchone fragment were also tested as reference compounds for the hybrids.

3.2 Cell lines and culture conditions

A panel of human gynecological cancer cell lines, including human breast carcinoma (MCF-7) as a model for ER+, human breast adenocarcinoma (MDA-MB-231) as a model for TNBC, cervical HPV 18+ adenocarcinoma (HeLa) and HPV 16+ squamous cell carcinoma (SiHa), with additional human leukemia cells HL-60 and non-cancerous mouse embryonic fibroblast cell line (NIH/3T3) were used as *in vitro* design to study the antitumor activity of the tested compounds. The SiHa and human leukemia HL-60 cells were obtained from the American Tissue Culture Collection (ATCC), Manassas, VA, USA, while all the other cell lines were from the European Collection of Cell Cultures (ECCAC), Salisbury, UK. According to the distributors' instructions, all human gynecological cancer cell lines and non-

cancerous mouse embryonic fibroblast cell line (NIH/3T3) were cultivated in flasks of 75 cm^2 in minimal essential medium (MEM) and enhanced with 10% heat-inactivated fetal bovine serum (FBS), 1% antibacterial-antimycotic solution (penicillin-streptomycin-amphotericin B) and 1% non-essential amino acids.

HL-60 leukemia cells were cultivated in RPMI 1640 medium containing 10% FBS, 1% antibacterial-antimycotic mixture and 1% L-glutamine, and incubated in a humidified atmosphere at 37°C enclosed with 5% carbon dioxide (CO_2). The density of the cells for each experiment was measured with a Luna Automatic Cell Counter (Seoul, South Korea) using trypan blue solution. All chemicals and media that were used in our research, if not specified otherwise, were purchased from Sigma-Aldrich Ltd. (Budapest, Hungary) and Lonza Group Ltd. (Basel, Switzerland), respectively [100,101].

3.3   Treatment with the compounds

The synthesized compounds were solubilized in dimethyl sulfoxide (DMSO) as a 50 and 10 mM standard solution for naringenin oxime and protoflavone derivatives, respectively, and stored at –20°C with minimal exposure to light to avoid oxidation. The stock solution was immediately diluted with a culture medium before each treatment to reach the final concentrations for the different experiments. Two concentrations (25 and 50 µM) were selected for screening the bioactivity of initial naringenin oxime derivatives on breast, cervical and HL-60 cancer cell lines, and the values of half-maximal inhibitory concentration (IC_{50}) were estimated only for those compounds that elicited antiproliferative activity with more than 75% growth inhibition at 50 µM, by repeating adjusted dilutions (1–50 µM) of the potent compound. On the other hand, the gynecological cells were exposed to ten different concentrations of each compound of protoflavone derivatives (0.039, 0.07, 0.1, 0.31, 0.62, 1.25, 2.5, 5, 10 and 20 µM). Cisplatin was used as a positive control (0.1, 0.3, 0.6, 1.25, 2.5, 5, 10, and 20 µM), while the negative control included the cells that were treated only with MEM.

HL-60 cells were seeded at $1×10^4$ cells per well and directly treated on the same day, whereas the gynecological and NIH/3T3 cells were seeded at $5×10^3$ cells per well, and overnight pre-incubation was done to permit the adhesion of the cells to the bottom of the well before the treatment (I, II).

3.4 Antiproliferative activity

The colourimetric ([3-(4,5-Dimethylthiazol-2-yl)-2,5-diphenyltetrazolium bromide]) MTT assay was employed to estimate the ability of the prepared compounds to suppress the proliferation of human gynecological (MDA-MB-231, MCF-7, HeLa and SiHa), human leukemia (HL-60) cells and non-cancerous mouse embryonic fibroblast (NIH/3T3) cell lines as previously characterized [102,103]. Briefly, the cells were seeded and treated in 96-well microplates with the final volume per well kept at 200μL and incubated for 72 hours in the same condition at 37°C in a humidified atmosphere of 5% CO_2. After incubation, 44 μL of MTT solution (5 mg/mL of PBS) was added to each well, and incubation continued for another four hours. Subsequently, the supernatant was removed carefully and the precipitated purple formazan crystals were solubilized by adding 100 μL/well of DMSO and gently shaking them for 1h at 37°C (Stat Fax-2200, Awareness Technology INC, USA). Absorbance was measured at a wavelength of 545 nm using an automatic microplate reader (Stat Fax-2100; Awareness Technology INC, USA). In the case of leukemia cells, the precipitated crystals were dissolved in 10% sodium dodecyl sulfate (SDS) with acid HCl 0.01 mM and incubated for 24 h, the absorbance read at 545 and 630 nm.

3.5 Cell cycle analysis

The cell cycle distribution was characterized by flow cytometry, as described by Sinka *et al*. [104], and the cellular DNA content was detected by staining with propidium iodide (PI). Briefly, adherent cancer cells were seeded in six-well plates at a density of 4×10^5 cells per well and allowed to grow for 24 h. On the second day, cells were treated with the testing compounds in two concentrations related to their IC_{50}, with an incubation period of 24 hours. Subsequently, cells were harvested with trypsin (250 μL/well), washed with PBS, re-suspended, and fixed with 70% cold ethanol, which was added dropwise to the cell pellet and maintained at -20°C until further analysis. Directly before the analysis, the fixed cells were washed with cold PBS, stained with a 300 μL of dye solution containing 0.1 mg/mL of PI in the presence of 0.02 mg/mL of RNAse, 0.003 mL/mL of Triton-X-100 and 1.0 mg/mL of sodium citrate in distilled water. Then they were incubated in the dark at room temperature for an hour. Finally, 700μL of PBS was added to detect the DNA contents by flow cytometry (Partec CyFlow, Partec GmbH, Munster, Germany). For each experiment, at least 20,000 events per sample were calculated. Also, the measured data and the distribution of the cells in the different cell cycle phases (subG1, G0/G1, S, and G2/M) were expressed as DNA

histograms by using ModFit LT 3.3.11 software (Verity Software House, Topsham, ME, USA).

3.6   Determination of caspase-3 activity

Caspase-3 colourimetric assay kit, purchased from Sigma-Aldrich, Saint Louis, MO, USA., was used to determine the cysteine-aspartic proteases-3 (Caspase-3) in conformity to the manufacturer's instructions and according to the procedure which had been published before [105]. Briefly, cells were seeded at a density of 12×10^6 cells in tissue culture flasks and allowed to grow and attach overnight. The adhered cells were treated with appropriate concentrations of the prepared compound and incubated for 24 or 48 h. Subsequently, the cells were scraped, harvested, centrifugated, and washed with PBS. They were re-suspended and incubated in lysis buffer on ice for 20 min, and the supernatant was used after the cold centrifugation of the lysates. Assays were performed in a 96-well plate with collected supernatant by incubating 5 µL of cell lysates with 10 µL of selective caspase-3 substrate in a final volume of 100µL of assay buffer, then incubated at 37°C in the dark for 24 h. Finally, the absorbance was measured at 405 nm with a microplate reader (Stat Fax 2100, Awareness Technology INC, USA). The changes in caspase-3 activity were determined after comparing the absorbance of the treated samples with the untreated controls.

3.7   Antioxidant activity

3.7.1   Diphenyl-2-picrylhydrazyl (DPPH) assay

The *in vitro* antioxidant activity of the NGOX derivatives was evaluated based on their efficiency to scavenge stable DPPH according to the method presented by Fukumoto and Mazza (2000) [106] with some modifications. 1,1′-Diphenyl-2-picrylhydrazyl (DPPH) was purchased from Sigma-Aldrich Hungary. The measurement was carried out on a 96-well microplate. Series microdilution of samples (starting with 150µL) was prepared from the stock solution (10 mM). To each well, 50 µL of DPPH reagent (100 µM in HPLC grade MeOH) was added to gain 200 µL working volume. The microplate was stored in the dark at room temperature for 30 min. Sample absorbance was measured at 550 nm by using a FluoStar Optima plate reader (software version 2.20R2, BMG Labtech Ortenberg, Germany). The percentage of free radical scavenging activity of the different samples was calculated by the following equation: Inhibition (%) = (A0 - As)/A0 × 100, and EC_{50} values were

calculated by Graph Pad Prism 6.05 software. Rutin (0.01 mg/mL in HPLC grade MeOH) was used as a reference standard and DMSO was used as a blank control.

3.7.2 Oxygen radical absorbance capacity (ORAC) assay

The ORAC assay was performed according to the method of Mielnik *et al.* (2011) [107]. Briefly, 20 µL of extracts (stock solution concentration of 0.002 mM) were mixed with 60 µL of AAPH (12 mM final concentration) and 120 µL of fluorescein solution (70 nM final concentration), then the fluorescence was measured through 3 h with 1.5-min cycle intervals with a BMG Labtech FluoStar Optima plate-reader. All experiments were carried out in triplicate, and trolox was used as a standard. The antioxidant capacity was expressed as µM Trolox Equivalent per µM of pure compound (µM TE/µM), as calculated by Graph Pad Prism 6.05.

3.7.3 Xanthine-oxidase inhibitory assay

To assess xanthine-oxidase (XO) inhibitory activity, a continuous spectrophotometric rate determination was used, based on a modified protocol of Sigma. The absorbance of XO-induced uric acid production from xanthine was measured at 290 nm for 3 min in a 96-well plate on a BMG Labtech FluoStar Optima plate-reader. The XO-inhibitory effect was determined via the decreased production of uric acid. The samples (10 mM stock solution) were prepared in DMSO. For enzyme-activity control, the final reaction mixture comprised 100 µL of xanthine solution (0.15 mM, pH = 7.5), 150 µL of buffer (potassium phosphate with 1 M KOH, pH = 7.5) and 50 µL of XO (0.2 units/mL) in a 300 µL well. The reaction mixture for inhibition was made with 100 µL of xanthine, 140 µL of buffer, 10 µL of sample and 50 µL of XO. Allopurinol was used as positive control. Test compound samples were added in appropriate volumes so that the final concentration of DMSO in the assay did not exceed 3.3% of the total volume. All experiments were conducted in triplicates. The reaction was initiated by the automatic addition of 50 µL of XO solution to a final concentration of 0.006 units/mL. The inhibitory percentage values were calculated by using Graph Pad Prism 6.05 software.

3.8 Combination study of relevant fragments vs hybrids 10b-d

Two combination studies were performed: a virtual and an experimental one. In the case of the virtual study, cell viability data obtained following treatment with the hybrid

compounds **3b-d** were analyzed in comparison with data obtained for their corresponding relevant fragments, such as compounds **1** and **8b-d**, and the hybrid compounds were considered as 1:1 ratio mixtures of compound **1** and the corresponding fragment. Two separate experiments were performed, each in triplicate. In the case of the experimental combination study, cell viability data obtained for equimolar mixtures of the above-mentioned fragments were tested in comparison with the corresponding single-treatment controls. In this bioassay, two separate experiments were performed, each in duplicate. Calculations were performed using CompuSyn software. In each case, raw cell viability data from all replicates were averaged, and the resulting single dataset was analyzed as suggested by Chou [108]. CI values obtained this way were then used to mathematically describe the extent of pharmacological benefit gained by the coupling (virtual combination) in comparison with a combined effect of the mixture of fragments (experimental combination). "Synergism" in the virtual combination means that the hybrid exerts significantly stronger cytotoxicity than just a sum of that of its fragments.

3.9   Other bioassays performed in collaboration

Cell death analysis by AV/PI labelling, and studies on the effect of compounds **10a-d** on the intracellular ROS/RNS levels, and on the depolarization of the mitochondrial membrane [109] were performed in cooperation with the group of Dr. Milica Pešić, Institute for Biological Research, Department of Neurobiology, University of Belgrade, Belgrade, Serbia.

DNA damage response studies were performed in cooperation with the group of Prof. Hui-Chun Wang, Graduate Institute of Natural Products, Kaohsiung Medical University, Kaohsiung, Taiwan. The effect of compounds **10a-d** on the ATR-dependent phosphorylation of checkpoint kinase-1 (Chk1) was evaluated on MCF-7 breast cancer cells by Western immunoblotting, as published before [110]. For more details see Ref. (I).

3.10   Statistical analysis

Data were collected from two separate experiments in triplicates for antiproliferative activity of protoflavone derivatives and cell cycle analysis or five replications for antiproliferative activity of naringenin oxime compounds and caspase-3 activity at each tested concentration; and evaluated by Graph Pad Prism 5.01 (Graph Pad Software, San Diego, CA, USA) using one-way ANOVA followed by Dunnett's post-hoc test for

comparison of multiple results. IC_{50} values were calculated by (log inhibitor vs normalized response) nonlinear regression model. The results were expressed as means ± standard error of the mean. The results were considered statically significant at *, ** and ***, $p < 0.05, p < 0.01$ and $p < 0.001$, respectively.

4   RESULTS

4.1   Naringenin oxime derivatives

As part of my own contribution to this work, naringenin oxime and oxime ethers were prepared. Two geometric isomers of naringenine oxime (**2** and **3**) were obtained from naringenin (NG; **1**) by reacting it with hydroxylamine hydrochloride in ethanol in the presence of potassium hydroxide, and purifying the products by column chromatography. After characterization by HRMS and ^{1}H-, and ^{13}C-NMR, compound **2** was identified as the *E* isomer, while compound **3** as the minor *Z* isomer, which was prepared by us for the first time. Five oxime ether derivatives (**4–8**) were also prepared by a similar one-step synthesis from the reaction of NG (**1**) with ethoxy-, methoxy-, allyloxy-, *t*-butoxy-, or benzyloxyamine hydrochloride, respectively, in the presence of pyridine. In these reactions, the exclusive formation of the *E* isomers was observed. After purification by using flash chromatography, the chemical structures of the prepared compounds were identified by NMR and HRMS techniques, and they are shown in Figure 2.
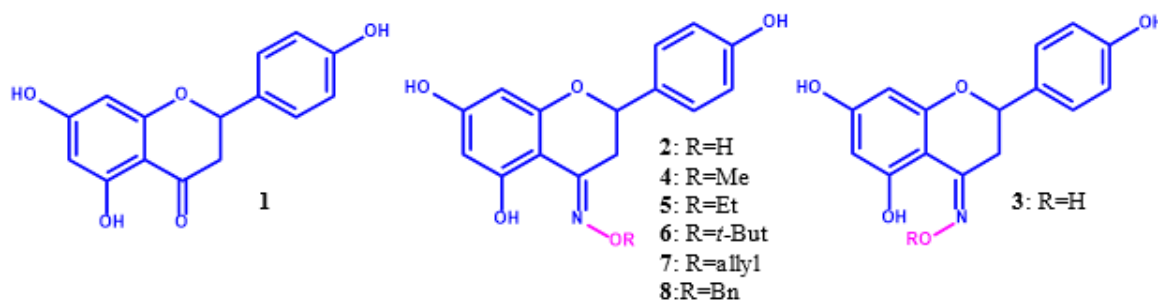
Figure 2. Chemical structures of naringenin (**1**) and its oxime (**2** and **3**), and oxime ether derivatives (**4-8**).

4.2   Pharmacological activities of naringenin oxime derivatives

4.2.1   Antiproliferative activity of naringenin oxime derivatives

The *in vitro* antiproliferative activity of NG (**1**) and its oximes (**2, 3**) and oxime ethers (**4-8**) were evaluated against four human adherent gynecological cancer cell lines, such as SiHa and HeLa (cervical), and MDA-MB-231 and MCF-7 (breast), and also against a human leukemia (HL-60) cell line. Cisplatin, a chemotherapeutic drug was used as a positive control. After the initial bioactivity screening by using MTT assay with two concentrations of 25 and 50 μM, IC_{50} values were determined only for those compounds that exhibited antiproliferative activity with an over 75% growth inhibition at 50 μM (Table 1). We found

that among all the applied compounds, the *t*-butyl substituted naringenin oxime ether (**6**) exerted significant and dose-dependent antiproliferative activity against all tested cancer cell lines.

In contrast, we found that naringenin (**1**) and *Z*-oxime (**3**) caused limited growth-inhibiting activity in the treated cancer cell lines. On the other hand, the *E* oxime (**2**) and the allyl-derivative (**7**) showed a limited growth inhibition in the MCF-7 and HeLa cancer cell lines at the higher concentration. Also, the methyl derivative (**4**) and benzyl-derivative (**8**) exerted conservative growth inhibition in MCF-7 and HL-60 cancer cell lines, respectively. Based on our results, we show for the first time that the *E*-oxime ethers are stronger antiproliferative agents as compared with naringenin and naringenin oximes, mainly if the ether is a bulky alkyl group as in the *t*-butyl derivative **6**. Further, we noted that compounds **1**-**8** did not demonstrate a marked cell line selectivity, but MCF-7 and HeLa cells seemed altogether more sensitive than MDA-MB-231 and SiHa cells (II).

Table 1. Antiproliferative activities of naringenin (**1**) and its oxime derivatives (**2-8**) against human gynecological cancer and leukemia cell lines. Cisplatin was used as a positive control; SEM: standard error of the mean; n = 5.

| Compound	Conc. (µM)	Growth inhibition (%) ± SEM [Calculated IC$_{50}$ value (µM)]				
		SiHa	HeLa	MDA-MB-231	MCF-7	HL-60
(**1**)	25	<20	<20	<20	<20	<20
	50	<20	23.9±2.09	<20	<20	<20
(**2**)	25	<20	<20	<20	<20	<20
	50	<20	28.75±2.44	<20	21.83±3.92	43.40±2.81
(**3**)	25	<20	<20	<20	<20	<20
	50	<20	<20	<20	<20	<20
(**4**)	25	<20	<20	<20	<20	37.67±1.29
	50	<20	31.36±2.97	24.35±1.88	48.44±3.27	57.89±1.13
(**5**)	25	<20	<20	<20	<20	<20
	50	<20	29.36±1.42	<20	44.06±2.18	44.89±0.48
(**6**)	25	<20	52.37±2.32	27.19±1.78	61.41±1.93	37.31±3.65
	50	88.54±1.51	92.22±1.03	90.33±0.58	87.00±0.61	88.07±0.10
		[35.41]	[23.49]	[29.74]	[19.46]	[31.76]
(**7**)	25	<20	<20	<20	<20	<20
	50	<20	25.04±2.4	<20	33.75±2.45	<20
(**8**)	25	<20	22.63±0.63	<20	24.29±1.86	<20
	50	<20	37.67±2.01	24.87±3.47	64.47±2.12	<20
Cisplatin	25	86.40±1.02	98.71±0.21	41.37±1.05	90.81±0.22	64.03±0.43
	50	96.72±0.36	99.09±0.24	84.43±0.4	98.49±0.11	84.88±0.41
		[13.63]	[11.79]	[25.82]	[5.15]	[5.75]

4.2.2 Cell cycle distribution affected by naringenin oxime derivatives

Among the prepared NGOX derivatives, compound **6** showed the most promising antiproliferative effects against gynecological cancer cells and was therefore selected for further *in vitro* studies, including flow cytometric cell cycle analyses, to distinguish the mechanism of action. Adherent cancer cells were exposed to compound **6** for 24 h at two concentrations in proportion to its IC_{50} and it is half IC_{50} -values, i.e., 18 or 36 µM for SiHa, 12 or 24 µM for HeLa, 15 or 30 µM for MDA-MB-231, and 10 or 20 µM for MCF-7 (Figure 3A). From the DNA content histogram, we demonstrated that the percentage of the hypodiploid (subG1) phase increased significantly in cervical SiHa and HeLa cancer cells, which is considered as apoptotic in these cell lines. Also, it was found that compound **6** caused a significant reduction in the percentage of the G1 phase with a consistent increase in the S phase of HeLa cells. SiHa cells showed different responses, which was characterized by a significant rise in the proportion of the G1 stage accompanied by a considerable decrease in the fraction S phase, which may be a consequence of the blockade of the G1–S transition of the cell cycle. However, in the MCF-7 cancer cells, the percentage of G1 and G2/M phase increased, whereas the proportion of S level decreased significantly. These data suggest that treatment with compound **6** induced G1 and G2/M phase cell cycle suppression in a concentration-dependent manner. On the other hand, no substantial action in TNBC was observed with either concentration after treatment for 24 h. Our results of cell cycle analysis revealed that compound **6** induced disturbance in the cell cycle distribution followed by cell death due to the apoptotic process in HeLa and SiHa cancer cell lines (II)

4.2.3 Caspase-3 activity affected by naringenin oxime derivatives

To verify the apoptotic activity of the *t*-butyl derivative (**6**), the activity of caspase-3, which plays a principal role in various apoptotic responses, has been additionally determined. HeLa cells were treated with two different concentrations representing the IC_{50} and its half value (12 and 24 µM) of compound **6** and were incubated for 24 h. The obtained results, summarized as fold activity shown in (Figure 3B), revealed that both used concentrations of the tested compound produced a considerable increase in caspase-3 activity in a concentration-dependent manner, with a rise in the number of measured apoptotic cells compared to the number of untreated control groups. Herein, for the first time, we asserted that apoptosis was induced in cervical Hela cell lines after handling with naringenin *t*-butyl oxime compound (II).
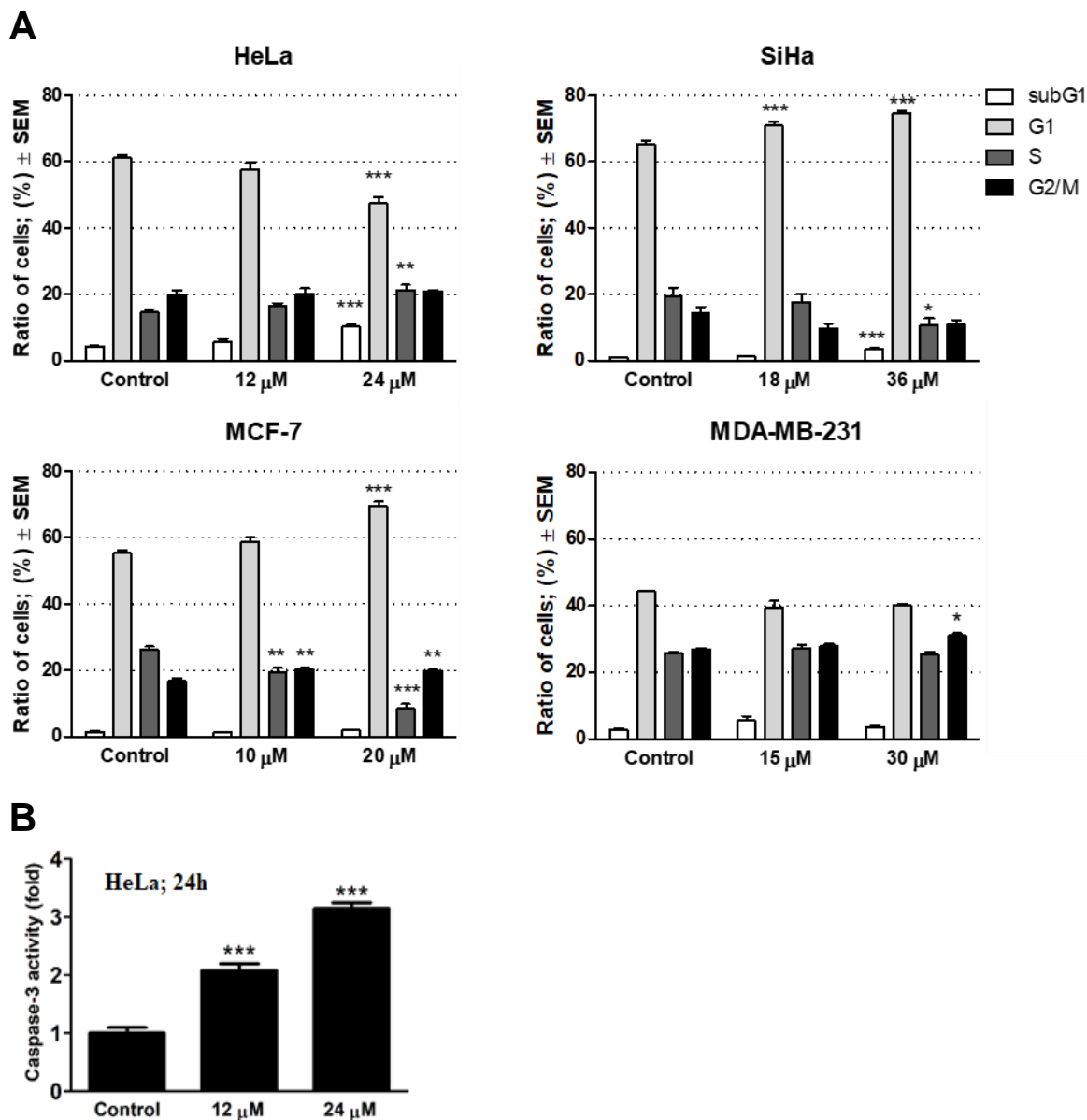
Figure 3. (**A**) Cell cycle distributions of human gynecological cancer cells after treatment with naringenin *t*-butyl oxime (**6**). (**B**) Effect of naringenin *t*-butyl oxime (**6**) on the caspase-3 activity of HeLa cells. Results from 5 replicates are represented as means ± SEM. *, ** and *** indicate $p < 0.05$, $p < 0.01$ and $p < 0.001$, respectively, by means of one-way ANOVA followed by Dunnett's post-hoc test.

4.2.4 Antioxidant activity of naringenin oxime derivatives

NG (**1**) and its oxime derivatives (**2–8**) were evaluated for their possible antioxidant activity by testing their ability to scavenge DPPH, and determining their ORAC value and XO inhibitory activity. The antioxidant results of its effects were clarified in (Table 2). Except for compound (**4**), all compounds exerted a weak activity in these bioassays when compared with the reference standard rutin (for direct scavenging activity) or allopurinol (for

XO inhibition). Surprisingly, the oxime methyl ether derivative (**4**) exhibited the most potent antioxidant activity in both the ORAC and DPPH assays, and this compound (**4**) was also the only one whose activity in the ORAC assay exceeded that of the positive control rutin. The *E*-Oxime (**2**) was much more active DPPH scavenger than NG (**1**), while the *Z*-Oxime (**3**) was an order of magnitude weaker than the *E*-oxime (**2**) in this regard. However, regardless of the oxime orientation, the ORAC activity of both compounds **2** and **3** was diminished as compared to NG (**1**). None of the compounds exerted a significant XO inhibitory activity at as high as 330 µM (II).

Table 2. Antioxidant activity XO inh, DPPH, and ORAC of naringenin (**1**), and its oxime derivatives (**2–8**). TE: Trolox equivalent; n.d.: not determined.

Compound	Antioxidant activity ± SD		
	ORAC (µmolTE/µmol	DPPH EC$_{50}$ (µM)	XO inh (%)
1	11.18±0.46	- [a]	12.31±4.60[b]
2	8.88±0.23	243.45±4.88	7.35±1.32
3	6.95±0.12	1776.00±123.71	2.13±0.78
4	16.63±1.68	212.20±32.59	4.00±1.81
5	5.54±0.41	1437.50±36.06	8.13±2.02
6	3.89±0.87	-	6.95±2.31
7	6.03±2.79	1164.00±226.27	12.84±3.01
8	1.38±0.41	-	9.06±0.79
Allopurinol	n.d.	n.d.	98.23±3.29
Rutin	12.35±0.38	39.88±1.34	n.d.

[a] Compounds eliciting DPPH scavenging activity less than 50% at the highest applied concentration were considered inactive, and the numerical results are not presented; [b] inhibition % at 330 µM

4.3 Pharmacological activities of protoflavone derivatives

4.3.1 Antiproliferative activity of protoflavone derivatives

The cytotoxic activity of relevant fragments (**9** and **11a-d**) and their newly synthesized hybrids (**10a-d**) were evaluated against human breast carcinoma cell lines MCF-7 and MDA-MB-231. Additionally, the cytotoxic effects of the target compounds were also estimated on HPV 16+ cervical squamous cell carcinoma (SiHa) and HPV 18+ human adenocarcinoma epithelial cervical carcinoma (HeLa) in comparison to non-cancerous mouse

embryonic fibroblast (NIH/3T3) cell lines. The antiproliferative activity was investigated after handling the cells with varying concentrations of each compound ranging between 30 nM and 20 μM for 72 h and using cisplatin, a conventional chemotherapeutic as a positive control group. The results are summarized as IC_{50} values and 95% in μM C.I. (Confidence Interval) in Table 3. All hybrid compounds displayed potent cytotoxic activity stronger than that of the positive control cisplatin, with considerable IC_{50} values limiting from 0.1 to 3.2 μM against all the investigated cancer cell lines. The results demonstrated that hybrid compounds (**10a-d**) of PrFl derivatives showed pronounced cytotoxicity compared to their fragment (**9** and **11b-d**) in a dose-dependent manner. Mainly, among these compounds, hybrids **10b** and **10c** exhibited an excellent antiproliferative activity on the examined cancer cell lines. In general, TNBC and cervical SiHa cells manifested exceptional susceptibility to exposure to hybrid compounds when compared to HeLa and MCF-7.

Moreover, fragment **11a** at all concentrations did not display any cytotoxic effects against all cancer cell lines. The most potent cytotoxic compounds **10b** and **10c** were also tested on non-cancerous mouse embryonic fibroblast 3T3, and their IC_{50} values were 0.99 and 0.89 μM respectively, demonstrating 3-4 times higher selectivity as compared to their effect on MDA-MB-231 cells. Furthermore, compounds **9** and **11b-d** themselves also exerted significant cytotoxic activity (I).

Table 3. Antiproliferative activity of hybrid compounds (**10a-d**), and their corresponding fragments (**9** and **11a-d**) on human gynecological cancer cell lines. C.I.: 95% confidence interval, n = 6 from two biological replicates (n = 3 each). Positive control: cisplatin, n = 10 from two biological replicates (n = 5 each).

| Compound	IC$_{50}$ [95% C.I.] (µM)			
	MCF-7	MDA-MB-231	HeLa	SiHa
9	1.742 [1.554 – 1.953]	2.525 [2.341 – 2.724]	1.659 [1.391 – 1.977]	2.342 [1.836 – 2.988]
10a	0.4712 [0.4511 – 0.4922]	0.3710 [0.3568 – 0.3858]	3.244 [2.820 – 3.732]	0.4659 [0.4334 – 0.5008]
10b	0.2522 [0.2271 – 0.2801]	0.2913 [0.2725 – 0.3113]	1.104 [0.9689 – 1.257]	0.1772 [0.1627 – 0.1929]
10c	0.2963 [0.2721 – 0.3227]	0.2223 [0.2075 – 0.2382]	0.7083 [0.6332 – 0.7924]	0.1533 [0.1327 – 0.1770]
10d	0.5125 [0.4805 – 0.5466]	0.3241 [0.3023 – 0.3474]	1.013 [0.9537 – 1.075]	0.1965 [0.1762 – 0.2192]
11a[a]	>20	>20	>20	>20
11b	15.07 [13.66 – 16.64]	11.11 [10.53 – 11.71]	23.60 [b] [21.22 – 26.24]	14.63 [13.55 – 15.80]
11c	2.510 [2.235 – 2.818]	4.399 [3.981 – 4.861]	10.32 [9.644 – 11.04]	3.020 [2.755 – 3.312]
11d	11.00 [10.20 – 11.85]	4.921 [4.521 – 5.356]	11.71 [10.93 – 12.53]	8.527 [8.139 – 8.932]
Cisplatin	5.347 [4.965 to 5.758]	26.15 [b] [24.18 to 28.27]	11.86 [10.63 to 13.22]	12.21 [10.90 to 13.69]

[a] **11a** exerted below 10% inhibition on each cell line at the highest tested concentration; therefore, it is considered as inactive. [b] Experimental data are available up to 20 µM, IC$_{50}$ value extrapolated from nonlinear curve fitting (log inhibitor vs normalized response model) by GraphPad Prism 5.0.

4.3.2 Cell cycle distribution affected by protoflavone derivatives

Flow cytometric examination was applied to investigate the cytotoxic mechanism of selected potent antiproliferative compounds **10b** and **10c** and to check their ability to induce alteration in the cell cycle progression and apoptosis induction towards SiHa and MDA-MB-231 cell lines. Cell cycle distributions were determined after the treatment of both cells with doses corresponding to IC$_{50}$ and its double concentrations for 24 h. The effects of the prepared compound on the cell cycle are explained in Figure 4. The flow cytometric assay, when compared with the control groups, showed that both cancer cell lines exhibited an increase in the proportion of apoptotic cells after treatment with compound **10b** and **10c** in a

dose-dependent manner. It indicated that both compounds in both cancer cell lines caused a substantial increase in the hypodiploid (sub-G1) proportions stage, and this influence was accompanied by a considerable decrease of the G1 step in MDA-MB-231 cells, while this decrease in the G1 of SiHa cells was insignificant.

Moreover, compound **10c** displayed potent effects in both tested cells. Together these data suggested that compound **10c** efficiently induced apoptosis in TNBC cells. Additionally, as noted with increased concentrations of both compounds in MDA-MB-231 and SiHa cells, it did not produce any substantial change in the proportion of cells in the S and G2/M aspects (I).
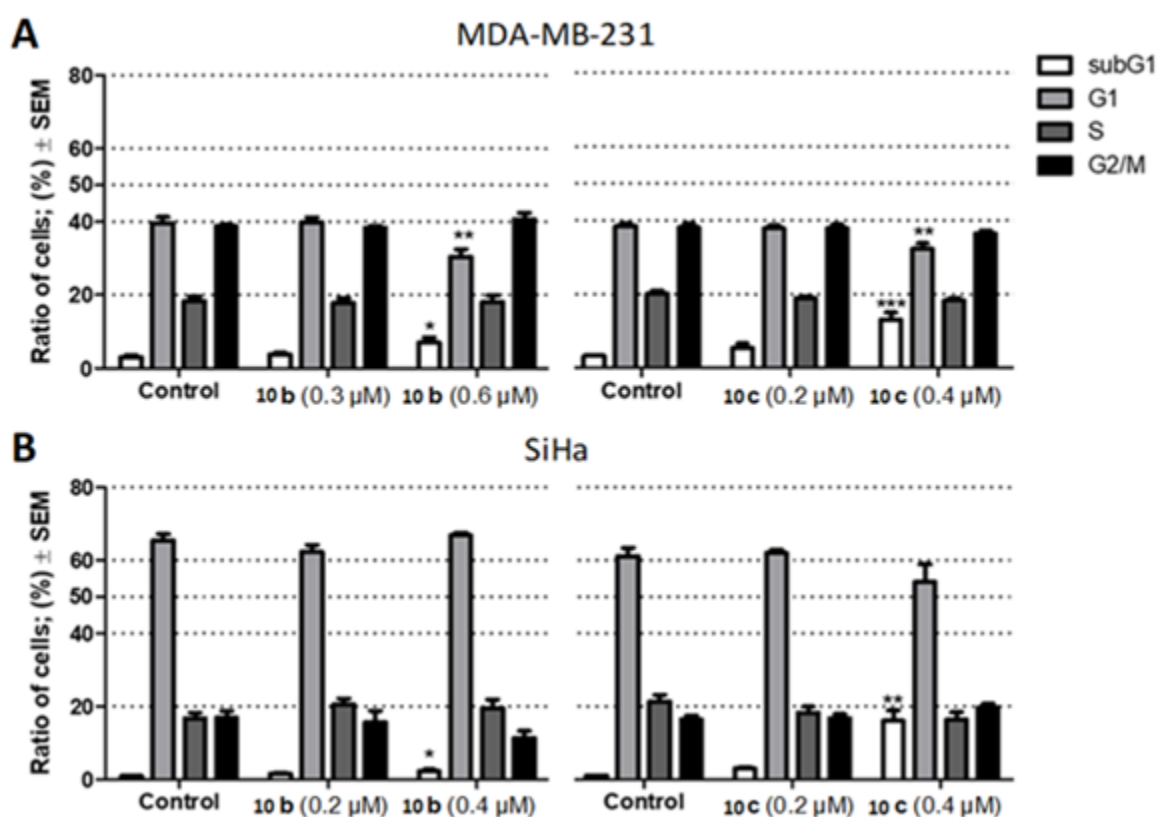
Figure 4. Effect of compounds (**10b** and **10c**) on the cell cycle distribution. (A) MDA-MB-231 and (B) SiHa cells. Cells treated for 24h; *, ** and ***: $p < 0.05$, $p < 0.01$ and $p < 0.001$, respectively, by means of one-way ANOVA followed by Dunnett's post-hoc test.

4.3.3 Caspase-3 activity affected by protoflavone derivatives

To investigate the apoptotic mechanism that is consistent with the cytotoxic property and cell cycle distribution of selected compound **10c** towards TNBC, caspase-3 enzymes, which play an essential role in the apoptotic responses, were used to discover if the cells were dying because of necrosis or apoptosis processes. The caspase-3 activity was analyzed in the

MDA-MB-231 cancer cells after exposure to compound **10c** with 0.2 and 0.4 μM (IC$_{50}$ and double corresponding concentration) and incubated for 24 h. The process showed that compound **10c** caused a significant increase (2-fold) in caspase-3 activity at a higher used level, while the lower concentration did not produce a significant increase in caspase-3 action, and apoptosis was induced in a concentration-dependent manner. Moreover, after increasing the concentration to 0.4 and 1.0 μM and the incubation period to 48 h, the compound produced a noticeable, significant elevation in the caspase-3 activity in both tested concentrations with increased activity (4- and 7-fold), as compared to the control group (Figures 5). The results confirm that compound **10c** induced apoptosis in TNBC cells through the activation of caspase-3 in a time- and concentration-dependent manner (I).
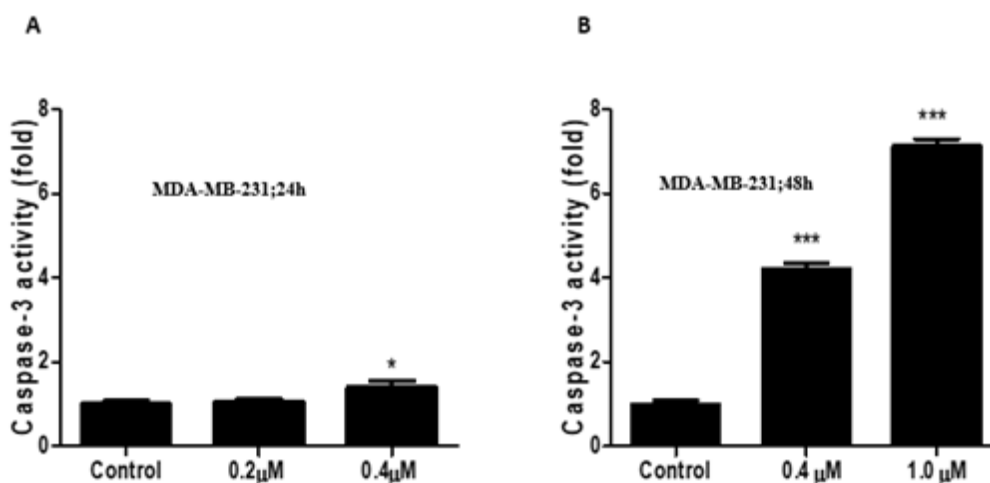
Figure 5. Effect of compound (**10c**) on the caspase-3 activity of MDA-MB-231 cells. (A) Cells treated for 24h (B) cells treated for 48h. *, and ***: $p < 0.05$, and $p < 0.001$, respectively, using one-way ANOVA followed by Dunnett's post-hoc test.

4.3.4 Combination study of protoflavone derivatives

When comparing the effect of the hybrids to their fragments, compound **10a** was found to be ca. 3.7 times more potent on MCF-7 cells, ca. 6.8 times more potent on MDA-MB-231 cells, and ca. 5 times more potent on SiHa cells than compound **9**. In contrast, it was ca. half as potent as compound **9** on the HeLa cells. It should be noted that compound **10a** could directly be compared with compound **9**, since the fragment coupled to **9**, i.e. **11a** itself did not exert any cytotoxic activity in the tested concentration range.

However, in the case of compounds **10b-d**, each fragment (**9** and **11b-d**) exhibited significant cytotoxic effects. Therefore, we performed a more sophisticated comparative evaluation to

quantitatively assess the added pharmacological benefit of linking the fragments into a hybrid molecule. In order to do this, we selected the Chou-Talalay method [108], which offers a well-established mathematical model for the calculation of drug-drug interactions, and two separate analyses were performed. The method was used in an unusual way that may be referred to as a "virtual combination study". Treatment with the hybrid molecules **10b-d** was considered as a 1:1 ratio combination treatment of their two relevant corresponding fragments (i.e., **9** and **11b** for **10b**, **9** and **11c** for **10c**, and **9** and **11d** for **10d**), and the cell viability data presented in Table 3 were re-evaluated accordingly by the CalcuSyn software. Further, a classical experimental combination study was also performed as a control, in which equimolar combinations of compounds **9** and **11b**, **11c**, or **11d** were analyzed in comparison with the corresponding single treatments. The results of these calculations are presented in Figure 6.

The virtual combination results clearly showed that the PrFl hybrid derivatives (**10b-d**) exerted stronger cytotoxic activities than their fragments alone, and the experimental combination showed that co-treatment with the fragments did not result in potent synergistic interactions. Therefore, it is clear that the activity increase is due to combining these fragments into hybrid molecules.

The activity increase was particularly high in the case of MDA-MB-231 and SiHa cells, as shown by the strong and very strong synergistic interactions [108], respectively, in the virtual combination results (I).
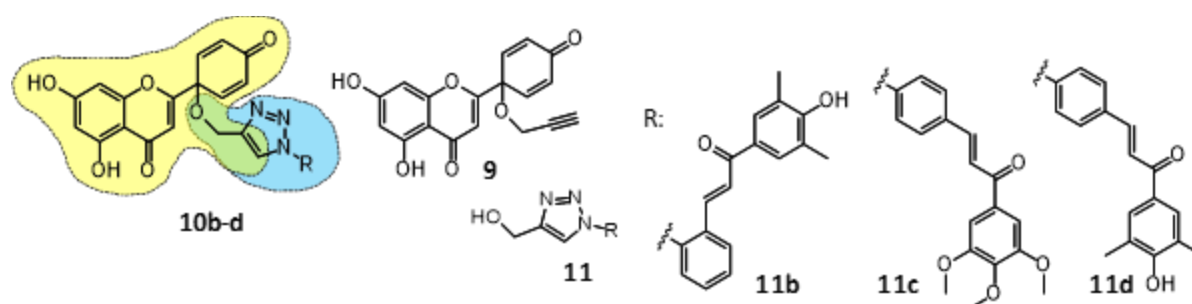
Cell line	Type of combo	Hybrid	Fragments combined	CI value at			Dm	m	r	CI_avg
				ED_{50}	ED_{75}	ED_{90}				
MCF-7	Virtual	10b	9 + 11b	0.22	0.19	0.17	0.31	2.48	0.993	0.18
		10c	9 + 11c	0.34	0.30	0.27	0.33	2.91	0.997	0.30
		10d	9 + 11d	0.39	0.36	0.34	0.53	2.38	0.998	0.35
	Exp.	10b	9 + 11b	0.70	0.71	0.73	2.18	2.51	0.989	0.72
		10c	9 + 11c	1.03	1.06	1.10	1.69	2.47	0.980	1.07
		10d	9 + 11d	0.98	0.93	0.87	2.38	2.55	0.997	0.91
MDA-MB-231	Virtual	10b	9 + 11b	0.18	0.15	0.13	0.25	3.36	0.982	0.14
		10c	9 + 11c	0.21	0.17	0.13	0.21	4.37	0.986	0.16
		10d	9 + 11d	0.23	0.20	0.17	0.27	3.01	0.982	0.19
	Exp.	10b	9 + 11b	0.75	0.96	1.22	1.28	2.01	0.972	1.05
		10c	9 + 11c	0.86	0.85	0.86	1.67	2.30	0.961	0.85
		10d	9 + 11d	0.77	0.79	0.80	1.53	1.86	0.972	0.79
HeLa	Virtual	10b	9 + 11b	0.48	0.51	0.56	0.74	1.73	0.994	0.53
		10c	9 + 11c	0.56	0.47	0.39	0.78	3.31	0.976	0.45
		10d	9 + 11d	0.72	0.58	0.48	1.03	3.37	0.997	0.56
	Exp.	10b	9 + 11b	1.05	1.14	1.32	1.95	1.97	0.962	1.22
		10c	9 + 11c	0.77	0.85	0.97	2.06	1.85	0.912	0.90
		10d	9 + 11d	0.89	0.97	1.09	2.32	2.31	0.952	1.01
SiHa	Virtual	10b	9 + 11b	0.10	0.07	0.05	0.25	4.72	0.984	0.06
		10c	9 + 11c	0.10	0.08	0.07	0.20	3.52	0.992	0.08
		10d	9 + 11d	0.11	0.10	0.09	0.24	2.47	0.994	0.10
	Exp.	10b	9 + 11b	0.95	1.13	1.40	1.43	1.79	0.964	1.24
		10c	9 + 11c	1.09	1.16	1.23	1.60	2.07	0.931	1.18
		10d	9 + 11d	0.78	0.94	1.16	1.76	2.90	0.843	1.02

Figure 6. Comparative analysis of the cytotoxic activity of the hybrid compounds **10b-d** by the Chou-Talalay method with that of their fragments (**9** and **11b-d**). Results of a virtual (hybrid vs. fragments alone) and an experimental (Exp.: equimolar mixture of fragments vs. fragments alone) combination study are shown at 50%, 75%, and 90% of inhibition. CI: combination index; $0 < CI < 1$, $CI = 1$, and $CI > 1$ represent synergism, additivity, and antagonism, respectively. Dm, m, and r represent the antilog of the x-intercept (activity), slope (shape of the dose-effect curve), and linear correlation coefficient (conformity of the data) of the median effect plot, respectively. $CI_{avg} = (CI_{50} + 2 \times CI_{75} + 3 \times CI_{90})/6$. The lowest CI_{avg} value demonstrates the highest added benefit of hybridization in terms of *in vitro* cytotoxic activity.

5   DISCUSSION

5.1   Naringenin oxime derivatives

5.1.1   Preparation of naringenin oximes and oxime ethers

Oximes or oxime ethers may have stronger antitumor activity than their corresponding oxo-compounds [95,97,98,111]. Therefore, we decided to synthesize such derivatives of NG, to possibly improve its anticancer activity.

By using the procedure previously described by Türkkan *et al*. (2012) [90], two NG oxime isomers and five different oxime ether derivatives were obtained.

The oxime derivatives of NG (**2,3**) were prepared from NG (**1**) by using hydroxylamine hydrochloride in the presence of potassium hydroxide and ethanol as solvent. The reaction resulted in two geometric isomers *E* and *Z,* which only differ in the oxime configuration, and the isolated yields were 38 and 3%, respectively. The *E* isomer has previously been prepared by others, and its antimicrobial, antioxidant, antigenotoxic, and antiproliferative effects were reported [90–94]. The minor *Z* isomer was prepared by us for the first time.

The five oxime ether derivatives (**4–8**) were analogously prepared from NG by applying the corresponding alkoxyamines, such as methoxy-, ethoxy-, tert-butoxy-, allyloxy-, and benzyloxyamine hydrochloride in pyridine, and the yields were 18, 52, 53, 58 and 5% respectively. In all these cases, only the formation of the *E*-oxime ether isomer was observed. The ethyl, *tert*-butyl and allyl ether derivatives were synthesized as new compounds, while the synthesis and characterization of the methyl and benzyl ether derivatives were previously reported by Liu *et al*. (2013), and their cytotoxicity was also evaluated on human gastric cancer cell line SGC-7901 [98].

5.1.2   Antiproliferative effects of naringenin oximes and oxime ethers

Several *in vitro* studies demonstrated that NG could suppress cell proliferation, influence cell cycle suppression, and induce apoptosis on cancer cell lines of various origin, including human pancreatic, ovarian, breast, and uterine cancer, and leukemia [112–114].

The present study was carried out to analyze the pharmacological effect of the NGOX derivatives against different types of cancer cell lines with more emphasis on the gynecological cancer cell types. The cytotoxic activity of eight compounds including NG and its oximes and oxime ethers was tested *in vitro* against human gynecological cancer cells, including four adherent cell lines: cervical (SiHa, HeLa) and breast (MDA-MB-231, MCF-7).

Additionally, the activity of the compounds was also tested on a human leukemia cell line (HL-60). First bioactivity screening was performed by MTT assay, which is based on the selective capacity of living cells to produce the mitochondrial enzymatic conversion of the yellow soluble salt of MTT to an insoluble purple precipitate of formazan crystals during a four-hour incubation period [115]. IC_{50} values were determined only for those compounds that demonstrated growth inhibition of higher than 75% at a concentration of 50 μM. The results showed that naringenin *t*-butyl oxime derivative (**6**) exerted the strongest antiproliferative effect on the tested cancer cell lines. Other compounds, such as the *E*-oxime (**2**), methyl derivative (**4**), allyl-derivative (**7**), and benzyl-derivative (**8**) exerted moderate growth inhibition.

In contrast, NG (**1**) and *Z*-oxime (**3**) did not present any antiproliferative activity on the examined cancer cell lines at any administered concentrations. At the same time, no marked cell line specificity was observed for the tested compounds. Our results were consistent with the related reports by Kocyigit *et al*. (2016) and Liu *et al*. (2013), suggesting that insertion of the oxime group to the structure of NG increased the cytotoxic activity of naringenin [92,98]. Furthermore, we proved for the first time that the elongation of the E-oxime ethers, and mainly if the ether is a *t*-butyl group at the carbonyl position in NG, results in a significant increase in the cytotoxic properties of the obtained compounds. Also, we observed that MCF-7 and HeLa cancer cells appear to be more sensitive than SiHa and MDA-MB-231 cells. Our results are consistent with previous studies of other authors who explained that the modification of the flavanone carbonyl group at C-4 position with an oxime group created new derivatives with stronger anticancer activity against different types of cancer cell lines. Besides, a significant increase was observed in their cytotoxic activity when used to treat human colon adenocarcinoma HT-29, epidermoid carcinoma (KB), small cell lung cancer (NCI-H187), hepatocellular carcinoma HepD2 and Human breast cancer T47D [94,97,116].

On the other hand, many of the flavonoid compounds were found to inhibit the proliferation of HL-60 cells to some extent [117]. Our recent data revealed that NG and its oxime derivatives had impotent inhibitory effects against HL-60 human leukemia and cervical SiHa cells. This is also in agreement with an observation by Kocyigit *et al*. (2016), who previously reported that treatment of human peripheral blood mononuclear cells (PBMC) with high concentrations of 1280 μM and 640 μM of NG and NGOX, respectively, did not produce more than 60% inhibitory effects [92]. However, at the same time these findings conflict with Park *et al*. (2008), who reported that NG induced significant antiproliferative and apoptotic

effects in human leukemia THP-1 cells. These contradictory results may be due to the dependence of cytotoxic potency on the tested cell lines or to the higher concentrations in their study because they used 200-400 μM, while in our research the maximum concentration was 50μM [114]. Our results agree with the results of Diaz *et al*. (2017) on the impacts of their synthesized flavone oxime ethers against MDA-MB-231 with a value of IC_{50} (28.7 μM), which was close to the effects of our potent compound against the same cells [96].

5.1.2 Cell cycle analysis

Measurement of the DNA content by flow cytometric cell cycle analysis is considered an attractive approach and played an essential role in cancer research screening or studying the mechanism of action of anticancer agents [118]. The cytotoxic activity of Fls was qualified for their effects on cell cycle progression and triggering apoptosis [119]. Based on the antiproliferative effects, our results showed that a new derivatized NGOX ether has a potent activity. Furthermore, flow cytometric cell cycle analyses were performed to prove *the in vitro* mechanism of action. Gynecological cancer cell lines that were treated with prepared compounds elicited a considerable rise in the number of hypodiploid cells (subG1 population) only in HeLa and SiHa cells after a 24 h incubation period, which indicates that the cytotoxic activity of compound **6** in HeLa and SiHa cells occurs via apoptosis. In addition, it also brought about a disruption in the cell cycle in a concentration-dependent manner. Stronger effects were observed on HeLa cells, which were accompanied by preventing the cancer cells from entering the G1 phase, which was detected from the significant decrease in the proportion of the G1 stage and the corresponding increase in the S phase, while in SiHa cells these effects were just the contrary. Besides, our study found that the tested compound did not interfere with the cell distribution of MDA-MB-231 cancer cells, not even at the highest concentration. These data suggest that the effect of NGOX ether (**6**) on the cell cycle progression depended on the cancer cell type. An earlier report showed that when treating two human nasopharyngeal carcinoma cell lines with WTC-01, a synthetic oxime-containing flavone caused G2/M phase suppression and increased apoptosis in a time- and dose-dependent manner [95]. This different cell cycle distribution may be dependent on cell lines and different tested types of flavonoid oxime.

5.1.3 Caspase-3 activity

Apoptosis, programmed cell death, is a highly regulated process that maintains an rquilibrium between cell proliferation and cell death. Hence, drugs that exhibit the ability to produce apoptosis and inhibit uncontrolled cell proliferation may be useful in managing and treating cancer disease. It was recorded that caspase-3 is a common effector enzyme that plays a principal role in the caspase-mediated apoptosis pathway, which can be detected by immunohistochemical, optical, and biochemical methods [120,121]. Khalilzadeh *et al.* (2018) described that caspase-3 has a vital role in both extrinsic and intrinsic pathways, and its detection is an essential tool for monitoring the competence of pharmaceuticals, chemo- and radiotherapy of cancers [122]. The antiproliferative and apoptosis activity of *t*-butyl derivative (**6**) was confirmed by measuring the proapoptotic property of caspase-3 level during 24 h on HeLa cells. The present study suggested that compound **6** induced apoptosis in a concentration-dependent manner, which was established by the significant increase in caspase-3 activity besides the considerable rise in the subG1 proportion. Our results confirmed that the *t*-butyl group added to NG significantly enhanced programmed cell death in HeLa cancer cells and thus could be considered as a promising agent that can be used for the treatment of cervical HeLa cancer cell lines. However, there is no available report demonstrating the caspase activity of this new oxime derivative compound on cancer cells. No previous scientific report has been published on the caspase activity of these oxime compounds against cancer cells; we were the first to investigate the caspase-3 effects of naringenin *t*-butyl oxime in the cancer cells.

5.1.4 Antioxidant activity

The free radicals are responsible for the induction of oxidative damage that leads to diseases, including cancer. Hunyadi (2019) mentions that antioxidants' secondary metabolites are able to decrease the oxidative stress through free radical scavenging or modulating the antioxidant and pro-oxidant enzymes [123]. This antioxidant activity fundamentally depends on the chemical structure of these compounds [124]. Therefore, the present research was carried out to evaluate the antioxidant activity of NG and their synthesized oxime derivatives by measuring oxygen radical absorbance capacity (ORAC), their ability to inhibit the xanthine oxidase (XO) activity, and scavenge diphenyl-2-picrylhydrazyl (DPPH) radical. Our results revealed that higher DPPH radical scavenging activity can only be observed in the case of *E*-oxime and oxime methyl ether and is still stronger than that of NG. Concerning the

DPPH scavenging activity here, our study was consistent and confirmed earlier findings according to which synthesized NGOX have an antioxidant capacity higher than their parent compounds [92]. Also, similarly to the study of Potaniec *et al*. (2014), it was observed that NGOX and flavanone oxime have stronger DPPH antioxidant properties than the corresponding substrates but comparable to ascorbic acid activity; they did not have any significant antioxidant effect [91]. Furthermore, we observed that E-oxime was an order of magnitude more potent in this respect than Z-oxime, these observations on the DPPH assay reveal that the scavenging activity of the prepared compound depends on the number and position of the hydroxyl (OH) group.

On the other hand, in exception of the oxime methyl ether derivative, which registered the highest antioxidant properties in both the ORAC and the DPPH assays, and this activity was more elevated than the positive control rutin in the ORAC assay, the other additional substitution on the synthesized NGOX including *t*-butyl caused reduction in XO inhibition and ORAC activity as compared to NG. This finding suggests that replacement at position C4 (C=O) of naringenin with oximes caused a reduction in antioxidant activity. Our results are in disagreement with Nile *et al*. (2018), who reported that flavonoid derivatives can be considered as potent antioxidants and XO inhibitors [61], and this difference in antioxidant effects might be due to various Fl derivatives. Moreover, our results demonstrated that NGOX derivatives, despite their *in vitro* cytotoxic effects, did not show any apparent correlation to their antioxidant capacities. This suggests that the potential antitumor action of these compounds is not related to their antioxidant properties.

5.2   Protoflavone derivatives

5.2.1   Antiproliferative effects

The present results displayed that synthesized hybrid derivatives (**10a-d**) and their relevant fragments (**9 and 11a-d**) were able to suppress significantly the proliferation of human breast and cervical cancer cells in a concentration-dependent character. They showed stronger activity than cisplatin, a conventional chemotherapeutic drug in all tested cancer cell lines. As demonstrated, their relevant fragments (**9 and 11b-d**) have a significant cytotoxic effect, while in contrast, particle (**11a**) did not show any antiproliferative effects. Additionally, we also observed that MDA-MB-231, a TNBC and SiHa, an HPV 16+ cervical squamous cell carcinoma, were considered sensitive to the cytotoxic action of hybrid

compounds. In a previous *in vitro* study, it was reported that PrFl derivatives provoke cytotoxic effects on TNBC and cervical cancer cells in a concentration-dependent manner [125–127]. Our results are concordant with the findings reported by Lin *et al*. (2007), Hunyadi *et al*. (2011) and Lin *et al*. (2005), concluding that modification analogs of synthetic and isolated protoapigenone from *Thelypteris torresiana* have intense antiproliferative activity against breast cancer cells MDA-MB-231 and MCF-7 [99,128,129]; and also consistent with a study conducted by Chen *et al*. (2013), indicating that protoapigenone derivative (WYC02) caused a concentration-dependent cytotoxic effect against HeLa and SiHa cells [130].

Moreover, the cytotoxicity of the potent compounds (**10b** and **10c**) was evaluated against non-cancerous mouse embryonic fibroblast cell lines (NIH/3T3) and it was found that both compounds exhibited less toxicity against these healthy cell lines. These data suggested that synthesized compounds have selective cytotoxicity on breast and cervical cancer cells. Fls can be considered as potential therapeutic agents due to their properties to kill tumor cells with less or no effect on healthy cells [131]. Our results are consistent with Yuan *et al*. (2012), indicating that protoapigenone analog (RY10-4) has potent cytotoxic effects on the MCF-7 and MDA-MB-231 cancer cells and offers satisfying selectivity for cancer cells with fewer cytotoxic effects against MCF-10A [132]. Also, they are in agreement with Danko *et al*. (2012), who found that methyl PrFl derivatives exhibited moderate selectivity toward MDR cancer cells [125].

In the present study, these data suggest that the antiproliferative activity of the newly tested hybrid PrFl derivatives was dependent on the position and nature of the fragment on the protoflavone-chalcone hybrids with triazole linker and showed that the presence of the methoxy group on the hybrid compound structure was the potent toxic effect.

5.2.2 Cell cycle analysis

Cell cycle regulation and apoptosis are supposed to be essential strategies in the development of antitumor agents [133]. To study the mechanism of action of the synthesized PrFl derivatives, we performed cell cycle analyses, and measured caspase-3 activity, DNA damage, cell death induction, and mitochondrial function. We evaluated the cell cycle progression of two compounds **10b** and **10c**, which exhibit potent cytotoxic effect in cervical SiHa and TNBC cells. The present study in both tested cancer cells observed that both tested compounds increase the cell population in the subG1 phase. In the case of MDA-MB-231, the

effect was associated with a reduction in the percentage of G1 phase cells in a concentration-dependent manner after 24h, which indicates a hallmark of enhanced apoptosis, with noticeable effects detected after exposure to compound **10c**. These results are consistent with a report conducted by Chen *et al.* (2011), who discovered that protoapigenone played a vital role in a concentration-dependent manner in inducing apoptosis by increasing the proportion of subG1 population in TNBC [127]. These results are in concord with those reported by Chang *et al.* (2008) and Chiu *et al.* (2009), who found that the treatment of human lung adenocarcinoma (H1299) and ovarian cancer cell lines (SKOV3 and MDAH-2774) with protoapigenone induced apoptosis and caused cell accumulation in the subG1 phase in a dose-dependent manner [134,135].

Moreover, Stankovic *et al.* (2015) demonstrated that 6-bromoprotoflavone derivative induced cell growth inhibition and decreased the level of the G1 phase of glioma MDR cancer cells [136]. Additionally, our results conflicted with Chen *et al.* (2013), who concluded that HeLa cells, when treated with WYC02, a synthetic protoapigenone derivative, caused cell cycle distribution and accumulation in the S and G2/M phases [130], while our tested compounds did not show any noticeable effects in these phases in both tested breast and cervical cancer cells. This may be due to the varied mechanisms of action of the various tested cancer cells and the different structure of the tested compounds.

5.2.3 Caspase-3 and apoptotic activity

Most of the anticancer therapeutic strategies and drug development aim to promote apoptosis in cancer cells [120]. The induction of apoptosis is considered one of the most critical points in the promising therapeutics for cancer. In particular, caspase-3, which is a member of the cysteine-aspartic acid protease family, plays an essential role as a crucial executioner protein of apoptotic pathways [1,137]. The activation of both the death extrinsic receptor and the mitochondria intrinsic receptor pathways of apoptosis converge in the activation of caspase-3, and its activation is considered as a hallmark for response estimation to anticancer therapy. Our results demonstrated that among all the synthetic and fragment hybrid PrFl compounds, **10c** was prominent in the cytotoxic and apoptotic effects through triggering caspase-3. **10c** was found to be potent inducing caspase apoptosis in the TNCS in a concentration- and time-dependent manner. Our data suggest that cytotoxic indication mediated by the PrFl derivatives was due to apoptotic cell death, which is in agreement with the findings of Wang *et al.* (2017), who reported that any drugs directly activating caspase-3

are of interest as anticancer agents [138]. This is also consistent with Chen *et al*. (2011), who demonstrated that protoapigenone activated caspase-3 in TNBC [127]. Furthermore, the importance of caspase activation to cause apoptosis in the breast cancer cells was supported and confirmed by the cooperation study data.

5.2.4   Combination study

ATM and ATR are attractive novel antitumor targets currently being investigated in several related clinical trials [139–141] . These two kinases are activated upon DNA damage induced by oxidative stress and they play an essential role in the regulation of DNA repair pathways [142]. Therefore, Hijova (2014) suggested that simultaneously targeting DDR and inducing oxidative stress may be a relevant antitumor strategy [143]. Protoflavones are efficient inhibitors of the ATR kinase, and, at the same time, they are also known to induce oxidative stress [110,127]. Chalcones may exert cytotoxic effect against cancer cell lines through various mechanisms of action, including the induction of oxidative stress and interfering with the mitochondrial membrane potential [144–146].

In our study, we explored the anticancer activities of a set of hybrid molecules obtained from our collaboration partners (Prof. Antal Csámpai, Institute of Chemistry, Eötvös Loránd University, Budapest, Hungary). These compounds represent an example for fragment-based drug design, and they were obtained from a protoflavone and a chalcone fragment through click reaction forming a triazol linker. According to the above considerations, they were hypothesized to combine complementary pharmacological properties.

When assessing the compounds' cytotoxicity on our gynecological cancer cell line panel, we found strong activities with IC_{50} values in a couple of hundreds nanomolar concentration range. Even though these activities were clearly much more potent than that of the protoflavone fragment, we decided to perform a more sophisticated mathematical evaluation to elaborate the pharmacological benefit of the hybrid coupling as compared to the separate bioactivity of the individual fragments. This clearly showed that, considering the hybrids as 1:1 ratio mixture combination treatment in a "virtual combination study", a strong synergism can be calculated, and therefore ample pharmacological benefit of the coupling may reasonably be concluded. This mathematical evaluation also provides extra information concerning the bioactivity of a hybrid molecule vs. that of its corresponding hybrids as compared to a simple intuitive comparison of the IC_{50} values. For example, compound **10c** was significantly more cytotoxic on MDA-MB-231 cells than **10b** by means of the non-

overlapping confidence intervals of their IC$_{50}$ values. When comparing the virtual combination indices of these two hybrids, however, the opposite trend may be observed, i.e. a more pronounced activity increase was gained when compound **10b** was formed from its fragments, as compared to the case of **10c**.

Using the Chou-Talalay method as a mathematical tool to perform a quantitative comparison between the bioactivity of two fragments and their corresponding hybrid is, to the best of our knowledge, a novel approach. We believe that with an appropriate selection of fragments to evaluate, such a virtual combination study provides a reasonable and easy-to-use platform to assess the bioactivity of hybrid compounds in general, therefore, we suggest an extension for the applicability of the Chou-Talalay method to analyze related bioactivity data.

5.2.5   Collaboration findings

The hybrid compounds were further tested within an international collaboration network including Serbian (Dr. Milica Pešić, Institute for Biological Research, Department of Neurobiology, University of Belgrade, Belgrade, Serbia), Taiwanese (Prof. Hui-Chun Wang, Graduate Institute of Natural Products, Kaohsiung Medical University, Kaohsiung, Taiwan) and Turkish (Prof. Engin Ulukaya, Istinye University, Istanbul, Turkey) partners. Their findings provided independent confirmation of our results, and provided some mechanistical background to the observed potent antitumor activity of the hybrid compounds. For more details see the Reference (I).

The potential of hybrid compounds **10a-d** to induce cell death in both tested breast cancer cell lines is shown in Figure 7.
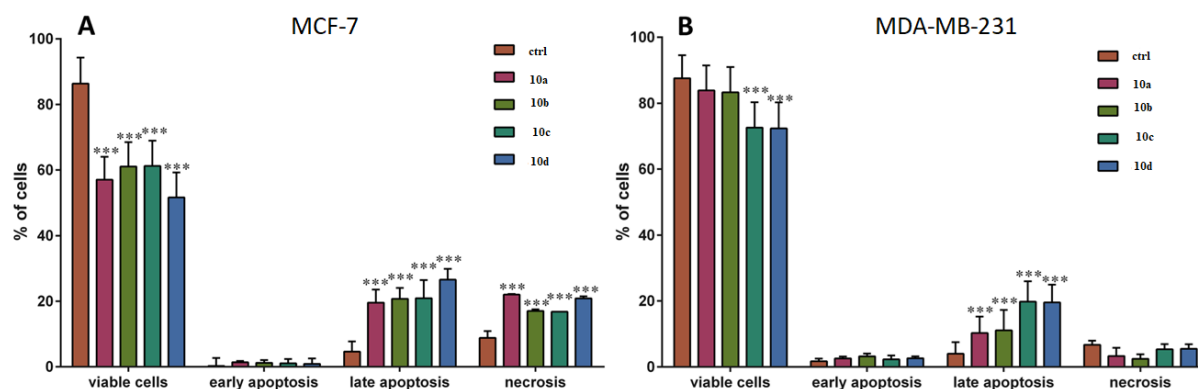
Figure 7. Cell death induction on the (A) MCF-7 and (B) MDA-MB-231 cells by the hybrid compounds (**10a-d**). After treatment with 500 nM of each compound for 72 h.

The compounds were also tested for their capacity to inhibit DNA damage response through the ATR-dependent signaling pahtway. Further, their effect on the intracellular ROS and RNS production was also tested (Figure 8).
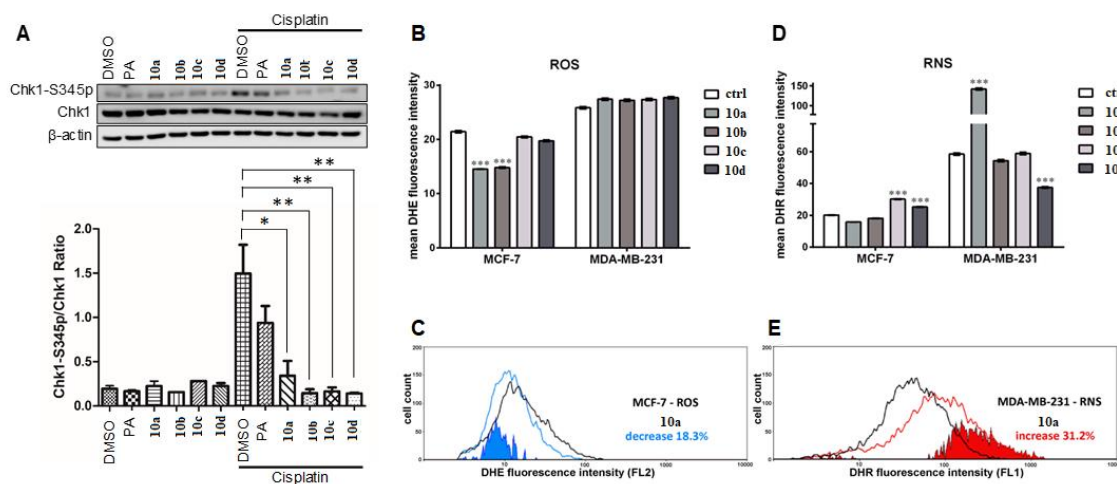
Figure 8. Effects of compounds (**10a-d)** on DNA damage response and redox balance in breast cancer cells. (A) Effect on Chk1 phosphorylation in MCF-7 cells, PA (protoapigenone); (B) Effect on ROS production; (C) Decrease in ROS production by **10a**; (D) Effect on RNS production; (E) Increase in RNS production by **10a**.

As shown in Figure 8A, the treatment with all tested compounds **10a-d** exhibited a significant suppression of cisplatin-induced Chk1-S345 phosphorylation and the activity was more potent than that of the positive control. Also, the hybrid compounds inhibited the DDR and were more potent than the ATR inhibitor fragment. Based on the pro-oxidant properties of both linked fragments, i.e., PrFl and chalcone, the intracellular ROS and RNS levels in the breast cancer cells were investigated after treatment with PrFl derivatives (Figure 8B-E).

The integrity of mitochondrial membrane potential (MMP) after the treatment of both cancer cell lines with the hybrid compounds **10a-d** was also tested (Figure 9).
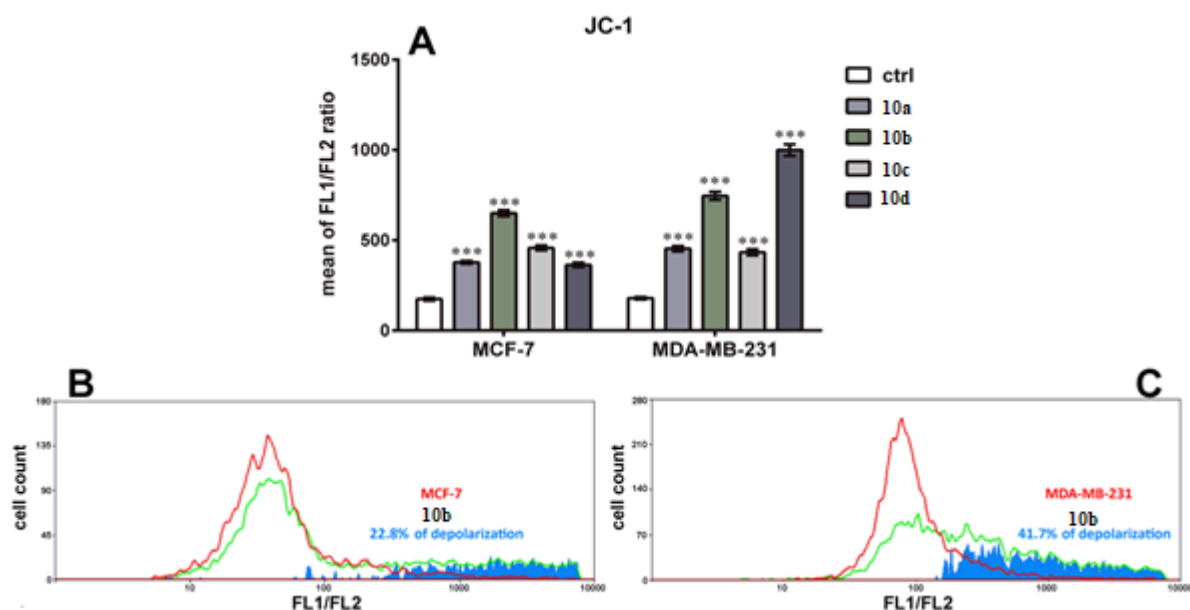
Figure 9. Hybrid-protoflavones induce mitochondrial membrane depolarization. (A) Increase in the ratio of green to red fluorescence (FL1/FL2) assessed by JC-1 staining in MCF-7 and MDA-MB-231 cells after 24 h treatments with one µM of compounds **10a-d**; (B) Illustration of the effect induced by **10b** in MCF-7 cells; (C) Illustration of effects caused by **10b** in MDA-MB-231 cells.

Our cooperator's *in vitro* findings further demonstrated that the hybrid compounds exhibited the ability to induce cell death with late apoptosis in both breast cancer cells and accompanied by necrotic cell death in the MCF-7 cells.

They observed that all treatments with hybrid compounds induced significant late apoptosis in both cell lines, while a substantial increase in primary necrosis was present only in the MCF-7 cells. On the other hand, only **10c** and **10d** caused a substantial decrease in the cell viability of MDA-MB-231 cells during the incubation period of this bioassay. It is worth noting that MCF-7 cells responded differently to the treatment when compared with the MDA-MB-231 cells. Moreover, substantial primary necrosis was observed in the MCF-7 cells.

Several ATR or checkpoint kinase inhibitors are currently being developed with an aim to selectively target tumors with or without a co-treatment with a DNA damaging chemotherapeutic agent [140,147]. Our current study showed that all hybrid compounds **10a-d** induced apoptotic cell death and DNA damage. These data support the previous results showing that protoapigenone and its derivatives caused DNA damage and cell death induction in the breast, prostate, and lung cancer cells [127,134,148]. In this regard, Kuo *et al.* (2016) reported that dietary Fls could inhibit Chk1 phosphorylation and impair DNA

repair pathways to increase breast cancer sensitivity to cisplatin treatment [149]. Similarly, our results were consistent with Wang *et al.* (2012) observing that PrFl derivatives (WYC0209 and WYC02) decreased the cisplatin-induced Chk1 phosphorylation in MDA-MB-231 breast cancer cells [110]. In view of these results in the current study, we suggest that effect on the DNA damage response plays an important role in the cytotoxicity of the hybrid compounds **10a**-**d**.

Among all the tested compounds, only **10a** and **10b** caused a significant decrease in ROS production in the MCF-7 cells, whereas TNBC did not show any noticeable effects. In respect to RNS levels, compounds **10c** and **10d** elicited a considerable increase in MCF-7 cells. Furthermore, the most noticeable effect on RNS levels was observed with **10a,** suggesting its significant pro-oxidant activity in MDA-MB-231 cells. On the other hand, **10d** significantly reduced the RNS levels in TNBC cells.

Numerous previous studies discussed that exposure of human glioma U87-TxR, breast MDA-MB-231, and prostate DU145 cancer cells to protoapigenone and its analogs increased the levels of intracellular ROS production [127,136,148]. On the contrary, our results on the protoflavone-chalcone hybrids showed that these compounds can scavenge ROS and induce RNS production in both tested breast cancer cells. Similar opposite effects on the ROS and RNS production were previously observed with ferrocene–quinidine hybrids [29] containing the same triazole-linked ferrocene moiety as compound **10a** [150].

While all the tested compounds **10a-c** displayed potent mitochondrial membrane depolarisation in MDA-MB-231 and MCF-7 cancer cells, compound **10d** showed pronounced selectivity towards MDA-MB-231 cells in this regard. Although this is just one aspect of a clear multitarget antitumor action of these compounds; it may still be worth noting that **10d** showed the highest selectivity towards MDA-MB-231 versus MCF-7 among the hybrids in the cytotoxicity assay. Further, it may be hypothesized that the induction of late apoptosis after 72 h treatment by **10d** and other hybrid compounds (Figure 7) is due to proapoptotic factors released from affected mitochondria whose proton leakage was observed after 24 h treatments.

6   SUMMARY

The present PhD work aimed to contribute to the knowledge available on the antitumor properties of flavonoids through the *in vitro* evaluation of the bioactivity of some uncommon semi-synthetic derivatives against a panel of breast and cervical cancer cell lines that are well-established models for certain types of gynecological cancer.

The work included the semi-synthetic preparation of seven naringenin oxime and oxime ether derivatives prior to their bioactivity testing, and the *in vitro* evaluation of nine protoflavone-chalcone hybrid compounds and their reference fragments against breast (hormone-dependent MCF-7 and triple-negative MDA-MB-231), and cervical (SiHa & HeLa) cancer cell lines in addition to human HL-60 leukemia cells and non-cancerous mouse embryonic fibroblasts (NIH/3T3). The work included cytotoxicity, cell cycle distribution, caspase-3 activity, and antioxidant activity evaluations. Further, the cytotoxic activity of the hybrid compounds was evaluated in comparison with that of their corresponding fragments in a virtual and experimental combination study.

In summary, our work led to the following results.

- Two naringenin oxime isomers and five oxime ether derivatives were synthesized, purified and characterized. Four of these compounds, such as the minor product naringenin *Z*-oxime, and the ethyl, allyl, and *tert*-butyl ethers of naringenin *E*-oxime were prepared as new compounds.

- When evaluating the *in vitro* cytotoxicity of the prepared derivatives of naringenin, *tert*-butyl oxime ether (**6**) showed the most potent effects on different gynecological cancer cells, with significant activity against MCF-7 and HeLa cells.

- The flow cytometric analysis of compound (**6**) on gynecological cancer cells revealed significant accumulation of cells in the hypodiploid (subG1) phase in HeLa & SiHa cell lines, indicating the apoptosis induction effect, and induced cycle suppression at G2/M stage in MCF-7 cancer cells. Further, the proapoptotic activity of this compound was confirmed in HeLa cells by detecting the increased activity of caspase-3.

- To our surprise, naringenin methyl oxime ether was more potent in the ORAC assay than its parent compound, while all other analogs were up to an order of magnitude less active. This suggests good peroxyl radical scavenging capacity for this compound.

- There was no apparent correlation between the *in vitro* cytotoxic and antioxidant activities of the tested compounds, suggesting that their anticancer effects are likely not related to their antioxidant properties.

- Four protoflavone hybrid compounds were identified as promising antitumor lead compounds based on their prominent *in vitro* cytotoxic effects and their selectivity on different breast and cervical cancer cells with antiproliferative effects better than cisplatin.

- The most potent compounds have an intense proapoptotic effect on TNBC, as evidenced by flow cytometric investigation and caspase-3 activity. It was shown that compound **10c** induces a considerable expansion in caspase-3 activity in a concentration-time dependent manner with a significant increase in the sub G1 phase.

- A novel approach was used to evaluate the bioactivity of the hybrid compounds in comparison with that of their corresponding fragments. A virtual combination study was performed by using the Chou-Talalay method as a mathematical tool, and results were compared to the corresponding experimental combinations of the cells with non-coupled fragments. This gave valuable extra information as virtual combination index values and confirmed that the studied hybrid compounds are much more potent than what would be expected by a mathematical sum of the bioactivity of their fragments.

- Based on the above, we demonstrated the use of a novel approach to evaluate the bioactivity of hybrid compounds in general, and suggested an extension of the applicability of the Chou-Talalay method, one of the currently available most popular platforms for drug-drug combination studies.

Altogether, our present study provided valuable information about the antitumor potential of two series of unusual semi-synthetic flavonoid derivatives, and made a significant contribution to identifying a set of highly potent hybrid lead compounds obtained through fragment-based drug design. Further, by providing a novel use for an existing convenient and very widely used mathematical platform, we believe our study may have contributed to the research of hybrid compounds also in a more general manner.

7 REFERENCES

1. Zhang, N.; An, B.; Zhou, Y.; Li, X.; Yan, M. Synthesis, evaluation, and mechanism study of new tepotinib derivatives as antiproliferative agents. *Molecules* **2019**, *24*, 1173.

2. World Health Organization *The Global Cancer Observatory, International agency for research on cancer, Breast, Source: Globocan 2018*; 2019;

3. Santos, M.B.; Bertholin Anselmo, D.; de Oliveira, J.G.; Jardim-Perassi, B. V.; Alves Monteiro, D.; Silva, G.; Gomes, E.; Lucia Fachin, A.; Marins, M.; de Campos Zuccari, D.A.P.; et al. Antiproliferative activity and p53 upregulation effects of chalcones on human breast cancer cells. *J. Enzyme Inhib. Med. Chem.* **2019**, *34*, 1093–1099.

4. Bray, F.; Ferlay, J.; Soerjomataram, I. Global cancer statistics 2018 : Globocan estimates of incidence and mortality worldwide for 36 cancers in 185 countries. *Cancer J Clin* **2018**, *68*, 394–424.

5. Ferlay, J.; Colombet, M.; Soerjomataram, I.; Dyba, T.; Randi, G. Cancer incidence and mortality patterns in Europe : Estimates for 40 countries and 25 major cancers in 2018. *Eur. J. Cancer* **2018**, *103*, 356–387.

6. Menyhárt, O.; Fekete, J.T.; Győrffy, B. Demographic shift disproportionately increases cancer burden in an aging nation : current and expected incidence and mortality in Hungary up to 2030. *Clin. Epidemiol.* **2018**, *10*, 1093–1108.

7. Gyulai, A.; Nagy, A.; Pataki, V.; Tonté, D.; Ádány, R.; Vokó, Z. General practitioners can increase participation in cervical cancer screening – a model program in Hungary. *BMC Fam. Pract.* **2018**, *19*, 67.

8. Kolozsvári, L.R.; Langmár, Z.; Rurik, I. Nationwide screening program for breast and cervical cancers in Hungary : special challenges , outcomes , and the role of the primary care provider. *Eur. J. Gynaecol. Oncol.* **2013**, 419–425.

9. Hartai, M.; Nyári, T.A.; McNally, R.J.Q. Trends in mortality rates in female genital organs and breast cancers in Hungary between 1979 and 2013. *Eur. J. Obstet. Gynecol. Reprod. Biol.* **2015**, *194*, 168–172.

10. Alwan, N.A.S.; Tawfeeq, F.N.; Mallah, N.A.G. Demographic and clinical profiles of female patients diagnosed with breast cancer in Iraq. *J Contemp Med Sci* **2019**, *5*, 14–19.

11. Al-janabi, A.M.; Hussein, A.; Algenabi, A.; Kamoona, T.H.; Alkhafaji, S.M. Association of HER2 [ILe655Val] gene polymorphism and breast cancer risk in Iraqi females population material and method : *Int. J. Adv. Res.* **2015**, *3*, 1483–1489.

12. Iriti, M.; Kubina, R.; Cochis, A.; Sorrentino, R.; Varoni, E.M.; Kabała-Dzik, A.; Azzimonti, B.; Dziedzic, A.; Rimondini, L.; Wojtyczka, R.D. Rutin, a quercetin glycoside, restores chemosensitivity in human breast cancer cells. *Phyther. Res.* **2017**, *31*, 1529–1538.

13. Oh, Y.J.; Seo, Y.H. A novel chalcone-based molecule, BDP inhibits MDA-MB-231 triple-negative breast cancer cell growth by suppressing Hsp90 function. *Oncol. Rep.* **2017**, *38*, 2343–2350.

14. Varghese, E.; Samuel, S.; Varghese, S.; Cheema, S.; Mamtani, R.; Büsselberg, D. Triptolide decreases cell proliferation and tnduces cell death in triple negative MDA-MB-231 breast cancer cells. *Biomolecules* **2018**, *8*, 163.

15. Cai, L.; Yu, R.; Hao, X.; Ding, X. Folate receptor-targeted bioflavonoid genistein-loaded chitosan nanoparticles for enhanced anticancer effect in cervical cancers. *Nanoscale Res. Lett.* **2017**, *12*, 509.

16. Chrysostomou, A.; Stylianou, D.; Constantinidou, A.; Kostrikis, L. Cervical Cancer Screening Programs in Europe: The transition towards HPV vaccination and population-based HPV testing. *Viruses* **2018**, *10*, 729.

17. Goodman, A. HPV testing as a screen for cervical cancer. *BMJ* **2015**, *350*, h2372–

h2372.

18. Wu, Z.; Wang, C.; Huang, M.; Tao, Z.; Yan, W.; Du, Y. Naturally occurring sesquiterpene lactone-santonin, exerts anticancer effects in multi-drug resistant breast cancer cells by inducing mitochondrial mediated apoptosis, caspase activation, cell cycle arrest, and by targeting Ras/Raf/MEK/ERK signaling pathw. *Med. Sci. Monit.* **2019**, *25*, 3676–3682.

19. Huang, T.; Wu, X.; Liu, T.; An, L.; Yin, X. Synthesis and anticancer activity evaluation of novel oxacalix[2]arene[2]pyrimidine derivatives. *Med. Chem. Res.* **2019**, *28*, 580–590.

20. Youns, M.; Abdel Halim Hegazy, W. The natural flavonoid fisetin inhibits cellular proliferation of hepatic, colorectal, and pancreatic cancer cells through modulation of multiple signaling pathways. *PLoS One* **2017**, *12*, 1–18.

21. Specian, A.F.L.; Serpeloni, J.M.; Tuttis, K.; Ribeiro, D.L.; Cilião, H.L.; Varanda, E.A.; Sannomiya, M.; Martinez-Lopez, W.; Vilegas, W.; Cólus, I.M.S. LDH, proliferation curves and cell cycle analysis are the most suitable assays to identify and characterize new phytotherapeutic compounds. *Cytotechnology* **2016**, *68*, 2729–2744.

22. Wen, L.; Guo, R.; You, L.; Abbasi, A.M.; Li, T.; Fu, X.; Liu, R.H. Major triterpenoids in Chinese hawthorn "Crataegus pinnatifida" and their effects on cell proliferation and apoptosis induction in MDA-MB-231 cancer cells. *Food Chem. Toxicol.* **2017**, *100*, 149–160.

23. Deng, X.; Wang, Z.; Liu, J.; Xiong, S.; Xiong, R.; Cao, X.; Chen, Y.; Zheng, X.; Tang, G. Design, synthesis and biological evaluation of flavonoid salicylate derivatives as potential anti-tumor agents. *RSC Adv.* **2017**, *7*, 38171–38178.

24. Yao, N.; Chen, C.-Y.; Wu, C.-Y.; Motonishi, K.; Kung, H.-J.; Lam, K.S. Novel flavonoids with anti-proliferative activities against breast cancer cells. *J Med Chem.* **2012**, *54*, 4339–4349.

25. Jayawardena, T.U.; Lee, W.W.; Fernando, I.P.S.; Sanjeewa, K.K.A.; Wang, L.; Lee, T.G.; Park, Y.J.; Ko, C.; Jeon, Y. Antiproliferative and apoptosis-inducing potential of 3β-hydroxy-Δ5-steroidal congeners purified from the soft coral Dendronephthya putteri. *J. Oceanol. Limnol.* **2019**, *37*, 1382–1392.

26. Li, X.; Yang, C.; Shen, H. Gentiopicroside exerts convincing antitumor effects in human ovarian carcinoma cells (SKOV3) by inducing cell cycle arrest , mitochondrial mediated apoptosis and inhibition of cell migration. *Jbuon* **2019**, *24*, 280–284.

27. Luan, T.; Cao, L.; Deng, H.; Shen, Q.; Tian, Y.; Quan, Z.-S. Design and synthesis of C-19 isosteviol derivatives as potent and highly selective antiproliferative agents. *Molecules* **2018**, *24*, 121.

28. Lou, J.; Yao, P.; Tsim, K.W.K. Cancer treatment by using traditional Chinese medicine: probing active compounds in anti-multidrug resistance during drug therapy. *Curr. Med. Chem.* **2018**, 5128–5141.

29. Liu, H.; Dong, A.; Gao, C.; Tan, C.; Xie, Z.; Zu, X.; Qu, L.; Jiang, Y. New synthetic flavone derivatives induce apoptosis of hepatocarcinoma cells. *Bioorg. Med. Chem.* **2010**, *18*, 6322–6328.

30. Graziela Moraes, G.; Mazziero, M.; Lovatto, M.; Dornelles, R.C.; Nogueira-Librelotto, D.R.; Reuter, C.P.; Ortolan, S.; da Silva, C. de M.; Manfron, M.P. Preliminary phytochemical analysis and evaluation of the antioxidant and anti-proliferative effects of Plinia peruviana leaves: an in vitro approach. *Nat. Prod. Res.* **2019**, *0*, 1–9.

31. Tungmunnithum, D.; Thongboonyou, A.; Pholboon, A.; Yangsabai, A. Flavonoids and other phenolic compounds from medicinal plants for pharmaceutical and medical aspects: An overview. *Medicines* **2018**, *5*, 93.

32. Galavi, H.R.; Saravani, R.; Shahraki, A.; Ashtiani, M. Anti-proliferative and apoptosis inducing potential of hydroalcoholic Achillea wilhelmsii C . koch extract on human breast adenocarcinoma cell lines MCF-7 and MDA-Mb-468. *Pak. J. Pharm. Sci* **2016**, *29*, 2397–2403.

33. Marvibaigi, M.; Amini, N.; Supriyanto, E.; Abdul Majid, F.A.; Kumar Jaganathan, S.; Jamil, S.; Hamzehalipour Almaki, J.; Nasiri, R. Antioxidant activity and ROS-dependent apoptotic effect of scurrula ferruginea (Jack) danser methanol extract in human breast cancer cell MDA-MB-231. *PLoS One* **2016**, *11*, 1–36.

34. Ahmed, N.; Konduru, N.K.; Ahmad, S.; Owais, M. Synthesis of flavonoids based novel tetrahydropyran conjugates (Prins products) and their antiproliferative activity against human cancer cell lines. *Eur. J. Med. Chem.* **2014**, *75*, 233–246.

35. Dei Cas, M.; Ghidoni, R. Cancer prevention and therapy with polyphenols: sphingolipid-mediated mechanisms. *Nutrients* **2018**, *10*, 940.

36. Park, H.J.; Choi, Y.J.; Lee, J.H.; Nam, M.J. Naringenin causes ASK1-induced apoptosis via reactive oxygen species in human pancreatic cancer cells. *Food Chem. Toxicol.* **2017**, *99*, 1–8.

37. Gattuso, G.; Barreca, D.; Gargiulli, C.; Leuzzi, U.; Caristi, C.; Organica, C.; Messina, U.; Sperone, S. Flavonoid composition of citrus juices. *molecules* **2007**, *12*, 1641–1673.

38. Zakaryan, H.; Arabyan, E.; Oo, A.; Zandi, K. Flavonoids: promising natural compounds against viral infections. *Arch. Virol.* **2017**, *162*, 2539–2551.

39. Chirumbolo, S.; Bjørklund, G.; Lysiuk, R.; Vella, A.; Lenchyk, L.; Upyr, T. Targeting cancer with phytochemicals via their fine tuning of the cell survival signaling pathways. *Int. J. Mol. Sci.* **2018**, *19*, 3568.

40. Cao, R.; Teskey, G.; Islamoglu, H.; Gutierrez, M.; Salaiz, O.; Munjal, S.; Fraix, M.; Sathananthan, A.; Nieman, D.; Venketaraman, V. Flavonoid mixture inhibits Mycobacterium tuberculosis survival and infectivity. *Molecules* **2019**, *24*, 851.

41. Chen, G.; Zhou, D.; Li, X.; Jiang, Z.; Tan, C.; Wei, X.; Ling, J.; Jing, J.; Liu, F.; Li, N. A natural chalcone induces apoptosis in lung cancer cells: 3D-QSAR, docking and an in vivo/vitro assay. *Sci. Rep.* **2017**, *7*, 10729.

42. Sudhakaran, M.; Sardesai, S.; Doseff, A.I. Flavonoids: New frontier for immuno-regulation and breast cancer control. *Antioxidants* **2019**, *8*, 103.

43. Rodriguez, J.; M. Gomez, L.; Gutierrez, A.C.; Mendez-Callejas, G.; Reyes, A.I.; Tellez, L.C.; Rodriguez, A.O.E.; Torrenegra, G.R.D. Source of flavonoids with antiproliferative and antioxidant activity. *Indian J. Sci. Technol.* **2018**, *11*, 1–7.

44. Smith, M.L.; Murphy, K.; Doucette, C.D.; Greenshields, A.L.; Hoskin, D.W. The dietary flavonoid fisetin causes cell cycle arrest, caspase-dependent apoptosis, and enhanced cytotoxicity of chemotherapeutic drugs in triple-negative breast cancer cells. *J. Cell. Biochem.* **2016**, *117*, 1913–1925.

45. Sudanich, S.; Tiyaworanant, S.; Yenjai, C. Cytotoxicity of flavonoids and isoflavonoids from crotalaria bracteata. *Nat. Prod. Res.* **2017**, *31*, 2641–2646.

46. Vukovic, N.L.; Obradovic, A.D.; Vukic, M.D.; Jovanovic, D.; Djurdjevic, P.M. Cytotoxic, proapoptotic and antioxidative potential of flavonoids isolated from propolis against colon (HCT-116) and breast (MDA-MB-231) cancer cell lines. *Food Res. Int.* **2018**, *106*, 71–80.

47. Jung, H.; Shin, S.Y.; Jung, Y.; Tran, T.A.; Lee, H.O.; Jung, K.-Y.; Koh, D.; Cho, S.K.; Lim, Y. Quantitative relationships between the cytotoxicity of flavonoids on the human breast cancer stem-like cells MCF7-SC and their structural properties. *Chem. Biol. Drug Des.* **2015**, *86*, 496–508.

48. Govindaiah, P.; Dumala, N.; Grover, P.; Jaya Prakash, M. Synthesis and biological evaluation of novel 4,7-dihydroxycoumarin derivatives as anticancer agents. *Bioorg. Med. Chem. Lett.* **2019**, *29*, 1819–1824.

49. Ketabforoosh, S.H.M.E.; Kheirollahi, A.; Safavi, M.; Esmati, N.; Ardestani, S.K.; Emami, S.; Firoozpour, L.; Shafiee, A.; Foroumadi, A. Synthesis and anti-cancer activity evaluation of new dimethoxylated chalcone and flavanone analogs. *Arch. Pharm. (Weinheim).* **2014**, *347*, 853–860.

50. Sak, K. Characteristic features of cytotoxic activity of flavonoids on human cervical cancer cells. *Asian Pacific J. Cancer Prev.* **2014**, *15*, 8007–8018.

51. Nugraha, A.T.; Ramadhan, V.; Pandapotan, H.; Romadhonsyah, F. A study of proliferative activity of herbs eriocaulon cinereum R.Br on cervical cancer cells (HeLa) with MTT assay method. *Int. J. Pharma Med. Biol. Sci.* **2017**, *6*, 73–76.

52. Alshatwi, A.A.; Ramesh, E.; Periasamy, V.S.; Subash-Babu, P. The apoptotic effect of hesperetin on human cervical cancer cells is mediated through cell cycle arrest, death receptor, and mitochondrial pathways. *Fundam. Clin. Pharmacol.* **2013**, *27*, 581–592.

53. Woo, Y.; Shin, S.Y.; Jiye Hyuni, S.D.L.; Lee, Y.H.; Lim, Y. Flavanones inhibit the clonogenicity of HCT116 cololectal cancer cells. *Int. J. Mol. Med.* **2011**, *29*, 403–408.

54. Deng, X.; Zhao, X.; Lan, Z.; Jiang, J.; Yin, W.; Chen, L. Anti-tumor effects of flavonoids from the ethnic medicine docynia delavayi (Franch.) schneid. and its possible mechanism. *J. Med. Food* **2014**, *17*, 787–794.

55. Méndez-Callejas, G.; Rodríguez-Mayusa, J.; Celis-Zambrano, C.; Rodríguez, O.; Torrenegra-Guerrero, R. Anticancer potential of (R) -5 , 7-dihydroxyflavanone from leaves of anticancer potential of (R) -5 , 7-dihydroxyflavanone from leaves of C hromolaena leivensis (Hieron) on cancer cells. *Int. J. Curr. Pharm. Rev. Res.* **2018**, *9*, 48–54.

56. Liu, X.; Ye, F.; Wu, J.; How, B.; Li, W.; Zhang, D.Y. Signaling proteins and pathways affected by flavonoids in leukemia cells. *Nutr. Cancer* **2015**, *67*, 238–249.

57. Tao, L.; Fu, R.; Wang, X.; Yao, J.; Zhou, Y.; Dai, Q.; Li, Z.; Lu, N.; Wang, W. LL-202, a newly synthesized flavonoid, inhibits tumor growth via inducing G2/M phase arrest and cell apoptosis in MCF-7 human breast cancer cells in vitro and in vivo. *Toxicol. Lett.* **2014**, *228*, 1–12.

58. Liu, H.; Jiang, W.; Xie, M. Flavonoids: Recent advances as anticancer drugs. *Recent Pat. Anticancer. Drug Discov.* **2010**, *5*, 152–164.

59. Sai, K.; Thapa, R.; Devkota, H.P. Phytochemical screening , free radical scavenging and α -amylase inhibitory activities of selected medicinal plants from western Nepal. *Medicines* **2019**, *6*, 1–9.

60. García, E.R.; Gutierrez, E.A.; Melo, F.C.S.A. de; Novaes, R.D.; Gonçalves, R.V. Flavonoids effects on hepatocellular carcinoma in murine models: A systematic review. *Evidence-Based Complement. Altern. Med.* **2018**, *1*, 1–23.

61. Nile, S.H.; Keum, Y.S.; Nile, A.S.; Jalde, S.S.; Patel, R. V Antioxidant, anti-inflammatory, and enzyme inhibitory activity of natural plant flavonoids and their synthesized derivatives. *J. Biochem. Mol. Toxicol.* **2018**, *32*, 1–8.

62. Das, S.; Mitra, I.; Batuta, S.; Niharul Alam, M.; Roy, K.; Begum, N.A. Design, synthesis and exploring the quantitative structure–activity relationship of some antioxidant flavonoid analogues. *Bioorg. Med. Chem. Lett.* **2014**, *24*, 5050–5054.

63. Salehi, B.; Fokou, P.; Sharifi-Rad, M.; Zucca, P.; Pezzani, R.; Martins, N.; Sharifi-Rad, J. The therapeutic potential of naringenin: A review of clinical trials. *Pharmaceuticals* **2019**, *12*, 11–29.

64. Testai, L.; Pozzo, E. Da; Piano, I.; Pistelli, L.; Gargini, C.; Breschi, M.C.; Braca, A.; Martini, C.; Martelli, A.; Calderone, V. The citrus flavanone naringenin produces cardioprotective effects in hearts from 1 year old rat , through activation of mitoBK channels. *Front. Pharmacol.* **2017**, *8*, 1–11.

65. Rebello, C.J.; Greenway, F.L.; Beyl, R.A.; Lertora, J.J.L.; Ravussin, E.; Ribnicky, D.M.; Poulev, A.; Kennedy, B.J.; Castro, H.F.; Campagna, S.R.; et al. Safety and pharmacokinetics of naringenin : A randomized , controlled , single-ascending-dose clinical trial. *Wiley* **2020**, 91–98.

66. Liu, S.-Y.; Zeng, J.; Peng, K.-J.; Zhang, L.-C.; Liu, L.-J.; Luo, Z.-Y.; Ma, D.-Y. Synthesis and antiproliferative properties of novel naringenin derivatives. *Med. Chem. Res.* **2017**, *26*, 2692–2698.

67. Taabodi, M.; May, E.B.; Mack, K.M.; Squibb, K.S.; Ishaque, A.B. Oxidative stress pathways of flavonoid toxicity in human breast tumor cells. *Int. J. Clin. Exp. Pathol.* **2017**, *10*, 2554–2567.

68. Palomares-alonso, F.; Rojas-tomé, I.S.; Palencia, G.; Jiménez-arellanes, M.A.; Macías-

rubalcava, M.L.; González-maciel, A.; Ramos-morales, A.; Santiago-reyes, R.; Castro, N.; González-hernández, I. In vitro and in vivo cysticidal activity of extracts and isolated flavanone from the bark of Prunus serotina : A bio-guided study. *Acta Trop.* **2017**, *170*, 1–7.

69. Chen, R.; Qi, Q.; Wang, M.; Li, Q. Therapeutic potential of naringin : an overview. *Pharm. Biol.* **2016**, *54*, 3203–3210.

70. Chien, A.; Liao, H.W.A.; Kuo, C.C.; Huang, Y.E.I.C. Naringenin inhibits migration of bladder cancer cells through downregulation of AKT and MMP - 2. *Mol. Med. Rep.* **2014**, *10*, 1531–1536.

71. Yoon, H.; Kim, T.W.; Shin, S.Y.; Park, M.J.; Yong, Y.; Kim, D.W.; Islam, T.; Lee, Y.H.; Jung, K.; Lim, Y. Design, synthesis and inhibitory activities of naringenin derivatives on human colon cancer cells. *Bioorg. Med. Chem. Lett.* **2013**, *23*, 232–238.

72. Kanno, S.; Tomizawa, A.; Ohtake, T.; Koiwai, K.; Ujibe, M.; Ishikawa, M. Naringenin-induced apoptosis via activation of NF- k B and necrosis involving the loss of ATP in human promyeloleukemia HL-60 cells. *Toxicol. Lett.* **2006**, *166*, 131–139.

73. Lee, J.; Kim, D.; Hoon, J. Combined administration of naringenin and hesperetin with optimal ratio maximizes the anti-cancer effect in human pancreatic cancer via down regulation of FAK and p38 signaling pathway. *Phytomedicine* **2019**, *58*, 152762.

74. Sabarinathan, D.; Mahalakshmi, P.; Vanisree, A.J. Chemico-biological interactions naringenin , a flavanone inhibits the proliferation of cerebrally implanted C6 glioma cells in rats. *Chem. Biol. Interact.* **2011**, *189*, 26–36.

75. Wang, K.; Chen, Z.; Huang, J.; Huang, L.; Luo, N.; Liang, X.; Liang, M.; Xie, W. Naringenin prevents ischaemic stroke damage via oxidant effects. *Clin Exp Pharmacol Physiol* **2017**, *44*, 862–871.

76. Arul, D.; Subramanian, P. Naringenin (citrus flavonone) induces growth inhibition , cell cycle arrest and apoptosis in human hepatocellular carcinoma cells. *Pathol. Oncol. Res.* **2013**, *19*, 763–770.

77. Wang, R.U.I.; Wang, J.; Dong, T.; Shen, J.U.N.; Gao, X.; Zhou, J.U.N. Naringenin has a chemoprotective effect in MDA - MB - 231 breast cancer cells via inhibition of caspase - 3 and - 9 activities. *Oncol. Lett.* **2019**, *17*, 1217–1222.

78. Zhao, Z.; Jin, G.; Ge, Y.; Guo, Z. Naringenin inhibits migration of breast cancer cells via inflammatory and apoptosis cell signaling pathways. *Inflammopharmacology* **2019**, *5*, 56–63.

79. Park, J.-H.; Lee, J.; Paik, H.; Cho, S.G.; Nah, S.; Park, Y.; Han, Y.S. Cytotoxic effects of 7-O-butyl naringenin on human breast cancer MCF-7 cells. *Food Sci. Biotechnol.* **2010**, *19*, 717–724.

80. Kim, J.-H.; Kim, H.; Bak, Y.; Kang, J.-W.; Lee, D.H.; Kim, M.S.; Park, Y.S.; Kim, E.-J.; Jung, K.-Y.; Lim, Y.; et al. Naringenin derivative diethyl (5,4′-dihydroxy flavanone-7-yl) phosphate inhibits cell growth and induces apoptosis in A549 human lung cancer cells. *J. Korean Soc. Appl. Biol. Chem.* **2012**, *55*, 75–82.

81. Shi, L.; Feng, X.E.; Cui, J.R.; Fang, L.H.; Du, G.H.; Li, Q.S. Synthesis and biological activity of flavanone derivatives. *Bioorg. Med. Chem. Lett.* **2010**, *20*, 5466–5468.

82. Lee, S.; Lee, C.; Moon, S.; Kim, E.; Kim, C.; Kim, B.; Bok, S.; Jeong, T. Naringenin derivatives as anti-atherogenic agents. *bioorganic Med. Chem. Lett.* **2003**, *13*, 3901–3903.

83. Daniëlle Copmansa; Adriana M. Orellana-Paucara, B.; Steurs, G.; Zhang, Y.; Ny, A.; Foubert, K.; Exarchou, V.; Siekierska, A.; Kim, Y.; Borggraeve, W. De; et al. Methylated flavonoids as anti-seizure agents: naringenin 4′,7- dimethyl ether attenuates epileptic seizures in zebrafish and mouse models. *Neurochem. Int.* **2017**, *112*, 124–133.

84. Brodowska, K.; Sykuła, A.; Garribba, E.; Łodyga-Chrus´cin´ska, E.; So´jka, M. Naringenin schiff base : antioxidant activity , acid – base profile , and interactions with DNA. *Transit. met chem* **2016**, *41*, 179–189.

85. Hoang, T.K.; Huynh, T.K.; Nguyen, T. Synthesis, characterization, anti-inflammatory

and anti-proliferative activity against MCF-7 cells of O-alkyl and O-acyl flavonoid derivatives. *Bioorg. Chem.* **2015**, *63*, 45–52.

86. Zaim, O.; Doganlar, O.; Zreigh, M.; Doganlar, Z.; And; Ozcan, H. Synthesis, cancer-selective antiproliferative and apoptotic effects of some (+_)-naringenin cycloaminoethyl derivatives. *Chem. Biodivers.* **2018**, *15*, 1–15.

87. Naik, N.; Harini, S.T. Synthesis of novel hespertin oxime esters: A new discernment in to their antioxidant potential. *Int. J. Pharm. Sci. Res.* **2014**, *5*, 1482–1489.

88. Acharya, P.C.; Bansal, R. Synthesis and antiproliferative activity of some androstene oximes and their O -alkylated derivatives. *Arch. Pharm. (Weinheim).* **2014**, *347*, 193–199.

89. Özyürek, M.; Akpınar, D.; Bener, M.; Türkkan, B.; Güçlü, K.; Apak, R. Novel oxime based flavanone, naringin-oxime: Synthesis, characterization and screening for antioxidant activity. *Chem. Biol. Interact.* **2014**, *212*, 40–46.

90. Türkkan, B.; Özyürek, M.; Bener, M.; Güçlü, K.; Apak, R. Synthesis, characterization and antioxidant capacity of naringenin-oxime. *Spectrochim. Acta Part A Mol. Biomol. Spectrosc.* **2012**, *85*, 235–240.

91. Potaniec, B.; Grabarczyk, M.; Stompor, M.; Szumny, A.; Zieliński, P.; Żołnierczyk, A.K.; Anioł, M. Antioxidant activity and spectroscopic data of isoxanthohomol oxime and related compounds. *Spectrochim. Acta Part A Mol. Biomol. Spectrosc.* **2014**, *118*, 716–723.

92. Kocyigit, A.; Koyuncu, I.; Taskin, A.; Dikilitas, M.; Bahadori, F.; Turkkan, B. Antigenotoxic and antioxidant potentials of newly derivatized compound naringenin-oxime relative to naringenin on human mononuclear cells. *Drug Chem. Toxicol.* **2016**, *39*, 66–73.

93. Koyuncu, I.; Kocyigit, A.; Gonel, A.; Arslan, E.; Durgun, M. The protective effect of naringenin-oxime on cisplatin-induced toxicity in rats. **2017**, *2017*, 19–21.

94. Kozłowska, J.; Grela, E.; Baczyńska, D.; Grabowiecka, A.; Anioł, M. Novel O-alkyl derivatives of naringenin and their oximes with antimicrobial and anticancer activity. *Molecules* **2019**, *24*, 679.

95. Chiang, C.; Wang, T.-C.; Lee, C.; Chen, C.; Wang, S.; Lin, Y.; Juang, S.-H. WTC-01, a novel synthetic oxime-flavone compound, destabilizes microtubules in human nasopharyngeal carcinoma cells in vitro and in vivo. *Br. J. Pharmacol.* **2015**, *172*, 4671–4683.

96. Díaz, J.; Martinez, D.; López, L.; Mendez, G.; Vera, R.; Loaiza, A. Synthesis and in vitro antiproliferative activity of flavone and 6-hydroxyflavone oxime ethers derivatives. *J. Braz. Chem. Soc.* **2017**, *29*, 177–184.

97. Yenjai, C.; Wanich, S. Cytotoxicity against KB and NCI-H187 cell lines of modified flavonoids from kaempferia parviflora. *Bioorg. Med. Chem. Lett.* **2010**, *20*, 2821–2823.

98. Liu, Z.; Wei, W.; Gan, C.; Huang, Y.; Liu, S.; Zhou, M.; Cui, J. Semisynthesis and cytotoxicity of E - naringenin oximes from naringin. *Chinese J. Org. Chem.* **2013**, *33,* 2551–2558.

99. Hunyadi, A.; Chuang, D.; Danko, B.; Chiang, M.Y.; Lee, C.; Wang, H.-C.; Wu, C.-C.; Chang, F.; Wu, Y. Direct semi-synthesis of the anticancer lead-drug protoapigenone from apigenin, and synthesis of further new cytotoxic protoflavone derivatives. *PLoS One* **2011**, *6*, 1–10.

100. Zupkó, I.; Molnár, J.; Réthy, B.; Minorics, R.; Frank, É.; Wölfling, J.; Molnár, J.; Ocsovszki, I.; Topcu, Z.; Bitó, T.; et al. Anticancer and multidrug resistance-reversal effects of solanidine analogs synthetized from pregnadienolone acetate. *Molecules* **2014**, *19*, 2061–2076.

101. Molnár, J.; Szebeni, G.; Csupor-Löffler, B.; Hajdú, Z.; Szekeres, T.; Saiko, P.; Ocsovszki, I.; Puskás, L.; Hohmann, J.; Zupkó, I. Investigation of the antiproliferative properties of natural sesquiterpenes from Artemisia asiatica and Onopordum acanthium on HL-60 Cells in vitro. *Int. J. Mol. Sci.* **2016**, *17*, 83.

102. Stefkó, D.; Kúsz, N.; Csorba, A.; Jakab, G.; Bérdi, P.; Zupkó, I.; Hohmann, J.; Vasas, A. Phenanthrenes from Juncus atratus with antiproliferative activity. *Tetrahedron* **2019**, *75*, 116–120.

103. Szabó, J.; Jerkovics, N.; Schneider, G.; Wölfling, J.; Bózsity, N.; Minorics, R.; Zupkó, I.; Mernyák, E. Synthesis and in vitro antiproliferative evaluation of C-13 epimers of triazolyl-d-secoestrone alcohols: The first potent 13α-d-secoestrone derivative. *Molecules* **2016**, *21*, 611.

104. Sinka, I.; Kiss, A.; Mernyák, E.; Wölfling, J.; Schneider, G.; Ocsovszki, I.; Kuo, C.-Y.; Wang, H.-C.; Zupkó, I. Antiproliferative and antimetastatic properties of 3-benzyloxy-16-hydroxymethylene-estradiol analogs against breast cancer cell lines. *Eur. J. Pharm. Sci.* **2018**, *123*, 362–370.

105. Bózsity, N.; Minorics, R.; Szabó, J.; Mernyák, E.; Schneider, G.; Wölfling, J.; Wang, H.-C.; Wu, C.-C.; Ocsovszki, I.; Zupkó, I. Mechanism of antiproliferative action of a new d -secoestrone-triazole derivative in cervical cancer cells and its effect on cancer cell motility. *J. Steroid Biochem. Mol. Biol.* **2017**, *165*, 247–257.

106. Fukumoto, L.; Mazza, G. Assessing antioxidant and prooxidant activities of phenolic compounds. *J. Agr. Food. Chem* **2000**, *48*, 3597–3604.

107. Mielnik, M.B.; Rzeszutek, A.; Triumf, E.C.; Egelandsdal, B. Antioxidant and other quality properties of reindeer muscle from two different Norwegian regions. *Meat Sci.* **2011**, *89*, 526–532.

108. Chou, T.-C. Theoretical basis, experimental design, and computerized simulation of synergism and antagonism in drug combination studies. *Pharmacol. Rev.* **2006**, *58*, 621–681.

109. Jung, J.; Lim, S.; Choi, H.; Cho, H.; Shin, H.; Kim, E.; Chung, W.; Park, K.; Park, J. Isoliquiritigenin induces apoptosis by depolarizing mitochondrial membranes in prostate cancer cells☆. *J. Nutr. Biochem.* **2006**, *17*, 689–696.

110. Wang, H.-C.; Lee, A.Y.-L.; Chou, W.-C.; Wu, C.-C.; Tseng, C.-N.; Liu, K.Y.-T.; Lin, W.-L.; Chang, F.-R.; Chuang, D.-W.; Hunyadi, A.; et al. Inhibition of ATR-dependent signaling by protoapigenone and its derivative sensitizes cancer cells to interstrand cross-link-generating agents in vitro and in vivo. *Mol. Cancer Ther.* **2012**, *11*, 1443–1453.

111. Kocyigit, A.; Koyuncu, I.; Dikilitas, M.; Bahadori, F.; Turkkan, B. Cytotoxic, genotoxic and apoptotic effects of naringenin-oxime relative to naringenin on normal and cancer cell lines. *Asian Pac. J. Trop. Biomed.* **2016**, *6*, 872–880.

112. Hatkevich, T.; Ramos, J.; Santos-sanchez, I.; Patel, Y.M. A naringenin – tamoxifen combination impairs cell proliferation and survival of MCF-7 breast cancer cells. *Exp. Cell Res.* **2014**, *327*, 331–339.

113. Abaza, M.S.I.; Orabi, K.Y.; Al-quattan, E.; Al-attiyah, R.J. Growth inhibitory and chemo-sensitization effects of naringenin , a natural flavanone purified from Thymus vulgaris , on human breast and colorectal cancer. *Cancer Cell Int.* **2015**, 1–19.

114. Park, J.H.; Jin, C.-Y.; Lee, B.K.; Kim, G.-Y.; Choi, Y.H.; Jeong, Y.K. Naringenin induces apoptosis through downregulation of Akt and caspase-3 activation in human leukemia THP-1 cells. *Food Chem. Toxicol.* **2008**, *46*, 3684–3690.

115. Bús, C.; Kúsz, N.; Jakab, G.; Senobar Tahaei, S.; Zupkó, I.; Endrész, V.; Bogdanov, A.; Burián, K.; Csupor-Löffler, B.; Hohmann, J.; et al. Phenanthrenes from Juncus compressus jacq. with promising antiproliferative and anti-HSV-2 activities. *Molecules* **2018**, *23*, 2085.

116. Yenjai, C.; Wanich, S.; Pitchuanchom, S.; Sripanidkulchai, B. Structural modification of 5 , 7-dimethoxyflavone from kaempferia parviflora and biological activities. *Arch Pharm Res* **2009**, *32*, 1179–1184.

117. Sonoda, M.; Nishiyama, T.; Matsukawa, Y.; Moriyasu, M. Cytotoxic activities of flavonoids from two Scutellaria plants in Chinese medicine. *J. Ethnopharmacol.* **2004**, *91*, 65–68.

118. Qiu, L.; Liu, M.; Pan, K. A triple staining method for accurate cell cycle analysis using multiparameter flow cytometry. *Molecules* **2013**, *18*, 15412–15421.

119. Tu, B.; Liu, Z.; Chen, Z.; Ouyang, Y.; Hu, Y. Understanding the structure–activity relationship between quercetin and naringenin: in vitro. *RSC Adv.* **2015**, *5*, 106171–106181.

120. Elvas, F.; Vanden Berghe, T.; Adriaenssens, Y.; Vandenabeele, P.; Augustyns, K.; Staelens, S.; Stroobants, S.; Van der Veken, P.; Wyffels, L. Caspase-3 probes for PET imaging of apoptotic tumor response to anticancer therapy. *Org. Biomol. Chem.* **2019**, *17*, 4801–4824.

121. Guan, G.; Lei, L.; Lv, Q.; Gong, Y.; Yang, L. Curcumin attenuates palmitic acid-induced cell apoptosis by inhibiting endoplasmic reticulum stress in H9C2 cardiomyocytes. *Hum. Exp. Toxicol.* **2019**, *38*, 655–664.

122. Khalilzadeh, B.; Shadjou, N.; Kanberoglu, G.S.; Afsharan, H.; de la Guardia, M.; Charoudeh, H.N.; Ostadrahimi, A.; Rashidi, M.-R. Advances in nanomaterial based optical biosensing and bioimaging of apoptosis via caspase-3 activity: a review. *Microchim. Acta* **2018**, *185*, 434.

123. Hunyadi, A. The mechanism(s) of action of antioxidants: from scavenging reactive oxygen/nitrogen species to redox signaling and the generation of bioactive secondary metabolites. *Med. Res. Rev.* **2019**, *39*, 2505–2533.

124. Vo, Q. V.; Nam, P.C.; Thong, N.M.; Trung, N.T.; Phan, C.-T.D.; Mechler, A. Antioxidant motifs in flavonoids: O–H versus C–H bond dissociation. *ACS Omega* **2019**, *4*, 8935–8942.

125. Danko, B.; Martins, A.; Chuang, D.W.; Wang, H.C.; Amaral, L. In vitro Cytotoxic activity of novel protoflavone analogs – selectivity towards a multidrug resistant cancer cell line. *Anticancer Res.* **2012**, *32*, 2863–2869.

126. Capistrano, I.R.; Wouters, A.; Foubert, K.; Baldé, A.M.; Apers, S.; Lardon, F.; Pieters, L.; Exarchou, V. Phytochemical characterisation of a cytotoxic stem bark extract of Steganotaenia araliacea and identification of a protoflavanone by LC-SPE-NMR. *Phytochem. Lett.* **2015**, *12*, 119–124.

127. Chen, W.; Hsieh, Y.; Tsai, C.; Kang, Y.-F.; Chang, F.-R.; Wu, Y.-C.; Wu, C.-C. Protoapigenone, a natural derivative of apigenin, induces mitogen-activated protein kinase-dependent apoptosis in human breast cancer cells associated with induction of oxidative stress and inhibition of glutathione S-transferase π. *Invest. New Drugs* **2011**, *29*, 1347–1359.

128. Lin, A.-S.; Nakagawa-Goto, K.; Chang, F.-R.; Morris-Natschke, S.; Wu, C.-C.; Chen, S.-L.; Wu, Y.-C.; Lee, K.-H. First total synthesis of protoapigenone and its analogs as potent cytotoxic agents. *Med Chem* **2007**, *50*, 3921–3927.

129. Lin, A.; Chang, F.-R.; Wu, C.-C.; Liaw, C.-C.; Wu, Y.-C. New cytotoxic flavonoids from thelypteris torresiana. *Planta Med.* **2005**, *71*, 867–870.

130. Chen, Y.; Kay, N.; Yang, J.; Lin, C.; Chang, H.-L.; Wu, Y.; Fu, C.; Chang, Y.; Lo, S.; Hou, M.-F.; et al. Total synthetic protoapigenone WYC02 inhibits cervical cancer cell proliferation and tumour growth through PIK3 signalling pathway. *Basic Clin. Pharmacol. Toxicol.* **2013**, *113*, 8–18.

131. Nguyen, L.T.; Lee, Y.-H.; Sharma, A.R.; Park, J.; Jagga, S.; Sharma, G.; Lee, S.; Nam, J. Quercetin induces apoptosis and cell cycle arrest in triple-negative breast cancer cells through modulation of Foxo3a activity. *Korean J. Physiol. Pharmacol.* **2017**, *21*, 205.

132. Yuan, Q.; Cai, S.; Zhang, X.; Liu, Z.; Li, Z.; Luo, X.; Xiong, C.; Wang, J.; Hu, J.; Ruan, J. A new protoapigenone analog RY10-4 induces apoptosis and suppresses invasion through the PI3K/Akt pathway in human breast cancer. *Cancer Lett.* **2012**, *324*, 210–220.

133. Fayed, E.A.; Sabour, R.; Harras, M.F.; Mehany, A.B.M. Design, synthesis, biological evaluation and molecular modeling of new coumarin derivatives as potent anticancer agents. *Med. Chem. Res.* **2019**, *28*, 1284–1297.

134. Chiu, C.-C.; Chang, H.-W.; Chuang, D.-W.; Chang, F.-R.; Chang, Y.-C.; Cheng, Y.; Tsai, M.-T.; Chen, W.-Y.; Lee, S.-S.; Wang, C.-K.; et al. Fern plant – derived protoapigenone leads to DNA damade, apoptosis, and G2/M arrest in lung cancer cell line H1299. *DNA Cell Biol.* **2009**, *28*, 501–506.

135. Chang, H.L.; Su, J.H.; Yeh, Y.T.; Lee, Y.C.; Chen, H.M.; Wu, Y.C.; Yuan, S.S.F. Protoapigenone, a novel flavonoid, inhibits ovarian cancer cell growth in vitro and in vivo. *Cancer Lett.* **2008**, *267*, 85–95.

136. Stanković, T.; Dankó, B.; Martins, A.; Dragoj, M.; Stojković, S.; Isaković, A.; Wang, H.C.; Wu, Y.C.; Hunyadi, A.; Pešić, M. Lower antioxidative capacity of multidrug-resistant cancer cells confers collateral sensitivity to protoflavone derivatives. *Cancer Chemother. Pharmacol.* **2015**, *76*, 555–565.

137. Moreira, J.; Ribeiro, D.; Silva, M.A.; Nazareth, N.; Monteiro, M.; Palmeira, A.; Pinto, M.; Bousbaa, H.; Cidade, H. New alkoxy flavone derivatives targeting caspases : Synthesis and antitumor activity evaluation. *molecules* **2019**, *24*.

138. Wang, Y.; Yuan, S.; Li, L.; Yang, D.; Xu, C.; Wang, S.; Zhang, D. Novel proapoptotic agent SM-1 enhances the inhibitory effect of 5-fluorouracil on colorectal cancer cells in vitro and in vivo. *Oncol. Lett.* **2017**, *13*, 4762–4768.

139. Dillon, M.T.; Harrington, K.J. *Targeting the DNA damage response for anti-cancer therapy*; Pollard, J., Curtin, N., Eds.; Cancer Drug Discovery and Development; Springer International Publishing: Cham, 2018; ISBN 978-3-319-75834-3.

140. Lecona, E.; Fernandez-Capetillo, O. Targeting ATR in cancer. *Nat. Rev. Cancer* **2018**, *18*, 586–595.

141. Sundar, R.; Brown, J.; Ingles Russo, A.; Yap, T.A. Targeting ATR in cancer medicine. *Curr. Probl. Cancer* **2017**, *41*, 302–315.

142. Yan, S.; Sorrell, M.; Berman, Z. Functional interplay between ATM/ATR-mediated DNA damage response and DNA repair pathways in oxidative stress. *Cell Mol Iife Sci* **2015**, *71*, 3951–3967.

143. Hijova, E. Bioavailability of chalcones bioavailability of chalcones. *Bratisl. Lek. Listy* **2014**, *107*, 80–84.

144. Sharma, R.; Kumar, R.; Kodwani, R.; Kapoor, S.; Khare, A.; Bansal, R.; Khurana, S.; Singh, S.; Thomas, J.; Roy, B.; et al. A review on mechanisms of anti tumor activity of chalcones. *Anticancer. Agents Med. Chem.* **2015**, *16*, 200–211.

145. Karthikeyan, C.; Narayana, N.S.H.; Ramasamy, S. Advances in chalcones with anticancer activities. *Recent Patents Anti-Cancer Discov.* **2015**, *10*, 97–115.

146. Mahapatra, D.K.; Bharti, S.K.; Asati, V. Anti-cancer chalcones: Structural and molecular target perspectives. *Eur. J. Med. Chem.* **2015**, *98*, 69–114.

147. Bian, X.; Lin, W. Targeting DNA replication stress and DNA double-strand break repair for optimizing SCLC treatment. *Cancers (Basel).* **2019**, *11*, 1289.

148. Chen, H.-M.; Chang, F.-R.; Hsieh, Y.-C.; Cheng, Y.-J.; Hsieh, K.-C.; Tsai, L.-M.; Lin, A.-S.; Wu, Y.-C.; Yuan, S.-S. A novel synthetic protoapigenone analogue, WYC02-9, induces DNA damage and apoptosis in DU145 prostate cancer cells through generation of reactive oxygen species. *Free Radic. Biol. Med.* **2011**, *50*, 1151–1162.

149. Kuo, C.; Zupkó, I.; Chang, F.; Hunyadi, A.; Wu, C. Dietary flavonoid derivatives enhance chemotherapeutic effect by inhibiting the DNA damage response pathway. *Toxicol. Appl. Pharmacol.* **2016**, *311*, 99–105.

150. Podolski-Renić, A.; Bősze, S.; Dinić, J.; Kocsis, L.; Hudecz, F.; Csámpai, A.; Pešić, M. Ferrocene–cinchona hybrids with triazolyl-chalcone linkers act as pro-oxidants and sensitize human cancer cell lines to paclitaxel. *Metallomics* **2017**, *9*, 1132–1141.

8   ACKNOWLEDGEMENTS

ANNEX

I.

Protoflavone-Chalcone Hybrids Exhibit Enhanced Antitumor Action through Modulating Redox Balance, Depolarizing the Mitochondrial Membrane, and Inhibiting ATR-Dependent Signaling

Ahmed Dhahir Latif [1,2,†,‡], Tamás Jernei [3,‡], Ana Podolski-Renić [4], Ching-Ying Kuo [5], Máté Vágvölgyi [2], Gábor Girst [2], István Zupkó [1,6], Sedef Develi [7], Engin Ulukaya [7], Hui-Chun Wang [5], Milica Pešić [4], Antal Csámpai [3,*] and Attila Hunyadi [2,6,*]

[1] Institute of Pharmacodynamics and Biopharmacy, Interdisciplinary Excellence Centre, University of Szeged, Eötvös str. 6, H-6720 Szeged, Hungary; latif.ahmed@pharmacognosy.hu (A.D.L.); zupko@pharm.u-szeged.hu (I.Z.)

[2] Institute of Pharmacognosy, Interdisciplinary Excellence Centre, University of Szeged, Eötvös str. 6, H-6720 Szeged, Hungary; vagvolgyi.mate@pharmacognosy.hu (M.V.); girst.gabor@pharmacognosy.hu (G.G.)

[3] Institute of Chemistry, Eötvös Loránd University, P.O. Box 32, H-1518 Budapest-112, Hungary; jernei@caesar.elte.hu

[4] Department of Neurobiology, Institute for Biological Research "Siniša Stanković"- National Institute of Republic of Serbia, University of Belgrade, Bulevar Despota Stefana 142, 11060 Belgrade, Serbia; ana.podolski@ibiss.bg.ac.rs (A.P.-R.); camala@ibiss.bg.ac.rs (M.P.)

[5] Graduate Institute of Natural Products, Kaohsiung Medical University, Shih-Chuan 1st Rd. 100, Kaohsiung 807, Taiwan; r980279@kmu.edu.tw (C.-Y.K.); wanghc@kmu.edu.tw (H.-C.W.)

[6] Interdisciplinary Centre for Natural Products, University of Szeged, Eötvös str. 6, H-6720 Szeged, Hungary

[7] Molecular Cancer Research Center, Istinye University, 34010 Topkapi, Istanbul, Turkey; elif.develi@stu.istinye.edu.tr (S.D.); eulukaya@istinye.edu.tr (E.U.)

* Correspondence: csampai@caesar.elte.hu (A.C.); hunyadi.a@pharm.u-szeged.hu (A.H.); Tel.: +36-62-546-456 (A.H.)

† On leave from Department of Pharmacology and Toxicology, Faculty of Medicine, Wasit University, 52001 Wasit, Iraq.

‡ Equal contribution from the first two authors.

Abstract: Hybrid compounds combine fragments with complementary targets to achieve a common pharmacological goal. This approach represents an increasingly popular strategy for drug discovery. In this work, we aimed to design antitumor hybrid compounds based on an inhibitor of ataxia-telangiectasia and Rad3-related protein (ATR)-dependent signaling, protoapigenone, and a pro-oxidant ferrocene or chalcone fragment. Four new triazole-coupled hybrids were prepared. The compounds were cytotoxic against human breast cancer cell lines in vitro, showing IC$_{50}$ values in the sub-micromolar range. The nature of interactions between relevant fragments of the hybrids was evaluated by the Chou–Talalay method. Experimental combination treatment with the fragments showed additive effects or slight/moderate synergism, while strong synergism was observed when the fragments were virtually combined into their hybrids, suggesting a relevant pharmacological benefit of the coupling. All hybrids were strong inhibitors of the ATR-mediated activation of Chk1, and they interfered with the redox balance of the cells leading to mitochondrial membrane depolarization. Additionally, they induced late apoptosis and primary necrosis in MDA-MB-231 and MCF-7 breast cancer cells, respectively. Our results demonstrate that coupling the ATR-dependent signaling inhibitor protoflavone with a pro-oxidant chalcone dramatically increases the

antitumor activity compared with either fragment alone. Such compounds may offer an attractive novel strategy for the treatment of various cancers.

Keywords: antitumor natural product; protoflavone; chalcone; ferrocene; hybrid compound; fragment-based drug design; DNA damage response; oxidative stress; virtual combination study

1. Introduction

Affecting 2.1 million people each year, breast cancer is the most common type of cancer among women, and it is one of the leading causes of cancer-related deaths. It is estimated that more than 600,000 women died of breast cancer in 2018, accounting for about 15% of all cancer deaths among women [1]. If diagnosed early, it is highly curable. However, the five-year survival rate of patients with metastatic breast cancer is poor. More devastatingly, almost a fifth of patients will develop local or distant recurrence within five years of diagnosis [2]. Therefore, new treatment options are essential, of which novel anticancer compounds are still desperately needed. This is particularly true for triple-negative breast cancer (TNBC), the most challenging breast cancer subtype to treat. Since it is resistant to first-line antiestrogen therapy, its current treatment options are limited and require the use of chemotherapeutic agents [3,4].

For fragment-based drug discovery, the design and preparation of hybrid compounds is an attractive strategy that has been increasingly popular in the search for new multitarget drugs, particularly against multifactorial chronic diseases [5–7]. In this context, molecular hybridization is also regarded as a highly efficient strategy to produce multitarget drug candidates with significantly enhanced anticancer activity, often due to a synergism associated with the cooperative effects of the individual molecular fragments.

Typically found in fern species (e.g., *Thelypteris* and *Pseudophegopteris*), protoflavones are rare natural flavonoids with an unusual non-aromatic B-ring [8]. Several of these compounds have been found to exert promising antitumor effects on a wide variety of cell lines in vitro [9–13] and various xenograft models in vivo [12,14–16]. Protoflavonoids were reported to induce apoptosis and cause S and G2/M phase cell cycle arrest [17,18], and this is closely associated with their ability to induce oxidative stress [19]. It is of particular interest that protoapigenone, the protoflavone analog of apigenin, is a potent inhibitor of the ataxia-telangiectasia and Rad3-related protein (ATR)-mediated activation of checkpoint kinase 1 (Chk-1), a crucial component of the replication-associated DNA damage response (DDR) [16]. Along with ataxia-telangiectasia mutated (ATM) kinase, this pathway is an attractive novel antitumor target that is currently being investigated in several related clinical trials [20–22]. Playing an essential role in the regulation of DNA repair pathways, ATR and ATM are activated upon DNA damage induced by oxidative stress [23]. Therefore, simultaneously targeting DDR and inducing oxidative stress may be a relevant antitumor strategy.

While protoflavones themselves already join these two pharmacological properties, we aimed to further exploit this by preparing hybrid compounds of a protoflavone (i.e., ATR inhibitor and oxidative stress inducer) and chalcones representing another type of fragment that may induce oxidative stress and are capable of uncoupling mitochondrial respiration to inhibit mitochondrial membrane potential [24]. Through a variety of molecular mechanisms, as discussed in recent reviews, chalcones have significant potential to cause cytotoxic effects against cancer cell lines [25–27]. In this context, we previously prepared antiproliferative hybrids comprising ferrocenyl-substituted chalcone and cinchona residues connected with triazole linkers, which were found to display marked cytotoxic activity against human liver cancer (HepG2) and human colon cancer (HT-29) cell lines [28]. Significantly, two representatives of these hybrids were found to act as pro-oxidants sensitizing three multidrug-resistant (MDR) human cancer cell lines and their sensitive counterparts (non-small cell lung carcinoma NCI-H460/R/NCI-H460, colorectal carcinoma DLD1-TxR/DLD1, and glioblastoma U87-TxR/U87) to paclitaxel [29]. We also established that these ferrocene-containing hybrids are not substrates for *P*-glycoprotein, a drug transporter responsible for the MDR phenotype, and that they

increase the production of reactive oxygen species (ROS), leading to mitochondrial damage in MDR cancer cells.

As a continuation of our search for potent anticancer hybrids with enhanced activity, we performed the synthesis, in vitro evaluation, and mechanistic study of novel hybrids containing a protoflavone and a chalcone residue. Both moieties may serve as promising building blocks of antitumor agents influencing redox homeostasis [30–32]. Therefore, in this study, we aimed to investigate if the addition of a potentially pro-oxidant fragment, such as a chalcone, can further enhance the antitumor activity of a protoflavone while maintaining or possibly further improving its inhibitory effect on ATR-mediated signaling.

2. Materials and Methods

2.1. General

All fine chemicals for synthesis were obtained from commercially available sources (Merck, Fluorochem, Molar Chemicals, VWR) and were used without further purification. Merck Kieselgel (230–400 mesh, 60 Å) was used for flash column chromatography. The ^{1}H- and ^{13}C-NMR spectra of all of the compounds were recorded in $CDCl_3$ or dimethyl sulfoxide (DMSO)-d_6 solution in 5 mm tubes at room temperature on a Bruker DRX-500 spectrometer at 500 (^{1}H) and 125 (^{13}C) MHz with the deuterium signal of the solvent as the lock and TMS as the internal standard. The HSQC and HMBC spectra, which support the exact assignment of ^{1}H- and ^{13}C NMR signals, were obtained using the standard Bruker pulse programs. HRMS spectra were recorded on a Q Exactive Plus hybrid quadrupole-orbitrap mass spectrometer (Thermo Scientific, Waltham, MA, USA) equipped with a heated electrospray ionization (HESI-II) probe that was used in the positive mode, and flow injection analysis was performed by an Abi 140C Syringe Pump.

For bioactivity assays, 96% ethanol was obtained from Molar Chemicals Ltd. (Halásztelek, Hungary). Dimethyl sulfoxide (DMSO) was purchased from Fisher Scientific Co. UK, Trypan Blue Solution was from Mediatech. Co. USA, Trypsin Replacement Enzyme was from Life Technologies UK, and cisplatin was obtained from Accord Healthcare France SAS. Penicillin-streptomycin-amphotericin B, non-essential amino acid (NEAA) mixture, phosphate-buffered saline (PBS), and minimal essential medium (MEM) were purchased from Lonza, Walkersville, USA. All plates, flasks, and cell culture vessels were purchased from Biologix Europe GmbH. Propidium iodide (PI), 3-(4, 5-dimethylthiazol-2-yl)-2, 5-diphenyltetrazolium bromide (MTT), Triton-X-100, ribonuclease A (RNase A), fetal bovine serum (FBS), the caspase 3 colorimetric assay kit and all other reagents, solvents, and chemicals were obtained from Sigma-Aldrich Co. (St. Louis, MO, USA).

2.2. Synthesis of Compound 1 from Apigenin

Protoapigenone 1'-*O*-propargyl ether (**1**) was synthesized as previously published [33]. Briefly, apigenin was dissolved to obtain a 1 mg/mL concentration in a 9:1 mixture of acetonitrile and propargyl alcohol. While stirring, two equivalents of [bis(trifluoroacetoxy)iodo]benzene were slowly added to the solution, and the reaction was left to develop for 1 h at 80 °C. After completion of the reaction, the mixture was cooled down, the solvent was evaporated under reduced pressure on a rotary evaporator, and the crude mixture was re-dissolved in methanol and adsorbed on silica. For purification, flash chromatography was performed on a CombiFlash Rf+ instrument (Teledyne Isco, Lincoln, NE, USA) with a 40 g HP Silica RediSep Rf Gold column (Teledyne Isco, Lincoln, NE, USA) with the eluent of the mixture of *n*-hexane:ethyl acetate:acetone (12:3:1, *v*/*v*/*v*). The reaction was repeated several times from a total of 1 g of apigenin, and the overall final isolated yield was 30%.

2.3. Synthesis of Hybrid Compounds 3a-d

The corresponding azide (**2a-d**; 0.31 mmol, 1.0 equation), 100 mg of 5,7-dihydroxy-2-(4-oxo-1-(prop-2-yn-1-yloxy)cyclohexa-2,5-dien-1-yl)-4*H*-chromen-4-one (**1**; 0.31 mmol, 1.0 equation), $CuSO_4$ (14 mg, 0.06 mmol, 0.2 equation), and sodium ascorbate (61 mg, 0.31 mmol, 1.0 equation) were

suspended in a 1:1 mixture of water and *n*-BuOH (1 mL). The reaction mixture was stirred at room temperature for 12 h, and then it was poured on brine (20 mL) and extracted with dichloromethane (DCM; 5 × 20 mL). The combined organic phases were dried over anhydrous Na_2SO_4, and the solvent was evaporated. The residue was purified by column chromatography on silica gel using a 20:1 mixture of DCM and methanol as eluent to obtain the pure product. After chromatography, the analytical sample was crystallized from DCM. Yields and characterization, along with detailed assignments and copies of ^1H- and ^{13}C NMR spectra, are found in the Supporting Information (Figures S1–S8).

2.4. Synthesis of the Reference Fragment 8a

This ferrocene derivative was prepared in two consecutive steps, (a) and (b), as follows:

2.4.1. (a) Synthesis of 2-(4-(Hydroxymethyl)-1*H*-1,2,3-triazol-1-yl)benzaldehyde (6)

Propargyl alcohol (**4**; 0.17 mL, 0.17 g, 3.0 mmol, 1.0 eq.), 2-azidobenzaldehyde (**5**; 0.44 g, 3.0 mmol, 1.0 eq.), $CuSO_4$ (0.10 g, 0.6 mmol, 0.2 eq.), and sodium ascorbate (0.59 g, 3.0 mmol, 1.0 equation) were suspended in a 1:1 mixture of water and *n*-BuOH (1 mL). The reaction mixture was stirred at room temperature for 12 h, and then it was poured on water (20 mL) and extracted with DCM (5 × 20 mL). The combined organic phase was dried on anhydrous Na_2SO_4, and the solvent was evaporated. The crude product was purified by column chromatography on silica gel using DCM as the eluent to obtain **6** as a pure product of which the yield and characterization, along with detailed assignments and copies of ^1H and ^{13}C NMR spectra, are found in the Supporting Information (Figures S9 and S10).

2.4.2. (b) Synthesis of (*E*)-1-Ferrocenyl-3-(2-(4-(hydroxymethyl)-1*H*-1,2,3-triazole-1-yl)phenyl)prop-2-en-1-one (8a)

2-(4-(Hydroxymethyl)-1*H*-1,2,3-triazole-1-yl)benzaldehyde (**6**; 0.20 g, 1.0 mmol, 1.0 eq.) and acetylferrocene (**7**; 0.23 g, 1.0 mmol, 1.0 eq.) were dissolved in 2 mL of EtOH. To this solution, 10% aqueous NaOH (0.2 mL) was added at room temperature, and the resulting mixture was stirred for 12 h and then poured on water (50 mL). The formed precipitate was collected by filtration, washed with water, dried, and subjected to column chromatography on a silica gel using DCM as the eluent to obtain **8a** as a pure product of which the yield and characterization, along with detailed assignments and copies of ^1H and ^{13}C NMR spectra, are found in the Supporting Information (Figures S11 and S12).

2.5. Synthesis of Reference Fragments 8b-d

The corresponding azide (**2b-d**; 1.0 mmol, 1.0 eq.), propargyl alcohol (**4**; 58 μL, 56 mg, 1.0 mmol, 1.0 eq.), $CuSO_4$ (32 mg, 0.2 mmol, 0.2 eq.), and sodium ascorbate (0.20 g, 1.0 mmol, 1.0 eq.) were suspended in a 1:1 mixture of water and *n*-BuOH (4 mL). The reaction mixture was stirred at room temperature for 12 h, and then it was poured on water (20 mL) and extracted with DCM (5 × 20 mL). The combined organic phase was dried on anhydrous Na_2SO_4, and the solvent was evaporated. The crude product was sequentially purified by column chromatography on a silica gel using DCM:MeOH (20:1 and 10:1) mixtures as eluents. After purification, the analytical sample was crystallized from MeOH. Yields and characterization, along with detailed assignments and copies of ^1H and ^{13}C NMR spectra, are provided as Supporting Information (Figures S13–S18).

2.6. Spectrofluorimetric Investigation of Compounds 3a-d

Fluorescence excitation and emission spectra were recorded on a Shimadzu RF-20A (Shimadzu Corp., Kyoto, Japan) spectrofluorometric HPLC detector equipped with a Xenon lamp. This unit was attached to a Shimadzu CBM-20A communication module that enabled PC-controlled investigation through the Class-VP software (Shimadzu Corp., Kyoto, Japan). A 10 ng/mL acetonitrile sample solution was prepared for each measurement and added into the detector chamber through a

capillary. Data were obtained by first recording the background spectrum of the solvent, followed by the analysis of the sample solution. The spectrum scanning option provided an automatic correction of spectral information with the previously recorded background. Before changing the sample or a mode of measurement, the detector capillary was washed multiple times with acetonitrile, and a new background value was consequently recorded. The emission spectra of derivatives were recorded between intervals of 500–750 nm using 488 nm as the excitation wavelength. The settings of the detector were as follows: "1X" detection gain, "high" sensitivity, and 120 nm/min scanning speed. The obtained background corrected emission spectra are shown in the Supporting Information, Figure S19.

2.7. Cell Lines

Human breast cancer (MDA-MB-231 cells and MCF-7 cells) cell lines were purchased from American Type Culture Collection (Rockville, MD, USA). These cell lines were cultured in MEM supplemented with 10% FBS, 1% non-essential amino acids and an antibiotic–antimycotic mixture (MTT assay, cell cycle analysis and caspase-3 assay), or Dulbecco's Modified Eagle's medium (DMEM) supplemented with 10% heat-inactivated FBS, 2 mM L-glutamine, 10,000 U/mL penicillin, and 10 mg/mL streptomycin (all other bioassays) at 37 °C in a humidified atmosphere containing 5% CO_2. All cell lines were sub-cultured using 0.25% trypsin/EDTA. The density of cells for each experiment was determined with a Luna Automatic Cell Counter (South Korea) using a hemocytometer and trypan blue solution [34,35].

2.8. Cell Viability Assay

The colorimetric MTT ([3-(4,5-dimethylthiazol-2-yl)-2,5-diphenyltetrazolium bromide]) assay was used to estimate the ability of prepared compounds to inhibit the proliferation of human breast cancer cells (MCF-7 and MDA-MB-231), as previously described [36,37]. Briefly, the cells were seeded in 96-well microplates at a density of 5000 cells/well in a final volume of 100 μL and allowed to adhere overnight under standard conditions. Prior to testing, compounds were dissolved in DMSO as a 10 mmol/L stock solution and stored at −20 °C with minimal exposure to light to avoid oxidation. The stock solution was diluted with the culture medium before each treatment to obtain the final concentrations for the different experiments. Cells were exposed to 10 different concentrations of each compound (0.039, 0.07, 0.1, 0.31, 0.62, 1.25, 2.5, 5, 10, and 20 μM). Cisplatin was used as a positive control (0.1, 0.3, 0.6, 1.25, 2.5, 5, 10, and 20 μM). The plates were incubated for 72 h in the same conditions at 37 °C in a humidified atmosphere of 5% CO_2. After incubation, 44 μL of the MTT solution (5 mg/mL PBS) was added to each well and incubated for 4 h. Subsequently, the supernatant was carefully removed, and insoluble purple formazan crystals were solubilized by adding 100 μL/well of DMSO and gently shaking them for 1 h at 37 °C (Stat Fax-2200, Awareness Technology INC, Palm City, FL, USA). Absorbance was measured at a wavelength of 545 nm using an automatic microplate reader (Stat Fax-2100; Awareness Technology INC, Palm City, FL, USA). Data were collected from two separate experiments performed in triplicate for each concentration and evaluated by Graph Pad Prism 5.01 (Graph Pad Software, San Diego, CA, USA). The half-maximal inhibitory concentration (IC_{50}) values were calculated by the nonlinear regression model log inhibitor vs. normalized response.

2.9. Combination Study of Relevant Fragments Compared with Their Hybrids 3b-d

Two combination studies were performed: a virtual and an experimental one. In the case of the virtual study, cell viability data obtained following treatment with the hybrid compounds **3b-d** were analyzed in comparison with data obtained for their corresponding relevant fragments, such as compounds **1** and **8b-d**, and the hybrid compounds were considered as 1:1 ratio mixtures of compound **1** and the corresponding fragment. Two independent experiments were performed, each in triplicate. In the case of the experimental combination study, cell viability data obtained for equimolar mixtures of the abovementioned fragments were tested in comparison with the

corresponding single-treatment controls. In this bioassay, two separate experiments were performed, each in duplicate.

Calculations were performed using the CalcuSyn software [38]. In each case, raw cell viability data from all replicates were averaged, and the resulting single dataset was analyzed as suggested by Chou [38]. CI values obtained this way were then used to mathematically describe the extent of pharmacological benefit gained by the coupling (virtual combination) in comparison with a combined effect of the mixture of fragments (experimental combination). "Synergism" in the virtual combination means that the hybrid exerts significantly stronger cytotoxicity than just a sum of that of its fragments.

2.10. Cell Death Analysis

The percentage of apoptotic, necrotic, and viable cells was determined by Annexin-V (AV)/PI labeling. Cells labeled with AV-FITC/PI were analyzed by flow cytometry. After 72 h treatments with 500 nM of each compound, both attached and floating cells of all samples (untreated and treated) were collected, washed in PBS to eliminate culture medium, and placed in 100 μL of binding buffer containing AV-FITC and PI in a ratio of 1:1 (*v/v*) (10 min at room temperature in the dark). Afterward, 400 μL of binding buffer was added to stop the reaction, and samples were analyzed within 1 h by flow cytometry. The fluorescence intensities of AV-FITC and PI were measured in the green (FL1) and red (FL2) channels on a CyFlow Space flow cytometer (Partec, Münster, Germany), respectively. In each sample, the fluorescence intensity of 20,000 cells was documented, while the amount of viable (AV−/PI−), early apoptotic (AV+/PI−), late apoptotic (AV+/PI+), and necrotic (AV−/PI+) cells was analyzed with Summit software (Dako Colorado Inc., USA). The experiments were performed in triplicate. For statistical analysis, two-way analysis of variance (ANOVA) with Dunnett's multiple comparisons test was conducted using GraphPad Prism 6 software. Differences were considered statistically significant in comparison with untreated controls when $p \leq 0.05$.

2.11. Cell Cycle Analysis in MDA-MB-231 Cells

To detect the cellular DNA content using PI staining, cell cycle distribution was determined by flow cytometry, as previously described [39]. Briefly, cells were seeded in six-well plates at a density of 4×10^5 cells per well. On the second day, the MDA-MB-231 cells were treated with compounds at their IC$_{50}$ or $2 \times$ IC$_{50}$ concentration. These concentrations were 0.2 and 0.4 μM (**3c**) or 0.3 and 0.6 μM (**3b**), respectively, while the control group was treated with MEM. Subsequently, cells were harvested with trypsin (250 μL/well), washed with PBS, resuspended and fixed with 70% EtOH, and kept at −20 °C. Directly before the assay, the fixed cells were washed with cold PBS and stained with PI in the presence of RNAse, Triton-X-100, and sodium citrate. Then, they were incubated in the dark at room temperature for 1 h. Finally, the DNA content was analyzed by flow cytometry (Partec CyFlow, Partec GmbH, Münster, Germany), with at least 20,000 cells being evaluated for each analysis. The experiment was performed in triplicate. Cell cycle distributions were determined by ModFit LT 3.3.11 software (Verity Software House, Topsham, ME, USA), and results are shown in the Supporting Information, Figure S20.

2.12. Effect of Compound 3c on Caspase-3 Activity in MDA-MB-231 Cells

Caspase-3 activity was determined using a Caspase-3 Colorimetric Assay Kit, according to the manufacturer's protocol, as previously published [40]. Briefly, cells were plated at the density of 12×10^6 cells per 175 cm^2 in a flask and allowed to attach and grow for 24 h. Then, they were treated with the appropriate concentrations of compound **3c** for 24 or 48 h, scraped, washed with PBS, and resuspended in Lysis Buffer. The supernatant was collected. Assays were performed in a 96-well plate by incubating 5 μL of the cell lysates in 100 μL of assay buffer containing 222 μM/L of the caspase-3 substrate at 37 °C in the dark for 24 h. Finally, the absorbance was measured at 405 nm with a microplate reader (Stat Fax 2100, Awareness Technology INC, Palm City, FL, USA). The comparison of the absorbance of the treated samples with the untreated controls to determine the change in

caspase activity was performed by Graph Pad Prism 5.0 using a one-way analysis of variance (ANOVA) followed by Dunnett's post-hoc test. Results are shown in the Supporting Information, Figure S21.

2.13. Effect of Compounds 3a-d on DNA Damage Response

The effect of compounds **3a-d** on the ATR-dependent phosphorylation of Chk1 was evaluated by western immunoblotting, as previously published [16]. Briefly, MCF7 cells were pretreated with 1 μM of the compounds for 30 min and exposed to 10 μM cisplatin in the presence or absence of the compounds for 8 h to induce DDR. The same concentration of protoapigenone was used as a positive control for inhibition. The primary antibody against S345 of Chk1 was purchased from Cell Signaling Technology (Danvers, MA, USA); Chk1 and β-actin antibodies were purchased from Santa Cruz Biotechnology Inc (Dallas, TX, USA). The protein expression signal on blots was quantified by Fujifilm Multi Gauge software (Tokyo, Japan). The ratio of Chk1-S345 to Chk1 expression was calculated, and the means between the groups were compared by a one-way ANOVA. Data represent the mean ± standard deviation from three independent experiments; *: $p < 0.05$, **: $p < 0.01$.

2.14. Effect of Compounds 3a-d on ROS/RNS Levels

DHE (life Technologies, D23107, NY, USA) and DHR (Sigma-Aldrich, D1054, MO, USA) fluorescent dyes were used to assess ROS and reactive nitrogen species (RNS) levels, respectively, in breast cancer cells. DHE fluorescence is activated by superoxide anion and corresponds to the intracellular ROS levels, while DHR fluorescence is activated by hydrogen peroxide and peroxynitrite anions and corresponds to the intracellular RNS levels. MCF-7 and MDA-MB-231 cells were plated and incubated overnight in 6-well plates at a density of 100,000 cells/well. After a 24 h incubation with 1 μM of each compound, adherent cells were harvested by trypsinization and placed in medium containing 5 μM of DHE or DHR for 30 min at 37 °C in the dark. Afterward, cells were washed twice in PBS. DHE and DHR fluorescence were assessed in the FL2 red channel and FL1 green channel, respectively. Data from a minimum of 20,000 cells were collected and assayed for each sample. These experiments were repeated three times. The samples were analyzed on a CyFlow Space flow cytometer (Partec, Münster, Germany). A two-way ANOVA with Dunnett's multiple comparisons test was performed using GraphPad Prism 6 software. Differences were considered statistically significant in the comparison with untreated controls when $p \leq 0.05$.

2.15. Assessing Mitochondrial Membrane Depolarization

JC-1 (BD Biosciences, San Diego, USA) is a cationic dye that can provide information about the mitochondrial membrane potential. JC-1 accumulates in healthy mitochondria as red fluorescent aggregates, while in depolarized dysfunctional mitochondria, JC-1 remains in the cytoplasm as green fluorescent monomers. During the depolarization of mitochondria, JC-1 labeled monomers leak out of the mitochondria into the cytoplasm, increasing the ratio of green to red fluorescence. MCF-7 and MDA-MB-231 cells were incubated overnight in 6-well plates (100,000 cells/well), and then treated for 24 h with 1 μM of each compound. Subsequently, the cells were incubated with the JC-1 reagent for 15 min at 37 °C. After two washing steps in 1X Assay Buffer, the cells were resuspended in PBS. Both red and green fluorescence emissions were detected, and their ratio was analyzed on a CyFlow Space flow cytometer (Partec, Münster, Germany). Data from a minimum of 20,000 cells were collected per sample. All experiments were performed in triplicate. A two-way ANOVA with Dunnett's multiple comparisons test was applied using GraphPad Prism 6 software. Differences were considered statistically significant in comparison with untreated controls when $p \leq 0.05$.

3. Results and Discussion

3.1. Chemistry

The protoflavone structure of protoapigenone 1'-*O*-propargyl ether (compound **1**) was prepared by a hypervalent iodine-induced oxidative de-aromatization from apigenin, using bis(trifluoroacetoxyiodo)benzene (PIFA) as previously published [33]. The terminal alkyne fragment of this compound was used for linking it to a preliminary selection of chalcone-based azide components **2a-d** by copper(I)-catalyzed click reactions [41] conducted under well-established ascorbate-conditions to generate the targeted protoflavone-chalcone hybrids with 1,4-disubstituted 1,2,3-triazole linkers (**3a-d**) in acceptable to good yields (Scheme 1). The synthesis of hydroxymethyl derivatives **8a-d**, serving as reference compounds for the combination studies, was also attempted under the same conditions using propargyl alcohol **4** as an alkyne (Scheme 1). While the conversion using **2a** as an azide component was not successful, and the reactions with azides **2b** and **2d** containing a 4-hydroxy-3,5-dimethylphenyl group produced **8b** and **8d** in low yields (7% and 9%, respectively), the cyclization of **2c** containing a 3,4,5-trimethoxyphenyl group resulted in the formation of **8c** in an average yield. The ferrocene analog **8a** was prepared by a two-step procedure, starting with the facile copper(I)-mediated cyclization of **4** and 2-azidobenzaldehyde **5** followed by the base-catalyzed condensation of the resulting triazole (**6**) with acetylferrocene (**7**).
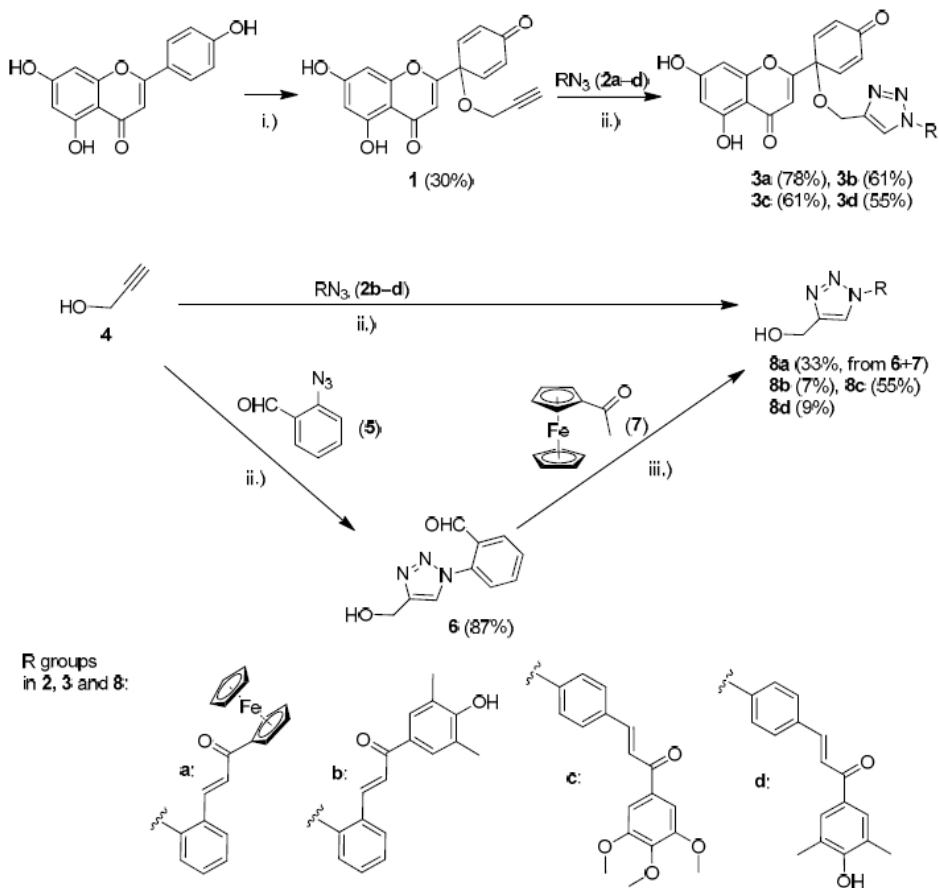
Scheme 1. Synthesis of the tested protoflavone-chalcone hybrids with triazole linkers (**3a–d**) and the corresponding hydroxymethyl derivatives (**8a–d**) serving as reference compounds for evaluating the pharmacological benefit gained by the coupling (see Figure 1). Reaction conditions: (i) PIFA (2.0 eq.), acetonitrile:propargyl alcohol (9:1), 80 °C, 1h; (ii) azide (1.0 eq.), alkyne (1.0 eq.), CuSO₄ (0.2 eq.),

sodium ascorbate (1.0 eq.), *n*-BuOH:water (1:1), rt, 12 h; (iii) 6 (1.0 eq.), 7 (1.0 eq.), NaOH, water, EtOH, room temperature, 12 h.

The compounds' structures were confirmed by high-resolution mass spectrometry (HRMS) and nuclear magnetic resonance (NMR) spectroscopy. The measured ^{1}H and ^{13}C NMR data of the novel compounds, including hybrids **3a-d** (see Supporting Information, Figures S1–S8), are consistent with their structure. However, the following remarks are necessary to make: (i) in **3a-d**, the connection of the protoflavone and chalcone fragments was unambiguously evidenced by the cross peaks discernible in the HMBC spectra generated by a three-bond interaction between the isotropic H15 protons in the OCH$_2$ group and the sp^3 quaternary C9 carbon in the cycloxehadienone ring; (ii) the singlet signal of H15 protons is also correlated with the ^{13}C NMR signals of the C16 and C17 triazole carbons generated by two-bond and three-bond interactions, respectively; (iii) an HMBC correlation was detected between H3 and C9 transmitted by a three-bond coupling; (iv) the *E*-configuration of the C=C double bond is reflected from the coupling constant of ca. 15 Hz characterizing the interaction involving the protons in the enone moiety. Complete NMR characterization and ^{1}H and ^{13}C NMR spectra of compounds **3a-d**, **6**, and **8a-d** are available in the Supporting Information (Figures S1–S18).

Spectrofluorimetric investigations were used to investigate the possibility of spectral interference related to the compounds' native fluorescence, considering the high degree of aromaticity of the hybrid compounds **3a-d** and the several fluorescence-based bioassays that we planned to perform on them (see below). Emission spectra were recorded between intervals of 500–750 nm using 488 nm as the excitation wavelength, and they are available in Supporting Information (Figure S19). None of these derivatives showed significant fluorescent emission under these experimental circumstances. Therefore, their fluorescent interference during the flow cytometry analyses was not expected.

3.2. Cell Viability Assay, Virtual and Experimental Combination Study

We evaluated the cytotoxic activity of relevant fragments and their hybrids (**3a-d**) on breast cancer cell lines by MTT assay. For the selection of relevant fragments, the following points were considered: (i) the *p*-quinol protoflavone containing a free OH group at position C-1' (i.e., protoapigenone in our case) is generally more toxic than its 1'-*O*-alkyl derivatives, and all hybrid molecules have an alkoxy-function at this position; and (ii) the free azide of compounds **2a-d** makes them potentially toxic in a way that does not have relevance in view of the hybrids. Therefore, for each hybrid compound of type **3**, protoapigenone 1'-*O*-propargyl ether (**1**) and the corresponding chalcone coupled to hydroxymethyltriazole (**8a-d**) were selected as reference fragments. Comparative testing of the cytotoxicity of these compounds provides a good assessment of the pharmacological benefit gained by the coupling, despite the slight overlap between the chemical structure of these fragments meaning a (necessary) compromise, as compared to evaluating the two halves of each hybrid molecule.

The MCF-7 cell line was used as a representative model for estrogen receptor (ER)-positive breast cancer, while the MDA-MB-231 cell line was used as a model of triple-negative breast cancer (TNBC). TNBCs are highly resistant to first-line antiestrogen therapy, and therefore their treatment relies on the use of chemotherapeutics. Both cell lines have an epithelial phenotype, although a mesenchymal marker, vimentin, was determined in the MDA-MB-231 cell line [42]. Both cell lines are tumorigenic and adherent while they differ in their tissue spatial organization. MCF-7 is a luminal subtype A human breast cell line [43], and MDA-MB-231 is a basal breast cell line originating from a metastatic site [44]. The cells were treated with each compound in the concentration range between 30 nM and 20 μM for 72 h; results are presented in Table 1.

Table 1. Cytotoxic activity of hybrid compounds 3a-d and their corresponding fragments 1 and 8a-d on human breast cancer cell lines. Confidence interval: 95% CI, $n = 6$ from two biological replicates ($n = 3$ each). Positive control: cisplatin, $n = 10$ from two biological replicates ($n = 5$ each).

| Compound | IC$_{50}$ [95% CI] (μM) | |
	MCF-7	MDA-MB-231
1	1.74 [1.55–1.95]	2.53 [2.34–2.72]
8a[a]	>20	>20
8b	15.07 [13.66–16.64]	11.11 [10.53–11.71]
8c	2.51 [2.24–2.82]	4.40 [3.98–4.86]
8d	11.00 [10.20–11.85]	4.92 [4.52–5.36]
3a	0.47 [0.45–0.49]	0.37 [0.36–0.39]
3b	0.25 [0.23–0.28]	0.29 [0.27–0.31]
3c	0.30 [0.27–0.32]	0.22 [0.21–0.24]
3d	0.51 [0.48–0.55]	0.32 [0.30–0.35]
Cisplatin	5.35 [4.97–5.76]	26.15[b] [24.18–28.27]

[a] 8a exhibited less than 10% inhibition on each cell line at the highest tested dose of 20 μM;
[b] Experimental data are available up to 20 μM, IC$_{50}$ value was extrapolated from the nonlinear curve fitting (log inhibitor vs. normalized response model) by GraphPad Prism 5.0.

All hybrid compounds showed a potent, dose-dependent cytotoxic effect against the tested cancer cell lines. Except for **3b**, the compounds were also slightly more effective against the TNBC cell line MDA-MB-231.

When comparing the effect of the hybrids to their fragments, compound **3a** was found to be ca. 3.7 times more potent on MCF-7 cells and ca. 6.8 times more potent on MDA-MB-231 cells than compound **1**. This demonstrates a strong potentiation of the cytotoxic effect when adding the non-cytotoxic fragment **8a** to the structure of the hybrid.

However, in the case of compounds **3b-d**, each fragment (**1** and **8b-d**, respectively) exhibited significant cytotoxic effects. Therefore, we performed a more sophisticated comparative evaluation to quantitatively assess the added pharmacological benefit of linking each pair of fragments into a hybrid molecule. To the end of performing this evaluation, we selected the Chou–Talalay method, which offers a well-established mathematical model for the calculation of drug–drug interactions [38]. Two separate analyses were performed. On one hand, the method was used in an unusual way that may be referred to as a "virtual combination study". Treatment with the hybrid molecules **3b-d** was considered as a 1:1 ratio combination treatment with their two relevant corresponding fragments (i.e., **1** and **8b**, **1** and **8c**, and **1** and **8d**, respectively), and the cell viability data presented in Table 1 were re-evaluated accordingly using the CalcuSyn software. Furthermore, a classical experimental combination study was also performed as a control, in which equimolar combinations of compounds **1** and **8b**, **8c**, or **8d** were analyzed in comparison with the corresponding single treatments. The results of these calculations are presented in Figure 1.
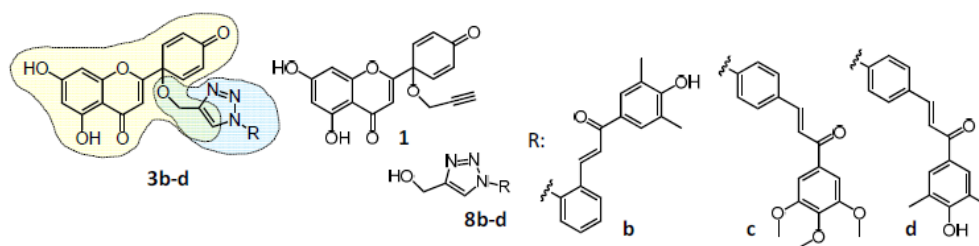
Cell line	Type of combo	Hybrid	Fragments combined	CI value at			Dm	m	r	CI$_{avg}$
				ED$_{50}$	ED$_{75}$	ED$_{90}$				
MCF-7	Virtual	3b	1 + 8b	0.216	0.191	0.170	0.306	2.477	0.993	0.184
		3c	1 + 8c	0.340	0.304	0.274	0.332	2.910	0.997	0.295
		3d	1 + 8d	0.392	0.363	0.335	0.526	2.382	0.998	0.354
	Exp.	3b	1 + 8b	0.700	0.712	0.732	2.183	2.511	0.989	0.720
		3c	1 + 8c	1.028	1.061	1.096	1.689	2.469	0.980	1.073
		3d	1 + 8d	0.980	0.925	0.873	2.384	2.549	0.997	0.908
MDA-MB-231	Virtual	3b	1 + 8b	0.181	0.150	0.125	0.248	3.365	0.982	0.143
		3c	1 + 8c	0.215	0.170	0.135	0.210	4.365	0.986	0.160
		3d	1 + 8d	0.230	0.197	0.169	0.269	3.010	0.982	0.188
	Exp.	3b	1 + 8b	0.751	0.957	1.221	1.276	2.009	0.972	1.055
		3c	1 + 8c	0.855	0.849	0.858	1.665	2.304	0.961	0.854
		3d	1 + 8d	0.772	0.786	0.801	1.535	1.861	0.972	0.791

Figure 1. Comparative analysis of the cytotoxic activity of the hybrid compounds **3b-d** by the Chou–Talalay method with that of their fragments. Results of a virtual (hybrid vs. fragments alone) and an experimental (Exp.: equimolar mixture of fragments vs. fragments alone) combination study are shown at 50%, 75%, and 90% of inhibition. CI: combination index; $0 < CI < 1$, $CI = 1$, and $CI > 1$ represent synergism, additivity, and antagonism, respectively. Dm, m, and r represent the antilog of the x-intercept (activity), slope (shape of the dose-effect curve), and linear correlation coefficient (conformity of the data) of the median effect plot, respectively [38]. CI$_{avg}$ = (CI$_{50}$ + 2 × CI$_{75}$ + 3 × CI$_{90}$)/6. The lowest CI$_{avg}$ value demonstrates the highest added benefit of hybridization in terms of *in vitro* cytotoxic activity.

The strong synergism observed by the virtual combination study for nearly every hybrid clearly showed that these compounds were much more potent than what would be expected by their corresponding building blocks. It is also evident that the co-treatment of cells with the fragments (see Exp. rows in the table of Figure 1) resulted in additive effects or moderate synergism at best. Our results therefore strongly suggest that the hybridization of these fragments offers a relevant pharmacological benefit.

Using the Chou–Talalay method as a mathematical tool to perform a quantitative comparison between the bioactivity of two fragments and their corresponding hybrid is, to the best of our knowledge, a novel approach. We believe that with an appropriate selection of fragments to evaluate, such a virtual combination study provides a reasonable and easy-to-use platform to assess the bioactivity of hybrid compounds in general, therefore, we suggest an extension for the applicability of the Chou–Talalay method to analyze related bioactivity data.

3.3. Cell Death Induction Analysis

To further investigate the effects of the hybrid compounds on the two breast cancer cell lines, cell death induction by compounds **3a-d** was analyzed (Figure 2).
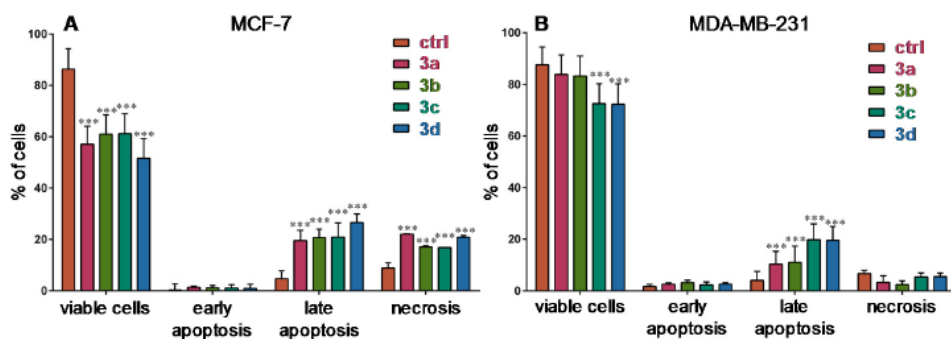
Figure 2. Cell death induction by the hybrid compounds in MCF-7 (**A**) and MDA-MB-231 cells (**B**). Cells were treated with 500 nM of each compound for 72 h, ***: $p < 0.001$ by two-way analysis of variance (ANOVA) followed by Dunnett's multiple comparisons test. Necrosis refers to primary necrosis.

While a substantial increase in primary necrosis was present only in MCF-7 cells, significant induction of late apoptosis was observed after all treatments in both cell lines. The viability of MCF-7 cells was significantly decreased by all of the compounds, whereas only **3c** and **3d** decreased the viability of MDA-MB-231 cells after 72 h. Of note, MCF-7 cells also responded differently to the treatment than MDA-MB-231 cells. Specifically, more necrosis (primary necrosis) was observed in MCF-7 cells. Cell type-dependent occurrence of either apoptotic or necrotic cell fate was previously observed for protoapigenone, and it was suggested that this may be connected to its effect on the DDR [16].

3.4. Cell Cycle Analysis and Effects of Compound 3c on Caspase-3 Activity in MDA-MB-231 Cells

Compound **3c** was also tested for its effect on the cell cycle and caspase-3 activity in this cell line, because its potent cytotoxic activity was the strongest against MDA-MB-231 cells. Cells were treated with IC$_{50}$ or double IC$_{50}$ concentrations of **3c**. The results of these bioassays are presented in Supporting Information (Figures S20 and S21). As a summary, it was concluded that, in comparison with the control groups, the treatment significantly increased the hypodiploid (subG1) phase, and this was associated with a significant decrease in the G1 phase in a dose-dependent manner after a 24 h treatment. These results (subG1 portion) indicate apoptotic cell death and that this hybrid compound inhibits DNA synthesis in a dose-dependent manner, which is consistent with previous results published for protoapigenone [45]. However, unlike protoapigenone [45], **3c** did not produce any significant effects on the proportion of cells in S and G2/M phases at the tested concentrations. Compound **3c** also caused a time- and concentration-dependent increase in caspase-3 activity, which is in agreement with previous reports on the pro-apoptotic activity of protoapigenone [12,17].

3.5. Effects of Compounds 3a–d on the ATR-Dependent Phosphorylation of Chk1

It was of primary interest to study whether the hybrid compounds retained activity on this target due to the bioactivity of the key fragment protoapigenone on the ATR-dependent inhibition of Chk1 in the DDR. Therefore, the effects of compounds **3a-d** on the cisplatin-induced activation of Chk1 were determined (Figure 3A). In comparison with the positive controls treated with protoapigenone, compounds **3a-d** significantly decreased and almost abolished cisplatin-induced Chk1-S345 phosphorylation. Checkpoint kinases play a critical role in the DDR to maintain genome integrity by mediating DNA repair or cell apoptosis. Agents that inhibit ATR or Chk1 have been developed in preclinical and clinical studies to improve tumor sensitivity by inducing tumor death in the presence or absence of DNA damaging therapies, such as radiotherapy and chemotherapy, or to exploit synthetic lethality interactions between Chk1 or ATR inhibition and genetic defects in other DDR genes [20,21]. Supporting the strong synergism identified in the virtual combination study, the hybrid compounds were more potent ATR inhibitors than their protoflavone fragment.

It is of interest that the expression levels of Chk1 and the capacity for DNA repair were most recently found to be associated with cancer sensitivity to DNA damaging agents, such as mitomycin C (MMC). In contrast with MMC-sensitive MCF-7 cells, MDA-MB-231 cells are resistant to MMC. This relates to the fact that MDA-MB-231 cells express high levels of Chk1 protein as well as MMC-induced Chk1-p and have a low DNA repair capacity [46]. This relative resistance of MDA-MB-231 cells to DNA damaging agents was also seen in our current study from their poor response to cisplatin treatment: we found them ca. five times more resistant to cisplatin as compared with MCF-7 cells. Cancer cells with higher Chk1 expression would expectably be sensitive to Chk1 inhibition. Further, it is known that the MDA-MB-231 cell line is a p53 mutant [47], in contrast with MCF-7 that contains wild-type p53 [48], and p53 mutations are among the factors that predict vulnerability of cancer cells to ATR inhibitors [49]. Taken together, it seems likely that potent inhibition of the ATR-dependent activation of Chk1 by compounds **3a-d** is among the reasons for their strong cytotoxicity on the TNBC cell line MDA-MB-231.

3.6. Effect on the Levels of Reactive Oxygen and Nitrogen Species

Based on the pro-oxidant properties of both protoflavone and chalcone, their effects on intracellular ROS and/or reactive nitrogen species (RNS) levels were studied (Figure 3B–E).
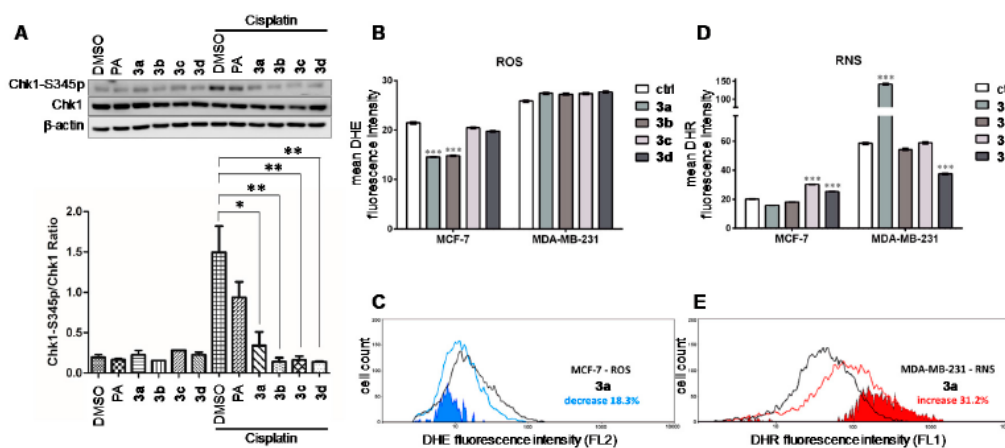
Figure 3. Effect of compounds **3a-d** on the DNA damage response and redox balance in breast cancer cells. (**A**) Effect of compounds **3a-d** on Chk1 phosphorylation in MCF-7 cells, PA: protoapigenone; (**B**) Changes in reactive oxygen species (ROS) production induced by 1 μM of compounds **3a-d** in MCF-7 and MDA-MB-231 cells assessed after 24 h; (**C**) Decrease in ROS production by **3a**; (**D**) Changes in reactive nitrogen species (RNS) production induced by 1 μM of compounds **3a-d** in MCF-7 and MDA-MB-231 cells assessed after 24 h; (**E**) Increase in RNS production by **3a**; ctrl: untreated cell control.

Although the results cannot point to a uniform pattern of action, such as antioxidant or pro-oxidant activity, all of the compounds demonstrated the ability to interfere with the redox system in breast cancer cells. Regarding ROS levels, **3a** and **3b** significantly decreased superoxide anion levels in MCF-7 cells. Additionally, **3c** and **3d** significantly increased RNS levels in MCF-7 cells. The most prominent effect on RNS levels was observed with **3a**, suggesting its significant pro-oxidant activity in MDA-MB-231 cells. In contrast, **3d** significantly decreased the RNS levels in MDA-MB-231 cells.

The changes of ROS and RNS after treatment with the hybrid compounds can be both time- and cell line-dependent. The end-point detection after 24 h showed that the cellular antioxidant capacity is modified by all tested compounds. Interestingly, according to our results, untreated MDA-MB-231 cells show increased production of ROS and RNS levels as compared with untreated MCF-7 cells (Figure 3B–E), indicating that this TNBC cell line has a higher oxidative status. Indeed, previous findings showed that in comparison with MCF-7 cells, MDA-MB-231 cells have higher FAD/NADPH redox ratio that is an indicator of oxidized mitochondrial state [50]. MCF-7 cells depend on energy

produced from oxidative phosphorylation in normoxic conditions but could switch to glycolytic activity under hypoxia, while MDA-MB-231 cells predominantly use glycolysis regardless of the availability of oxygen [51]. In addition, MCF-7 cells possess high levels of glutathione peroxidase, while MDA-MB-231 cells contain increased levels of glutathione transferase [52]. Therefore, high oxygen consumption of MCF-7 cells requires more efficient antioxidant system than that of MDA-MB-231 cells that do not depend on oxygen. Consequently, MDA-MB-231 cells may be more vulnerable to pro-oxidants than MCF-7 cells. This may explain obvious discrepancy in the effect of **3a**, a compound with a prominent antioxidant effect in MCF-7 cells as seen from the decrease in ROS levels (Figure 3B,C), and with a prominent pro-oxidative effect in MDA-MB-231 cells as seen from the increase in RNS levels (Figure 3D,E). Similar opposite effects on the ROS and RNS production were previously observed with ferrocene–quinidine hybrids [29] containing the same triazole-linked ferrocene moiety as compound **3a**.

It is worth mentioning that the administration of pro-oxidants to exploit oxidative stress-related vulnerabilities of cancer may also lead to unwanted toxicity in healthy cells and tissues. Therefore, it will be particularly important to conduct future studies elaborating related properties of our hybrid compounds and/or to assure their adequate selective targeting at the tumor site.

3.7. Effect on Mitochondrial Membrane Depolarization

Activating the mitochondrial apoptosis pathway, chalcones are commonly associated with the ability to interfere with the mitochondrial electron chain [53,54], and changes in the ROS and RNS levels may also affect mitochondrial function. Therefore, we determined the ability of hybrid compounds **3a-d** to change the mitochondrial membrane potential in MCF-7 and MDA-MB-231 breast cancer cells (Figure 4).
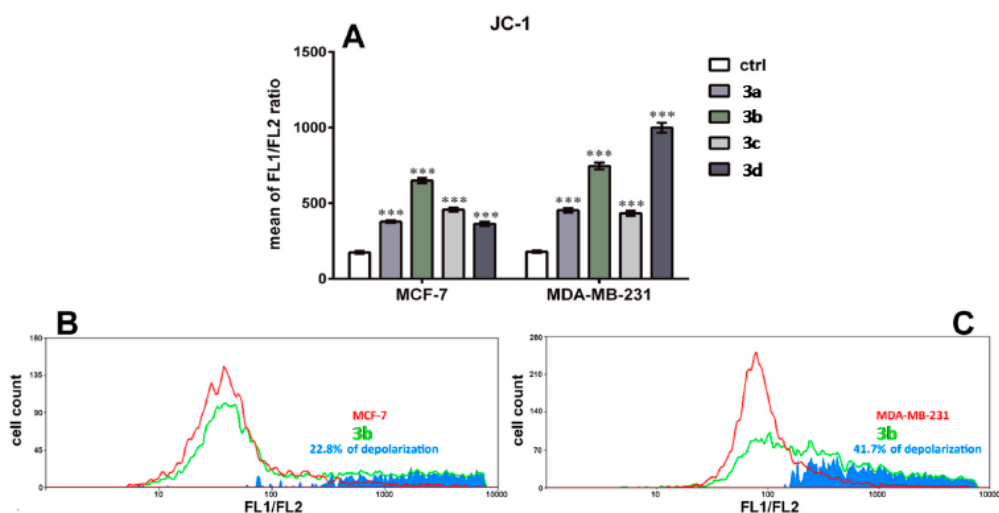
Figure 4. Hybrid-protoflavones induce mitochondrial membrane depolarization. (**A**) Increase in the ratio of green to red fluorescence (FL1/FL2) assessed by JC-1 staining in MCF-7 and MDA-MB-231 cells after 24 h treatments with 1 μM of compounds **3a-d**; (**B**) Illustration of the effect induced by **3b** in MCF-7 cells; (**C**) Illustration of the effect induced by **3b** in MDA-MB-231 cells.

All of the compounds induced significant depolarization of the mitochondrial membrane in both cell lines. While the effects of compounds **3a-c** were similar in MCF-7 and MDA-MB-231 cells, compound **3d** showed a >2-fold increase in selectivity toward MDA-MB-231 cells in this regard. While this is just one aspect of a clearly multitarget antitumor action of these compounds, it may still be worth noting that **3d** also showed the highest selectivity toward MDA-MB-231 cells vs. MCF-7 cells among the hybrids in the cytotoxicity assay (see Table 1). In addition, the induction of late apoptosis after 72 h treatment by **3d** and other hybrid compounds (Figure 2) is probably due to pro-

apoptotic factors released from affected mitochondria whose proton leakage was observed after 24 h treatments.

4. Conclusions

The hybrid compounds prepared in this study exhibited a significant increase in their antitumor activity compared with either fragment alone, resulting in potent antitumor leads active in the sub-micromolar concentration range against breast cancer cell lines. The strong activity of these compounds against the TNBC model is particularly promising since the treatment of this disease is challenging due to its resistance to first-line therapies. In this respect, compound **3a** deserves to be further studied as a pro-oxidant, as well as compound **3d**, which exerted the most pronounced effect on mitochondrial depolarization.

The triazole coupling of the ATR inhibitor protoflavone and a chalcone fragment resulted in hybrids that clearly act on multiple targets. They exert a significantly stronger activity on the cisplatin-induced activation of Chk1 as compared with their parent fragment protoapigenone, interfere with the redox balance of cells, and strongly depolarize the mitochondrial membrane. The potency and multitarget antitumor action of these hybrid compounds make them valuable starting points for possible further developments.

References

1. Union for International Cancer Control. New Global Cancer Data: GLOBOCAN 2018. Availabe online: https://www.uicc.org/news/new-global-cancer-data-globocan-2018 (accessed on 28 August 2019).

2. Elder, E.E.; Kennedy, C.W.; Gluch, L.; Carmalt, H.L.; Janu, N.C.; Joseph, M.G.; Donellan, M.J.; Molland, J.G.; Gillett, D.J. Patterns of breast cancer relapse. *Eur. J. Surg. Oncol.* **2006**, *32*, 922–927. doi:10.1016/j.ejso.2006.06.001.

3. Park, J.H.; Ahn, J.H.; Kim, S.B. How shall we treat early triple-negative breast cancer (TNBC): From the current standard to upcoming immuno-molecular strategies. *ESMO Open* **2018**, *3*, e000357. doi:10.1136/esmoopen-2018-000357.

4. Bergin, A.R.T.; Loi, S. Triple-negative breast cancer: Recent treatment advances. *F1000Res.* **2019**, *8*. doi:10.12688/f1000research.18888.1.

5. Luciana, S.; Francisco Jaime Bezerra, M.-J.; Marcus, T.S. Editorial (Thematic Issue: Hybrid Compounds as Multitarget Agents in Medicinal Chemistry–Part II). *Curr. Top. Med. Chem.* **2017**, *17*, 957–958. doi:10.2174/156802661709170213205211.

6. de Oliveira Pedrosa, M.; Duarte da Cruz, R.M.; de Oliveira Viana, J.; de Moura, R.O.; Ishiki, H.M.; Barbosa Filho, J.M.; Diniz, M.F.F.M.; Scotti, M.T.; Scotti, L.; Bezerra Mendonca, F.J. Hybrid Compounds as Direct

Multitarget Ligands: A Review. *Curr. Top. Med. Chem.* **2017**, *17*, 1044–1079. doi:10.2174/1568026616666160927160620.

7.   Azizeh, A.; Jahan, B.G. Dual-acting of Hybrid Compounds–A New Dawn in the Discovery of Multi-target Drugs: Lead Generation Approaches. *Curr. Top. Med. Chem.* **2017**, *17*, 1096–1114. doi:10.2174/1568026616666160927151144.

8.   Hunyadi, A.; Martins, A.; Danko, B.; Chang, F.R.; Wu, Y.C. Protoflavones: A class of unusual flavonoids as promising novel anticancer agents. *Phytochem. Rev.* **2014**, *13*, 69–77. doi:10.1007/s11101-013-9288-2.

9.   Danko, B.; Martins, A.; Chuang, D.W.; Wang, H.C.; Amaral, L.; Molnar, J.; Chang, F.R.; Wu, Y.C.; Hunyadi, A. In vitro cytotoxic activity of novel protoflavone analogs–selectivity towards a multidrug resistant cancer cell line. *Anticancer Res.* **2012**, *32*, 2863–2870.

10. Pouny, I.; Etievant, C.; Marcourt, L.; Huc-Dumas, I.; Batut, M.; Girard, F.; Wright, M.; Massiot, G. Protoflavonoids from ferns impair centrosomal integrity of tumor cells. *Planta Med.* **2011**, *77*, 461–466. doi:10.1055/s-0030-1250407.

11. Tranah, G.J.; Manini, T.M.; Lohman, K.K.; Nalls, M.A.; Kritchevsky, S.; Newman, A.B.; Harris, T.B.; Miljkovic, I.; Biffi, A.; Cummings, S.R.; et al. Mitochondrial DNA variation in human metabolic rate and energy expenditure. *Mitochondrion* **2011**, *11*, 855–861. doi:10.1016/j.mito.2011.04.005.

12. Chang, H.-L.; Wu, Y.-C.; Su, J.-H.; Yeh, Y.-T.; Yuan, S.-S.F. Protoapigenone, a novel flavonoid, induces apoptosis in human prostate cancer cells through activation of p38 mitogen-activated protein kinase and c-Jun NH2-terminal kinase 1/2. *J. Pharmacol. Exp. Ther.* **2008**, *325*, 841–849. doi:10.1124/jpet.107.135442.

13. Lin, A.-S.; Chang, F.-R.; Wu, C.-C.; Liaw, C.-C.; Wu, Y.-C. New cytotoxic flavonoids from Thelypteris torresiana. *Planta Med.* **2005**, *71*, 867–870. doi:10.1055/s-2005-871292.

14. Chen, Y.-J.; Kay, N.; Yang, J.-M.; Lin, C.-T.; Chang, H.-L.; Wu, Y.-C.; Fu, C.-F.; Chang, Y.; Lo, S.; Hou, M.-F.; et al. Total synthetic protoapigenone WYC02 inhibits cervical cancer cell proliferation and tumour growth through PIK3 signalling pathway. *Basic Clin. Pharmacol. Toxicol.* **2013**, *113*, 8–18. doi:10.1111/bcpt.12057.

15. Chen, Y.-J.; Chen, H.-P.; Cheng, Y.-J.; Lin, Y.-H.; Liu, K.-W.; Hou, M.-F.; Wu, Y.-C.; Lee, Y.-C.; Yuan, S.-S. The synthetic flavonoid WYC02-9 inhibits colorectal cancer cell growth through ROS-mediated activation of MAPK14 pathway. *Life Sci.* **2013**, *92*, 1081–1092. doi:10.1016/j.lfs.2013.04.007.

16. Wang, H.C.; Lee, A.Y.; Chou, W.C.; Wu, C.C.; Tseng, C.N.; Liu, K.Y.; Lin, W.L.; Chang, F.R.; Chuang, D.W.; Hunyadi, A.; et al. Inhibition of ATR-dependent signaling by protoapigenone and its derivative sensitizes cancer cells to interstrand cross-link-generating agents in vitro and in vivo. *Mol. Cancer Ther.* **2012**, *11*, 1443–1453. doi:10.1158/1535-7163.mct-11-0921.

17. Chang, H.L.; Su, J.H.; Yeh, Y.T.; Lee, Y.C.; Chen, H.M.; Wu, Y.C.; Yuan, S.S. Protoapigenone, a novel flavonoid, inhibits ovarian cancer cell growth in vitro and in vivo. *Cancer Lett.* **2008**, *267*, 85–95. doi:10.1016/j.canlet.2008.03.007.

18. Chen, H.M.; Chang, F.R.; Hsieh, Y.C.; Cheng, Y.J.; Hsieh, K.C.; Tsai, L.M.; Lin, A.S.; Wu, Y.C.; Yuan, S.S. A novel synthetic protoapigenone analogue, WYC02-9, induces DNA damage and apoptosis in DU145 prostate cancer cells through generation of reactive oxygen species. *Free Radic. Biol. Med.* **2011**, *50*, 1151–1162. doi:10.1016/j.freeradbiomed.2011.01.015.

19. Chen, W.Y.; Hsieh, Y.A.; Tsai, C.I.; Kang, Y.F.; Chang, F.R.; Wu, Y.C.; Wu, C.C. Protoapigenone, a natural derivative of apigenin, induces mitogen-activated protein kinase-dependent apoptosis in human breast cancer cells associated with induction of oxidative stress and inhibition of glutathione S-transferase pi. *Investig. New Drugs* **2011**, *29*, 1347–1359. doi:10.1007/s10637-010-9497-0.

20. Dillon, M.T.; Harrington, K.J. Targeting ATR for Cancer Therapy: ATR-Targeted Drug Candidates. In *Targeting the DNA Damage Response for Anti-Cancer Therapy*; Pollard, J., Curtin, N., Eds.; Springer International Publishing: Manhattan, NY, USA, 26 May 2018; pp. 99–127. doi:10.1007/978-3-319-75836-7_5.

21. Lecona, E.; Fernandez-Capetillo, O. Targeting ATR in cancer. *Nat. Rev. Cancer* **2018**, *18*, 586–595. doi:10.1038/s41568-018-0034-3.

22. Sundar, R.; Brown, J.; Ingles Russo, A.; Yap, T.A. Targeting ATR in cancer medicine. *Curr. Probl. Cancer* **2017**, *41*, 302–315. doi:10.1016/j.currproblcancer.2017.05.002.

23. Yan, S.; Sorrell, M.; Berman, Z. Functional interplay between ATM/ATR-mediated DNA damage response and DNA repair pathways in oxidative stress. *Cell. Mol. Life Sci.* **2014**, *71*, 3951–3967. doi:10.1007/s00018-014-1666-4.

24. Hijova, E. Bioavailability of chalcones. *Bratisl. Lek. Listy* **2006**, *107*, 80–84.

25. Sharma, R.; Kumar, R.; Kodwani, R.; Kapoor, S.; Khare, A.; Bansal, R.; Khurana, S.; Singh, S.; Thomas, J.; Roy, B.; et al. A Review on Mechanisms of Anti Tumor Activity of Chalcones. *Anti-Cancer Agents Med. Chem.* **2015**, *16*, 200–211.

26. Karthikeyan, C.; Moorthy, N.S.; Ramasamy, S.; Vanam, U.; Manivannan, E.; Karunagaran, D.; Trivedi, P. Advances in chalcones with anticancer activities. *Recent Pat. Anti-Cancer Drug Discov.* **2015**, *10*, 97–115.

27. Mahapatra, D.K.; Bharti, S.K.; Asati, V. Anti-cancer chalcones: Structural and molecular target perspectives. *Eur. J. Med. Chem.* **2015**, *98*, 69–114. doi:10.1016/j.ejmech.2015.05.004.

28. Kocsis, L.; Szabo, I.; Bosze, S.; Jernei, T.; Hudecz, F.; Csampai, A. Synthesis, structure and in vitro cytostatic activity of ferrocene-Cinchona hybrids. *Bioorg. Med. Chem. Lett.* **2016**, *26*, 946–949. doi:10.1016/j.bmcl.2015.12.059.

29. Podolski-Renic, A.; Bosze, S.; Dinic, J.; Kocsis, L.; Hudecz, F.; Csampai, A.; Pesic, M. Ferrocene-cinchona hybrids with triazolyl-chalcone linkers act as pro-oxidants and sensitize human cancer cell lines to paclitaxel. *Metallomics* **2017**, *9*, 1132–1141. doi:10.1039/c7mt00183e.

30. Patra, M.; Gasser, G. The medicinal chemistry of ferrocene and its derivatives. *Nat. Rev. Chem.* **2017**, *1*, 1–12. doi:10.1038/s41570-017-0066.

31. Ramirez-Tagle, R.; Escobar, C.A.; Romero, V.; Montorfano, I.; Armisén, R.; Borgna, V.; Jeldes, E.; Pizarro, L.; Simon, F.; Echeverria, C. Chalcone-Induced Apoptosis through Caspase-Dependent Intrinsic Pathways in Human Hepatocellular Carcinoma Cells. *Int. J. Mol. Sci.* **2016**, *17*, 260. doi:10.3390/ijms17020260.

32. dos Santos, M.B.; Bertholin Anselmo, D.; de Oliveira, J.G.; Jardim-Perassi, B.V.; Alves Monteiro, D.; Silva, G.; Gomes, E.; Lucia Fachin, A.; Marins, M.; de Campos Zuccari, D.A.P.; et al. Antiproliferative activity and p53 upregulation effects of chalcones on human breast cancer cells. *J. Enzym. Inhib. Med. Chem.* **2019**, *34*, 1093–1099. doi:10.1080/14756366.2019.1615485.

33. Hunyadi, A.; Chuang, D.W.; Danko, B.; Chiang, M.Y.; Lee, C.L.; Wang, H.C.; Wu, C.C.; Chang, F.R.; Wu, Y.C. Direct semi-synthesis of the anticancer lead-drug protoapigenone from apigenin, and synthesis of further new cytotoxic protoflavone derivatives. *PLoS ONE* **2011**, *6*, e23922. doi:10.1371/journal.pone.0023922.

34. Zupko, I.; Molnar, J.; Rethy, B.; Minorics, R.; Frank, E.; Wolfling, J.; Molnar, J.; Ocsovszki, I.; Topcu, Z.; Bito, T.; et al. Anticancer and multidrug resistance-reversal effects of solanidine analogs synthetized from pregnadienolone acetate. *Molecules* **2014**, *19*, 2061–2076. doi:10.3390/molecules19022061.

35. Nicolov, M.; Ghiulai, R.M.; Voicu, M.; Mioc, M.; Duse, A.O.; Roman, R.; Ambrus, R.; Zupko, I.; Moaca, E.A.; Coricovac, D.E.; et al. Cocrystal Formation of Betulinic Acid and Ascorbic Acid: Synthesis, Physico-Chemical Assessment, Antioxidant, and Antiproliferative Activity. *Front. Chem.* **2019**, *7*, 92. doi:10.3389/fchem.2019.00092.

36. Roza, O.; Lai, W.C.; Zupkó, I.; Hohmann, J.; Jedlinszki, N.; Chang, F.R.; Csupor, D.; Eloff, J.N. Bioactivity guided isolation of phytoestrogenic compounds from Cyclopia genistoides by the pER8:GUS reporter system. *South Afr. J. Bot.* **2017**, *110*, 201–207. doi:10.1016/j.sajb.2016.06.001.

37. Stefkó, D.; Kúsz, N.; Csorba, A.; Jakab, G.; Bérdi, P.; Zupkó, I.; Hohmann, J.; Vasas, A. Phenanthrenes from Juncus atratus with antiproliferative activity. *Tetrahedron* **2019**, *75*, 116–120. doi:10.1016/j.tet.2018.11.039.

38. Chou, T.C. Theoretical basis, experimental design, and computerized simulation of synergism and antagonism in drug combination studies. *Pharmacol. Rev.* **2006**, *58*, 621–681. doi:10.1124/pr.58.3.10.

39. Sinka, I.; Kiss, A.; Mernyak, E.; Wolfling, J.; Schneider, G.; Ocsovszki, I.; Kuo, C.Y.; Wang, H.C.; Zupko, I. Antiproliferative and antimetastatic properties of 3-benzyloxy-16-hydroxymethylene-estradiol analogs against breast cancer cell lines. *Eur. J. Pharm. Sci.* **2018**, *123*, 362–370. doi:10.1016/j.ejps.2018.07.029.

40. Gyovai, A.; Minorics, R.; Kiss, A.; Mernyák, E.; Schneider, G.; Szekeres, A.; Kerekes, E.; Ocsovszki, I.; Zupkó, I. Antiproliferative Properties of Newly Synthesized 19-Nortestosterone Analogs Without Substantial Androgenic Activity. *Front. Pharmcol.* **2018**, *9*, 825–825. doi:10.3389/fphar.2018.00825.

41. Rostovtsev, V.V.; Green, L.G.; Fokin, V.V.; Sharpless, K.B. A Stepwise Huisgen Cycloaddition Process: Copper(I)-Catalyzed Regioselective "Ligation" of Azides and Terminal Alkynes. *Angew. Chem. Int. Ed.* **2002**, *41*, 2596–2599. doi:10.1002/1521-3773(20020715)41:14<2596::aid-anie2596>3.0.co;2-4.

42. Sommers, C.L.; Walker-Jones, D.; Heckford, S.E.; Worland, P.; Valverius, E.; Clark, R.; McCormick, F.; Stampfer, M.; Abularach, S.; Gelmann, E.P. Vimentin rather than keratin expression in some hormone-independent breast cancer cell lines and in oncogene-transformed mammary epithelial cells. *Cancer Res.* **1989**, *49*, 4258–4263.

43. Soule, H.D.; Vazquez, J.; Long, A.; Albert, S.; Brennan, M. A human cell line from a pleural effusion derived from a breast carcinoma. *J. Natl. Cancer Inst.* **1973**, *51*, 1409–1416. doi:10.1093/jnci/51.5.1409.

44. Visagie, M.H.; Mqoco, T.V.; Liebenberg, L.; Mathews, E.H.; Mathews, G.E.; Joubert, A.M. Influence of partial and complete glutamine-and glucose deprivation of breast-and cervical tumorigenic cell lines. *Cell Biosci.* **2015**, *5*, 37. doi:10.1186/s13578-015-0030-1.

45. Chiu, C.-C.; Chang, H.-W.; Chuang, D.-W.; Chang, F.-R.; Chang, Y.-C.; Cheng, Y.-S.; Tsai, M.-T.; Chen, W.-Y.; Lee, S.-S.; Wang, C.-K.; et al. Fern Plant–Derived Protoapigenone Leads to DNA Damage, Apoptosis, and G2/M Arrest in Lung Cancer Cell Line H1299. *DNA Cell Biol.* **2009**, *28*, 501–506. doi:10.1089/dna.2009.0852.

46. Meyer, F.; Becker, S.; Classen, S.; Parplys, A.C.; Mansour, W.Y.; Riepen, B.; Timm, S.; Ruebe, C.; Jasin, M.; Wikman, H.; et al. Prevention of DNA Replication Stress by CHK1 Leads to Chemoresistance Despite a DNA Repair Defect in Homologous Recombination in Breast Cancer. *Cells* **2020**, *9*, 238. doi:10.3390/cells9010238.

47. Olivier, M.; Eeles, R.; Hollstein, M.; Khan, M.A.; Harris, C.C.; Hainaut, P. The IARC TP53 database: New online mutation analysis and recommendations to users. *Hum. Mutat.* **2002**, *19*, 607–614.

48. Lu, X.; Errington, J.; Curtin, N.J.; Lunec, J.; Newell, D.R. The impact of p53 status on cellular sensitivity to antifolate drugs. *Clin. Cancer Res.* **2001**, *7*, 2114–2123.

49. Middleton, F.K.; Pollard, J.R.; Curtin, N.J. The Impact of p53 Dysfunction in ATR Inhibitor Cytotoxicity and Chemo- and Radiosensitisation. *Cancers* **2018**, *10*, 275.

50. Sun, N.; Xu, H.N.; Luo, Q.; Li, L.Z. Potential Indexing of the Invasiveness of Breast Cancer Cells by Mitochondrial Redox Ratios. *Adv. Exp. Med. Biol.* **2016**, *923*, 121–127. doi:10.1007/978-3-319-38810-6_16.

51. Theodossiou, T.A.; Wälchli, S.; Olsen, C.E.; Skarpen, E.; Berg, K. Deciphering the Nongenomic, Mitochondrial Toxicity of Tamoxifens As Determined by Cell Metabolism and Redox Activity. *ACS Chem. Biol.* **2016**, *11*, 251–262. doi:10.1021/acschembio.5b00734.

52. Theodossiou, T.A.; Olsen, C.E.; Jonsson, M.; Kubin, A.; Hothersall, J.S.; Berg, K. The diverse roles of glutathione-associated cell resistance against hypericin photodynamic therapy. *Redox Biol.* **2017**, *12*, 191–197. doi:10.1016/j.redox.2017.02.018.

53. Díaz-Tielas, C.; Graña, E.; Reigosa, M.J.; Sánchez-Moreiras, A.M. Biological activities and novel applications of chalcones. *Planta Daninha* **2016**, *34*, 607–616.

54. Jung, J.I.; Lim, S.S.; Choi, H.J.; Cho, H.J.; Shin, H.K.; Kim, E.J.; Chung, W.Y.; Park, K.K.; Park, J.H. Isoliquiritigenin induces apoptosis by depolarizing mitochondrial membranes in prostate cancer cells. *J. Nutr. Biochem.* **2006**, *17*, 689–696. doi:10.1016/j.jnutbio.2005.11.006.

II.

Article

Synthesis and In Vitro Antitumor Activity of Naringenin Oxime and Oxime Ether Derivatives

Ahmed Dhahir Latif [1,2,†,‡], **Tímea Gonda** [2,†], **Máté Vágvölgyi** [2], **Norbert Kúsz** [2], **Ágnes Kulmány** [1],
Imre Ocsovszki [3], **Zoltán Péter Zomborszki** [2], **István Zupkó** [1,4,*] and **Attila Hunyadi** [2,4,*]

[1] Institute of Pharmacodynamics and Biopharmacy, Interdisciplinary Excellence Centre, University of Szeged,
    6720 Szeged, Hungary; latif.ahmed@pharmacognosy.hu (A.D.L.); agnes.kulmany@gmail.com (Á.K.)
[2] Institute of Pharmacognosy, Interdisciplinary Excellence Centre, University of Szeged,
    6720 Szeged, Hungary; gonda.timea@pharm.u-szeged.hu (T.G.);
    vagvolgyi.mate@pharm.u-szeged.hu (M.V.); kusz.norbert@pharm.u-szeged.hu (N.K.);
    zombozope@pharmacognosy.hu (Z.P.Z.)
[3] Department of Biochemistry, University of Szeged, 6720 Szeged, Hungary; imre@biochem.szote.u-szeged.hu
[4] Interdisciplinary Centre for Natural Products, University of Szeged, 6720 Szeged, Hungary
[*] Correspondence: zupko@pharm.u-szeged.hu (I.Z.); hunyadi.a@pharm.u-szeged.hu (A.H.);
    Tel.: +36-62-546-839 (I.Z.); +36-62-546-456 (A.H.)
[†] These authors contributed equally to this work.
[‡] Previous address: Department of Pharmacology and Toxicology, Faculty of Medicine, Wasit Univesty,
    52001 Wasit, Iraq.

check for
updates

Abstract: Naringenin is one of the most abundant dietary flavonoids exerting several beneficial biological activities. Synthetic modification of naringenin is of continuous interest. During this study our aim was to synthesize a compound library of oxime and oxime ether derivatives of naringenin, and to investigate their biological activities. Two oximes and five oxime ether derivatives were prepared; their structure has been elucidated by NMR and high-resolution mass spectroscopy. The antiproliferative activity of the prepared compounds was evaluated by MTT assay against human leukemia (HL-60) and gynecological cancer cell lines isolated from cervical (HeLa, Siha) and breast (MCF-7, MDA-MB-231) cancers. *Tert*-butyl oxime ether derivative exerted the most potent cell growth inhibitory activity. Moreover, cell cycle analysis suggested that this derivative caused a significant increase in the hypodiploid (subG1) phase and induced apoptosis in Hela and Siha cells, and induced cell cycle arrest at G2/M phase in MCF-7 cells. The proapoptotic potential of the selected compound was confirmed by the activation of caspase-3. Antioxidant activities of the prepared molecules were also evaluated with xanthine oxidase, DPPH and ORAC assays, and the methyl substituted oxime ether exerted the most promising activity.

Keywords: naringenin-oxime; oxime ether; naringenin derivative; antioxidant; cell cycle analysis; antiproliferative; caspase activity

1. Introduction

Naringenin (**1**) is one of the most abundant dietary flavonoids predominantly found in citrus fruits and grapes. This compound exerts several beneficial pharmacological activities including antioxidant, antiviral, anti-inflammatory, anticarcinogenic and cardioprotective effects [1–3]. Several *in vitro* studies showed that naringenin can inhibit cell proliferation and migration, and that it can induce cell cycle arrest and apoptosis in cancer cell lines, including human leukemia, hepatocellular carcinoma, colon, bladder, uterine and breast cancer [4–11]. Due to these biological activities, the design and synthesis of new naringenin derivatives is of continuous interest. With modification of the phenolic groups,

several derivatives were synthesized. Esterification and alkylation of the 7-OH group with bulky substituents yielded compounds with improved anticancer effect against human colon cancer cells [12]. Such semi-synthetic modifications also afforded derivatives with significant anti-atherogenic effect in high-cholesterol fed rabbits [13]. Recently it was also found that a 4′- and 7-O-methylated naringenin derivative attenuates epileptic seizures in zebrafish and mouse models [14]. Modification on the keto group also yields pharmacologically interesting compounds. Synthetic thiosemicarbazone derivatives were found to exert antioxidative effects and demonstrated significant DNA binding properties [15].

The synthesis and characterization of naringenin *E*-oxime (NOX) has recently been reported. Investigation of its antioxidant and reactive oxygen species (ROS) scavenging properties demonstrated significantly enhanced activity as compared to naringenin itself [16,17]. Further studies confirmed that both naringenin and its *E*-oxime protect cells against hydrogen peroxide-induced oxidative damage [18]. Furthermore, NOX has recently been reported to exert protective effect against cisplatin induced hepatotoxicity, nephrotoxicity and genotoxicity in rats [19]. On the other hand, both naringenin and NOX were found to exert cytotoxic, genotoxic and apoptotic effects by increasing ROS levels in cancer cells, although very high doses were needed (cytotoxic IC_{50} values ranged from ca. 500 to 1000 μM) [20]. Apart from the pharmacological investigations, the chelating capability of NOX makes this compound also interesting from the chemical point of view. The synthesis of Ni(II)-NOX complex was reported, and the prepared ligand was successfully applied in Mizoroki-Heck reaction as a catalyst [21]. In a more recent study, *E*-oximes were prepared from several *O*-alkyl derivatives of naringenin and demonstrated to exert stronger cytotoxic activity on HT-29 cells as compared to their respective parent compounds [22]. However, even though the synthesis and pharmacological investigation of naringenin oxime is reported in several articles [16–21], only a few oxime ether derivatives have been mentioned in the literature [23].

During the current work, our aim was to synthesize a set of oxime and oxime ether derivatives of naringenin, and to test their antitumor activity on different cancer cell lines as well as their antioxidant capacity.

2. Results and Discussion

2.1. Synthesis of Naringenin Oximes and Naringenin Oxime Ethers

Oxime derivatives of racemic naringenin (**1**) were synthesized by using hydroxylamine hydrochloride in the presence of potassium hydroxide and ethanol as solvent. The reaction afforded racemates of two geometric isomers (**2** and **3**), purified by column chromatography and characterized by NMR and HRMS. The ^{1}H NMR spectrum of compound **3** displayed resonances of a para disubstituted benzene ring (δ_H 7.18 and 6.75, d, *J* = 8.2 Hz), the overlapping signals of two meta coupled aromatic protons (δ_H 5.87 br s), and an isolated –CH(O)–CH$_2$– spin system (δ_H 5.45 br t, *J* = 9.5 Hz; 3.92 dd, *J* = 10.5 Hz, 17.9 Hz; 3.44 dd, *J* = 8.6 Hz, 17.9 Hz). In the ^{13}C NMR spectrum 15 carbon resonances were detected, which were then categorized based on their chemical shifts and HSQC cross peaks. The structure of compound **3** was finally established by means of an HMBC experiment. It was obvious that compounds **2** and **3** only differ in the oxime configuration, as suggested by the considerably downfield-shifted C-3 and H-3a/b in compound **3** as compared to **2** (δ_H 3.44 dd and 3.92 dd vs. 2.77 dd and 3.25 dd; δ_C 45.7 vs. 29.0). Compound **2** was identified as the *E* isomer of naringenin oxime by the literature data [16], thus the minor compound **3** had to be the *Z* isomer. When a ketone is converted into a corresponding oxime derivative, signals of the carbonyl carbon and both adjacent α-carbons shift upfield, and the extent of these changes show a consistent pattern since the α-syn carbons are always more shielded than the α-anti carbons [24]. This structural feature was also clearly seen in compounds **2** and **3**, which further supports the assignation of the two isomers. It is also worth mentioning that the steric hindrance present in compound **3** explains why the formation of the *E* isomer is energetically more favorable. According to HPLC measurements on the crude product mixture, the major and minor products were formed at a ratio of 91:9 during the reaction. Notably, while the preparation of the

E isomer was discussed in several articles [16–23], this is the first evidence on the formation of the *Z* isomer.

An oxime ether library (**4–8**) was also prepared from naringenin (**1**). Five derivatives were synthesized applying methoxy-, ethoxy-, *tert*-butoxy-, allyloxy-, and benzyloxyamine hydrochloride in pyridine. In all cases, the exclusive formation of the *E* isomer was detected (Figure 1). After purification by flash chromatography, the structures were confirmed by NMR and HRMS techniques.
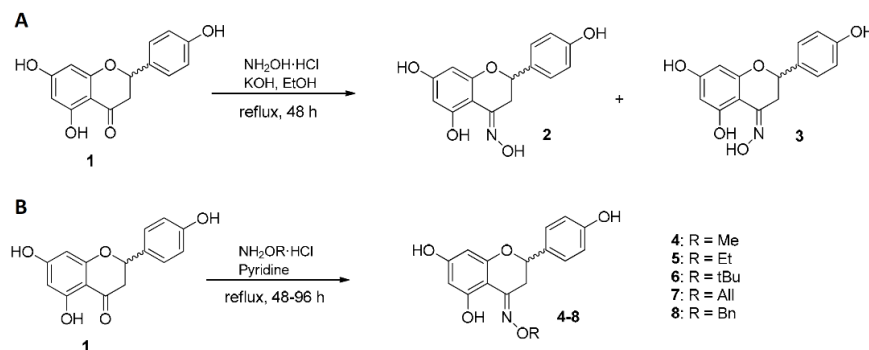
Figure 1. Synthesis of naringenin oximes (**2** and **3**) (**A**) and oxime ethers (**4–8**) (**B**).

2.2. Biological Activity

2.2.1. Antiproliferative Assay

Antiproliferative activity of naringenin (**1**) and the prepared oximes (**2**, **3**) and oxime ethers (**4–8**) was determined in vitro against five human cancer cell lines, including adherent gynecological cell lines isolated from cervical (HeLa, Siha) and breast (MCF-7, MDA-MB-231) carcinomas, and a human leukemia (HL-60) cell line. Two concentrations (25 and 50 µM) were selected for initial bioactivity screening by using an MTT assay, and IC_{50} values were calculated only for those compounds which elicited higher than 75% growth inhibition at 50 µM (Table 1).

Among the tested compounds, the *tert*-butyl substituted derivative (**6**) exerted the most potent antiproliferative effect on the tested cancer cell lines. In contrast, neither naringenin (**1**) nor the *Z*-oxime (**3**) inhibited the growth of the tested cancer cell lines at any of the applied concentrations. In case of the allyl-derivative (**7**) and the *E* oxime (**2**) only a limited growth inhibition was observed. The benzyl-derivative (**8**) exerted moderate growth inhibition on MCF-7 cells, similarly to the methyl derivative (**4**) on HL-60 cells. Our results confirm the previous evidences [20,23] on the increased (but still very weak) antiproliferative activity of naringenin *E*-oxime as compared to that of naringenin (**1**). Further, we show for the first time that the *E*-oxime ethers are much more potent in this regard, particularly if the ether is a bulky alkyl group as in compound **6**. No marked cell line selective action could be demonstrated, though HeLa and MCF-7 cells seem to be more sensitive than SiHa and the triple negative MDA-MB-231 cells.

Table 1. Antiproliferative activities of naringenin and its oxime derivatives against four human gynecological cancer cell lines and HL-60 leukemia cells. Cisplatin was used as positive control; SEM: standard error of the mean; $n = 5$.

Compound	Conc. (µM)	Growth Inhibition (%) ± SEM (Calculated IC$_{50}$ Value (µM))				
		HeLa	SiHa	MCF-7	MDA-MB-231	HL-60
(1)	25	<20	<20	<20	<20	<20
	50	23.9 ± 2.09	<20	<20	<20	<20
(2)	25	<20	<20	<20	<20	<20
	50	28.75 ± 2.44	<20	21.83 ± 3.92	<20	43.40 ± 2.81
(3)	25	<20	<20	<20	<20	<20
	50	<20	<20	<20	<20	<20
(4)	25	<20	<20	<20	<20	37.67 ± 1.29
	50	31.36 ± 2.97	<20	48.44 ± 3.27	24.35 ± 1.88	57.89 ± 1.13
(5)	25	<20	<20	<20	<20	<20
	50	29.36 ± 1.42	<20	44.06 ± 2.18	<20	44.89 ± 0.48
(6)	25	52.37 ± 2.32	<20	61.41 ± 1.93	27.19 ± 1.78	37.31 ± 3.65
	50	92.22 ± 1.03	88.54 ± 1.51	87.00 ± 0.61	90.33 ± 0.58	88.07 ± 0.10
		[23.49]	[35.41]	[19.46]	[29.74]	[31.76]
(7)	25	<20	<20	<20	<20	<20
	50	25.04 ± 2.4	<20	33.75 ± 2.45	<20	<20
(8)	25	22.63 ± 0.63	<20	24.29 ± 1.86	<20	<20
	50	37.67 ± 2.01	<20	64.47 ± 2.12	24.87 ± 3.47	<20
Cisplatin	25	98.71 ± 0.21	86.40 ± 1.02	90.81 ± 0.22	41.37 ± 1.05	64.03 ± 0.43
	50	99.09 ± 0.24	96.72 ± 0.36	98.49 ± 0.11	84.43 ± 0.4	84.88 ± 0.41
		[11.79]	[13.63]	[5.15]	[25.82]	[5.75]

2.2.2. Cell Cycle Analysis

Based on its outstanding efficacy, compound **6** was selected to subject additional in vitro assays including cell cycle analyses by flow cytometry to characterize the mechanism of action. Cells were treated with compound **6** for 24 h at concentrations corresponding to its half IC$_{50}$ or IC$_{50}$ values, i.e., 12 or 24 µM for HeLa, 18 or 36 µM for SiHa, 10 or 20 µM for MCF-7, and 15 or 30 µM for MDA-MB-231 (Figure 2).

A significant increase in the hypodiploid (subG1) phase was found only in HeLa and SiHa cells after the treatment with the higher concentrations (24 and 36 µM, respectively), indicating the induction of apoptosis in these cell lines. In addition, SiHa exhibited significant accumulation of cells in G1 phase with a corresponding decrease in the fraction of cells in the S phase, which may be a consequence of blockade of the G1–S transition of the cell cycle. In HeLa cells, however, significant decrease was observed in the G1 phase accompanied by a significant increase in the S phase. In case of the MCF-7 cells, the proportion of cells in the G1 and G2/M phase increased, whereas the proportion in the S phase decreased, suggesting cell cycle arrest at G1 and G2/M phase. On the other hand, no substantial action was observed on MDA-MB-231 cells at 15 and 30 µM concentrations after 24 h of treatment. Our results indicate that compound **6** induced apoptosis in HeLa and Siha cell lines and exerted a disturbance in the cell cycle.
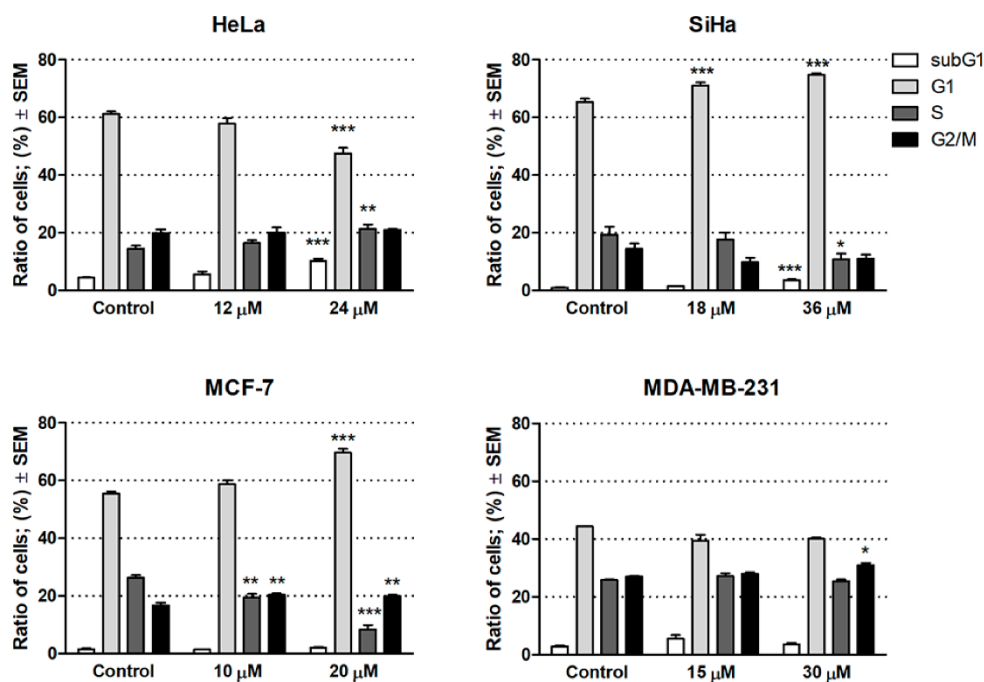
Figure 2. Cell cycle distributions of human gynecological cancer cell lines HeLa, SiHa, MCF-7 and MDA-MB-231 after treatment with compound **6**. *, ** and *** indicate $p < 0.05$, $p < 0.01$ and $p < 0.001$, respectively, by means of one-way ANOVA followed by Dunnett's post-hoc test.

2.2.3. Caspase Activity

As the *tert*-butyl derivative (**6**) exerted pronounced antiproliferative activity by inducing apoptosis, its effect on caspase-3 activity was also tested. HeLa cells were treated for 24 h with compound **6** in two different concentrations (12 and 24 μM). Compound **6** induced a concentration-dependent and significant increase of caspase-3 activity (Figure 3).
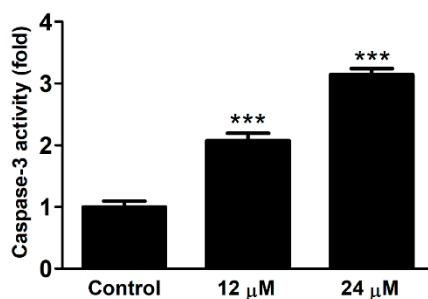
Figure 3. Effect of compound 6 on the caspase-3 activity in HeLa cells as compared to the untreated control. Results are means ± standard error of the mean from 5 replicates. *** indicates $p < 0.001$, by means of one-way ANOVA followed by Dunnett's post-hoc test.

2.2.4. Antioxidant Activity

Antioxidant activity of naringenin (**1**) and its oxime derivatives (**2**–**8**) was analyzed through assessing their capacity to scavenge diphenyl-2-picrylhydrazyl (DPPH) radical and determining their oxygen radical absorbance capacity (ORAC) and xanthine-oxidase (XO) inhibitory activity (Table 2).

Table 2. Antioxidant activity of compounds **1–8**. TE: trolox equivalent; XO inh: xanthine oxidase inhibition. [a] Compounds eliciting less than 50% scavenging of diphenyl-2-picrylhydrazyl (DPPH) at the highest applied concentration were considered inactive and the numerical results are not presented; [b] inhibition % at 330 μM, n.d.: not determined; SD: standard deviation.

Compound	Antioxidant Activity ± SD		
	DPPH EC$_{50}$ (μM)	ORAC (μmolTE/μmol)	XO inh (%)
1	- [a]	11.18 ± 0.46	12.31 ± 4.60 [b]
2	243.45 ± 4.88	8.88 ± 0.23	7.35 ± 1.32
3	1776.00 ± 123.71	6.95 ± 0.12	2.13 ± 0.78
4	212.20 ± 32.59	16.63 ± 1.68	4.00 ± 1.81
5	1437.50 ± 36.06	5.54 ± 0.41	8.13 ± 2.02
6	-	3.89 ± 0.87	6.95 ± 2.31
7	1164.00 ± 226.27	6.03 ± 2.79	12.84 ± 3.01
8	-	1.38 ± 0.41	9.06 ± 0.79
Rutin	39.88 ± 1.34	12.35 ± 0.38	n.d.
Allopurinol	n.d.	n.d.	98.23 ± 3.29

Previously, Türkkan et al. showed that the 4-oxime substitution increases the antioxidant activity of naringenin [16], which here we can confirm concerning the DPPH scavenging activity. However, it is now also clear that a favorable increase in this activity can only be observed for the *E*-oxime (**2**). While it is still stronger DPPH scavenger than naringenin (**1**), the *Z*-oxime (**3**) was an order of magnitude weaker in this regard than the *E*-oxime (**2**). However, regardless of the orientation of the oxime, the ORAC activity of both compounds **2** and **3** was decreased as compared to naringenin (**1**). Surprisingly, the oxime methyl ether derivative (**4**) showed the highest antioxidant activity in both the DPPH and the ORAC assays, and this was the only compound that was more potent in the ORAC assay than the positive control rutin. Since rutin has a catechol-type B-ring that makes it a particularly efficient ROS scavenger, this finding suggests that an oxime methyl ether moiety on the flavanone C-ring is highly favorable in terms of such activity. Accordingly, it may be hypothesized that the 4-oxime methyl ether of eriodictyol (the catechol B-ring analog of naringenin) would be an even stronger antioxidant in vitro. All other compounds, including the *tert*-butyl derivative **6**, exhibited much weaker antioxidant activity than rutin, and they were also proven practically inactive in terms of XO inhibition.

Structure-activity relationships observed for the antioxidant activity of naringenin oxime derivatives did not show any apparent correlation to those of the in vitro antiproliferative activity, suggesting that the antitumor potential of these compounds is likely not, or at least not entirely due to their antioxidant properties. Further studies are needed to reveal the exact mechanism of action. Nevertheless, it is now clear that the introduction of a bulky alkyl (e.g., *tert*-butyl) group as an oxime ether to the flavanone B-ring greatly increases the antitumor potential of such compounds, which finding shows new paths towards the design and optimization of new, bioactive flavonoid analogs.

3. Materials and Methods

3.1. Chemical Methods

Starting material naringenin (purity: 98%) was purchased from Indofine Chemical Company Inc. (Hillsborough, NJ, USA), and used without further purification. All reagents were purchased from Sigma (Sigma Aldrich Co., St. Louis, MO, USA). Ethanol 96% was obtained from Molar Chemicals Ltd. (Halásztelek, Hungary). Reaction progress was monitored by normal phase thin-layer chromatography (TLC) (Silica gel 60F254, E. Merck, Darmstadt, Germany). Purification was carried out applying flash chromatography on a CombiFlash Rf+ Lumen Instrument (Teledyne Isco, Lincoln, NE, USA) with integrated UV-Vis, photodiode-array (PDA) and evaporative light-scattering (ELS) detection on commercially available pre-filled columns (Teledyne Isco, Lincoln, NE, USA) for normal-phase separations in a detection range of 210–366 nm. Naringenin oximes and oxime ethers were characterized

by means of NMR and MS. ^{1}H (500.1 MHz) and ^{13}C (125.6 MHz) NMR spectra were recorded on a Bruker Avance DRX-500 spectrometer (Bruker, Billerica, MA, USA).

3.2. Cell Culture

All cell lines were obtained from ECCAC (European Collection of Cell Cultures, Salisbury, UK) except the SiHa and human leukemia cells HL-60, which were obtained from ATCC (American Tissue Culture Collection, Manassas, VA, USA). The human gynecological cancer cell lines were cultivated in minimal essential medium (MEM) supplemented with 10% fetal bovine serum, 1% non-essential amino acids and an antibiotic–antimycotic mixture. HL-60 cells were grown in RPMI 1640 medium containing 10% heat inactivated fetal calf serum (FCS), 1% L-glutamine, and 1% penicillin-streptomycin. The cell lines were cultured at 37 °C in a humidified atmosphere 5% CO_2. All media and chemicals used in our experiment, if otherwise not specified, were purchased from from Lonza Group Ltd. (Basel, Switzerland) and Sigma-Aldrich Ltd. (Budapest, Hungary). [25,26].

3.3. Antiproliferative Assay

Inhibitory growth effects of the compounds evaluated on human leukemia cells (HL-60) and human gynecological adherent cancer cell lines (HeLa, SiHa, MCF-7, MDA-MB-231) isolated from cervical and breast cancer has been carried out according to our previously published procedures [27,28] by using MTT ([3-(4,5 dimethylthiazol-2-yl)-2,5-diphenyltetrazolium bromide]) assay. Briefly, adherent cells were seeded in 96-well microplates (5000 cells/well) and overnight preincubation allowed attachment to the bottom of the well before treatment, while the HL-60 cells seeded at 10,000 cells/well and treated the same day. Thereafter, 50 mM of the compounds were dissolved in dimethyl sulfoxide (DMSO), and the cells were treated with two concentrations (25 and 50 μM) and incubated for 72 h. Then the solution of 5 mg/mL MTT was added to the samples and incubated for another 4 h. For adherent cancer cell lines, the medium was removed, and the precipitated crystals were dissolved by adding 100 μL DMSO under stirring for 1 h, at 37 °C and the absorbance was read at 545 nm, using a microplate reader. In the case of leukemia cells, the precipitated crystals were dissolved in 10% sodium dodecyl sulfate with acid HCl 0.01 mM, and incubated for 24 h, the absorbance was read at 545 and 630 nm. The determination of the antiproliferative compound was repeated with a set of dilutions (1–50 μM) to calculate the IC_{50} value. Calculations and statistical analyses (One-Way ANOVA followed by Dunnett's post-hoc test) were performed by Graph Pad Prism 5.01 (Graph Pad Software; San Diego, CA, USA). All measurements in all experiments were carried out in duplicate reading with at least five parallel wells.

3.4. Cell Cycle Analysis

Estimation of cellular DNA content has been carried out using flow cytometric analysis with DNA-specific fluorescent dye, propidium iodide (PI) as published before [29]. Briefly, adherent cancer cells were plated in a 6-well plate at a density of 400,000 cells/well, and allowed to grow for 24 h, cells were treated with the compound in two concentrations: 12 to 24 μM for Hela; 18 to 36 μM for Siha; 15 to 30 μM for MDA-MB-231 and 10 to 20 μM for MCF-7 with incubation period of 24 h. The cells were washed with phosphate-buffered saline (PBS), following dissociation with trypsin, cells were centrifuged at 2200 rpm, 4 °C for 15 min. After the washing step, the cells were fixed in 1 mL 70% cold ethanol which was added dropwise to the cell pellet and the cells were kept at −20 °C until DNA staining. Prior to analysis, the cells were stained with 300 μL dye solution containing 0.02 mg/mL RNAse A, 0.1 mg/mL PI, 0.003 mL/mL Triton-X and 1.0 mg/mL sodium citrate in distilled water, incubated in the dark place for 60 min at room temperature. Finally, 700 μL PBS was added and mixed to the sample. Flow cytometric analyses were carried out using a flow cytometer PartecCyFlow instrument (Partec GmbH, Münster, Germany). In each analysis, 20,000 events were counted, and ModFit Software (Verity Software House, Topsham, ME, USA) was used to determine the different percentages of cell cycle phases (subG1, G1, S and G2/M). The results were statistically evaluated by

Graph Pad Prism 5.0. (GraphPad Software Inc., San Diego, CA, USA) using one-way ANOVA for two biological replicates.

3.5. Caspase Activity

Caspase-3 activity was determined by using Caspase-3 Colorimetric Assay Kit as published before [30]. Briefly, HeLa cells were seeded at 12 million cells /flask density and allowed to grow overnight. The cells were treated with compound 6 and incubated for 24 h. Then they were scraped, centrifuged and washed with physiological buffer saline, re-suspended in lysis buffer (1 million cells/10 μL) and incubated on ice for 20 min, then cold centrifuged (16,000× g, 4 °C for 15 min). Then the supernatant was used for measurement of caspase-3 activity. The concentration of the protein was measured with the substrate Assay Kit, by incubating 5.0 μL of treated and untreated lysates samples with 10 μL selective caspase-3 substrate in a final volume of 100 μL in assay buffer, and for the experiment control 5.0 μL of 24 μM sample was added with 10 μL caspase-3 substrate and 10 μL caspase-3 inhibitor, in a final volume of 100 μL in assay buffer in 96-well plates. After an incubation period of 24 h at 37 °C, 5% CO_2, the absorbance was measured at 405 nm with a microplate reader. The results were statistically evaluated by Graph Pad Prism 5.0. using one-way ANOVA.

3.6. Antioxidant Activity

3.6.1. Diphenyl-2-picrylhydrazyl (DPPH) Assay

DPPH (1,1′-diphenyl-2-picrylhydrazyl) was purchased from Sigma-Aldrich Hungary. DPPH free radical scavenging assay was performed according to the method of Fukomoto et al. [31] with some modifications. The measurement was carried out on a 96-well microplate. Microdilution series of samples (10 mM stock solution, dissolved in DMSO) were made starting with 150 μL. To each well 50 μL of DPPH reagent (100 μM in HPLC grade MeOH) was added to gain 200 μL working volume. The microplate was stored at room temperature in dark conditions. The absorbance was measured after 30 min at 550 nm using a FluoStar Optima plate reader (software version 2.20R2, BMG Labtech Ortenberg, Germany). For the blank control DMSO was used instead of the sample. As a standard, rutin (0.01 mg/mL, in HPLC grade MeOH) was used. The scavenging activity was calculated as Inhibition (%) = $(A_0 − A_s)/A_0 × 100$, and EC_{50} values were calculated by Graph Pad Prism 6.05 software.

3.6.2. Oxygen Radical Absorbance Capacity (ORAC) Assay

AAPH ((2,2′-Azobis(2-methyl-propionamidine) dihydrichloride) free radical and trolox standard ((±)-6hydroxy-2,5,7,8-tetramethyl-chromane-2-carboxylic acid) were purchased from Sigma-Aldrich Hungary. Fluorescein was purchased from Fluka Analytical, Tokyo, Japan. The ORAC assay was carried out on a 96-well microplate according to the method of Mielnik et al. [32]. Briefly, 20 μL of extracts (stock solution concentration of 0.002 mM) were mixed with 60 μL of AAPH (12 mM final concentration) and 120 μL of fluorescein solution (70 nM final concentration), then the fluorescence was measured through 3 h with 1.5-min cycle intervals with a BMG Labtech FluoStar Optima plate-reader. All experiments were carried out in triplicate, and trolox was used as standard. The antioxidant capacity was expressed as μM Trolox Equivalent per μM of pure compound (μM TE/μM), as calculated by Graph Pad Prism 6.05.

3.6.3. Xantine-Oxidase Inhibitory Assay

To assess xanthine-oxidase (XO) inhibitory activity, a continuous spectrophotometric rate determination was used, based on a modified protocol of Sigma. The absorbance of XO-induced uric acid production from xanthine was measured at 290 nm for 3 min in a 96-well plate on a BMG Labtech FluoStar Optima plate-reader. The XO-inhibitory effect was determined via the decreased production of uric acid. The samples (10 mM stock solution) were prepared in DMSO. For enzyme-activity control,

the final reaction mixture comprised of 100 µL of xanthine solution (0.15 mM, pH = 7.5), 150 µL of buffer (potassium phosphate with 1 M KOH, pH = 7.5) and 50 µL of XO (0.2 units/mL) in a 300 µL well. The reaction mixture for inhibition was made with 100 µL of xanthine, 140 µL of buffer, 10 µL of sample and 50 µL of XO. Allopurinol was used as positive control. Test compound samples were added in appropriate volumes so that the final concentration of DMSO in the assay did not exceed 3.3% of the total volume. All experiments were conducted in triplicates. The reaction was initiated by the automatic addition of 50 µL of XO solution to a final concentration of 0.006 units/mL. The inhibitory percentage values were calculated by using Graph Pad Prism 6.05 software.

4. Experimental

4.1. Procedure for the Synthesis of Naringenin-Derived Oximes

Naringenin (1.00 g) was dissolved in 100 mL EtOH, then 3 equiv. of KOH (0.62 g) and 3 equiv. of hydroxylamine hydrochloride (0.77 g) were added. The reaction mixture was refluxed for 48 h, then the solvent was evaporated under vacuo. The residue was re-dissolved in water (100 mL) and the aqueous phase was extracted with EtOAc (3×100 mL). The organic phase was combined and dried (Na_2SO_4), then evaporated to dryness. The crude product was purified by flash chromatography using *n*-hexane—EtOAc—formic acid (15:4:0.25, *v/v/v*) solvent system on silica.

(E)-5,7-dihydroxy-2-(4-hydroxyphenyl)chroman-4-one oxime (**2**)

Yield: 38%, white solid. ^{1}H NMR (500 MHz, DMSO-d_6): δ 11.23 (1H, s), 11.20 (1H, br s), 9.80 (1H, br s), 9.53 (1H, br s), 7. 28 (2H, d, *J* = 8.4 Hz), 6.78 (2H, d, *J* = 8.4 Hz), 5.90 (1H, d, *J* = 1.8 Hz), 5.85 (1H, d, *J* = 1.8 Hz), 5.02 (1H, dd, *J* = 2.5 Hz, 11.5 Hz), 3.25 (1H, dd, *J* = 2.7 Hz, 17.0 Hz), 2.77 (11.7 Hz, 17.0 Hz). ^{13}C NMR (MHz, DMSO-d_6): δ 160.3, 159.1, 157.9, 157.5, 153.3, 129.9, 128.0, 115.1, 97.0, 96.4, 95.2, 75.8, 29.0 HR-HESI-MS $C_{15}H_{14}NO_5$ [M + H]$^+$ calcd. 288.0871, found: 288.0884.

(Z)-5,7-dihydroxy-2-(4-hydroxyphenyl)chroman-4-one oxime (**3**)

Yield: 3%, white solid. ^{1}H NMR (500 MHz, DMSO-d_6): δ 10.25 (2H, br s), 9.75 (1H, br s), 9.50 (1H, br s), 7.18 (2H, d, *J* = 8.2 Hz), 6.75 (2H, d, *J* = 8.2 Hz), 5.87 (2H, s), 5.45 (1H, br t, *J* = 9.5 Hz), 3.92 (1H, dd, *J* = 10.5 Hz, 17.9 Hz), 3.44 (1H, dd, *J* = 8.6 Hz, 17.9 Hz). ^{13}C NMR (MHz, DMSO-d_6): δ 160.7, 158.9, 157.8, 157.3, 153.9, 130.7, 127.7, 115.3, 95.3, 94.7, 80.2, 45.7. HR-HESI-MS $C_{15}H_{14}NO_5$ [M + H]$^+$ calcd. 288.0871, found: 288.0888.

4.2. General Procedure for the Synthesis of Naringenin Oxime Ethers

To begin with, 100 mg naringenin was dissolved in 15 mL pyridine, then 3 equiv. of the corresponding alkyl or aryloxyhydroxylamine hydrochloride were added and the mixture was refluxed for 48–96 h. When the reaction was completed (monitored by means of TLC), the solvent was evaporated under vacuo. Water (50 mL) was added to the residue and the aqueous phase was extracted with EtOAc (3×50 mL). The combined organic phase was dried over Na_2SO_4, filtered and evaporated to dryness. Each crude product was purified with flash chromatography on silica.

(E)-5,7-dihydroxy-2-(4-hydroxyphenyl)chroman-4-one *O*-methyl oxime (**4**)

Purified by using *n*-hexane—EtOAc—formic acid (15:4:0.25, *v/v/v*), yield: 18%, white solid. ^{1}H NMR (500 MHz, DMSO-d_6): δ10.71 (1H, s), 9.98 (1H, br s), 9.58 (1H, br s), 7.27 (2H, d, *J* = 8.3 Hz), 6.77 (2H, d, *J* = 8.3 Hz), 5.92 (1H, br s), 5.87 (1H, br s), 5.03 (1H, dd, *J* = 2.4 Hz, 11.9 Hz), 3.88 (3H, s), 3.23 (1H, dd, *J* = 2.4 Hz, 17.1 Hz), 2.82 (1H, dd, *J* = 11.9 Hz, 17.1 Hz). ^{13}C NMR (MHz, DMSO-d_6): δ 161.1, 159.1, 158.4, 157.5, 154.4, 129.6, 128.1, 115.2, 96.5, 96.2, 95.5, 75.6, 62.1, 29.5. HR-HESI-MS $C_{16}H_{16}NO_5$ [M + H]$^+$ calcd. 302.1028, found: 302.1023.

(E)-5,7-dihydroxy-2-(4-hydroxyphenyl)chroman-4-one *O*-ethyl oxime (**5**)

Purified by dichloromethane—methanol (99:1, *v/v*), yield: 52%, white solid. ^{1}H NMR (500 MHz, DMSO-d_6): δ 10.82 (1H, s), 9.94 (1H, br s), 9.55 (1H, br s), 7.28 (2H, d, *J* = 8.5 Hz), 6.77 (2H, d, *J* = 8.5 Hz), 5.92 (1H, d, *J* = 2.2 Hz). 5.87 (1H, d, *J* = 2.2 Hz), 5.03 (1H, dd, *J* = 2.7 Hz, 11.9 Hz), 4.13 (2H, m), 3.23 (1H, dd, *J* = 2.7 Hz, 17.1 Hz), 2.83 (1H, dd. *J* = 11.9 Hz, 17.1 Hz), 1.24 (3H, t, *J* = 7.0 Hz).^{13}C NMR (MHz, DMSO-d_6): δ 160.9, 159.1, 158.4, 157.6, 154.1, 129.6, 128.2, 115.1, 96.5, 96.4, 96.4, 75.7, 69.6, 29.6, 14.2. HR-HESI-MS $C_{17}H_{18}NO_5$ [M + H]$^+$ calcd. 316.1185, found: 316.1181.

(E)-5,7-dihydroxy-2-(4-hydroxyphenyl)chroman-4-one *O*-(tert-butyl) oxime (**6**)

Purified by dichloromethane—methanol (99:1, *v/v*), yield: 53%, white solid. ^{1}H NMR (500 MHz, DMSO-d_6): δ 11.10 (1H, s), 9.90 (1H, br s), 9.55 (1H, br s), 7.28 (2H, d, *J* = 8.5 Hz), 6.77 (2H, d, *J* = 8.5 Hz), 5.91 (1H, d, *J* = 2.2 Hz). 5.86 (1H, d, *J* = 2.2 Hz), 5.03 (1H, dd, *J* = 2.6 Hz, 11.9 Hz), 3.21 (1H, dd, *J* = 2.6 Hz, 17.1 Hz), 2.82 (1H, dd, *J* = 11.9 Hz, 17.1 Hz), 1.29 (9H, s). ^{13}C NMR (MHz, DMSO-d_6): δ160.7, 159.1, 158.3, 157.6, 153.5, 129.7, 128.2, 115.1, 96.9, 96.4, 95.4, 78.9, 75.9, 29.6, 27.1. HR-HESI-MS $C_{19}H_{22}NO_5$ [M + H]$^+$ calcd. 344.1498, found: 344.1496.

(E)-5,7-dihydroxy-2-(4-hydroxyphenyl)chroman-4-one *O*-allyl oxime (**7**)

Purified by dichloromethane—methanol (95:5, *v/v*), yield: 58%, white solid. ^{1}H NMR (500 MHz, DMSO-d_6): δ 10.72 (1H, s), 9.95 (1H, br s), 9.54 (1H, br s), 7.28 (2H, d, *J* = 8.5 Hz), 6.77 (2H, d, *J* = 8.5 Hz), 5.99 (1H, m), 5.91 (1H, d, *J* = 2.2 Hz), 5.86 (1H, d, *J* = 2.2 Hz), 5.35 (1H, dd, *J* = 1.3 Hz, 17.3 Hz), 5.25 (1H, br d, *J* = 10.4 Hz), 5.05 (1H, dd, *J* = 2.7 Hz, 11.8 Hz), 4.60 (2H, d, *J* = 5.7 Hz), 3.25 (1H, dd, *J* = 2.7 Hz, 17.1 Hz), 2.86 (1H, dd, *J* = 11.8 Hz, 17.1 Hz).^{13}C NMR (MHz, DMSO-d_6): δ 161.0, 159.1, 158.4, 157.5, 154.4, 134.1, 129.6, 123.1, 118.5, 115.1, 96.5, 96.4, 95.4, 75.7, 74.6, 29.6. HR-HESI-MS $C_{19}H_{22}NO_5$ [M + H]$^+$ calcd. 344.1498, found: 344.1496.

(E)-5,7-dihydroxy-2-(4-hydroxyphenyl)chroman-4-one *O*-benzyl oxime (**8**)

Purified by dichloromethane—methanol (99:1, *v/v*): yield: 5%, white solid. ^{1}H NMR (500 MHz, DMSO-d_6): δ 10.63 (1H, s), 9.94 (1H, s), 9.53 (1H, s), 7.42–7.32 (5H, m), 7.26 (2H, d, *J* = 8.4 Hz), 6.76 (2H, d, *J* = 8.4 Hz), 5.87 (1H, d, *J* = 2.2 Hz), 5.85 (1H, d, *J* = 2.2 Hz), 5.14 (2H, s), 5.04 (1H, dd, *J* = 2.9 Hz, 11.7 Hz), 3.25 (1H, dd, *J* = 3.0 Hz, 17.1 Hz), 2.90 (1H, dd, *J* = 11.7 Hz, 17.1 Hz). ^{13}C NMR (MHz, DMSO-d_6): δ 161.0, 159.0, 158.3, 157.5, 154.6, 137.2, 129.5, 128.4, 128.4 128.1, 128.0, 115.1, 96.5, 96.3, 95.4, 75.6, 75.6, 29.5. HR-HESI-MS $C_{22}H_{20}NO_5$ [M + H]$^+$ calcd. 378.1341, found: 378.1342.

Conflicts of Interest: The authors declare no conflict of interest. The founding sponsors had no role in the design of the study; in the collection, analyses, or interpretation of data; in the writing of the manuscript, and in the decision to publish the results.

References

1. Erlund, I. Review of the flavonoids quercetin, hesperetin and naringenin. Dietary sources, bioactivities, bioavailability and epidemiology. *Nutr. Res.* **2004**, *24*, 851–874. [CrossRef]

2. Khan, M.K.; Zill-E-Huma; Dangles, O. A comprehensive review on flavanones, the major citrus polyphenols. *J. Food Compos. Anal.* **2014**, *33*, 85–104. [CrossRef]

3. Testai, L.; Da Pozzo, E.; Piano, I.; Pistelli, L.; Gargini, C.; Breschi, M.C.; Braca, A.; Martini, C.; Martelli, A.; Calderone, V. The citrus flavanone naringenin produces cardioprotective effects in hearts from 1 year old rat, through activation of mitoBK channels. *Front. Pharmacol.* **2017**, *8*. [CrossRef]

4. Liao, A.C.H.; Kuo, C.-C.; Huang, Y.-C.; Yeh, C.-W.; Hseu, Y.-C.; Liu, J.-Y.; Hsu, L.-S. Naringenin inhibits migration of bladder cancer cells through downregulation of AKT and MMP-2. *Mol. Med. Rep.* **2014**, *10*, 1531–1536. [CrossRef]

5. Hatkevich, T.; Ramos, J.; Santos-Sanchez, I.; Patel, Y.M. A naringenin-tamoxifen combination impairs cell proliferation and survival of MCF-7 breast cancer cells. *Exp. Cell Res.* **2014**, *327*, 331–339. [CrossRef]

6. Ahamad, M.S.; Siddiqui, S.; Jafri, A.; Ahmed, S.; Afzal, M. Induction of apoptosis and antiproliferative activity naringenin in human epidermoid carcinoma cell through ROS generation and cell cycle arrest. *PLoS ONE* **2014**, *10*, e110003. [CrossRef]

7. Arul, D.; Subramanian, P. Naringenin (citrus flavonone) induces growth inhibition, cell cycle arrest and apoptosis in human hepatocellular carcinoma cells. *Pathol. Oncol. Res.* **2013**, *19*, 763–770. [CrossRef] [PubMed]

8. Bao, L.; Liu, F.; Guo, H.; Li, Y.; Tan, B.; Zhang, W. Naringenin inhibits proliferation, migration, and invasion as well as induces apoptosis of gastric cancer SGC7901 cell line by downregulation of AKT pathway. *Tumor Biol.* **2016**, 11365–11374. [CrossRef]

9. Abaza, M.S.I.; Orabi, K.Y.; Al-Quattan, E.; Al-Attiyah, R.J. Growth inhibitory and chemo-sensitization effects of naringenin, a natural flavanone purified from Thymus vulgaris, on human breast and colorectal cancer. *Cancer Cell Int.* **2015**, *15*, 46–65. [CrossRef]

10. Hee, J.; Jin, C.; Kyu, B.; Kim, G.; Hyun, Y.; Kee, Y. Naringenin induces apoptosis through downregulation of Akt and caspase-3 activation in human leukemia THP-1 cells. *Food Chem. Toxicol.* **2008**, *46*, 3684–3690. [CrossRef]

11. Wang, K.; Chen, Z.; Huang, J.; Huang, L.; Luo, N.; Liang, X.; Liang, M.; Xie, W. Naringenin prevents ischaemic stroke damage via anti-apoptotic and anti-oxidant effects. *Clin. Exp. Pharmacol. Physiol.* **2017**, *44*, 862–871. [CrossRef] [PubMed]

12. Yoon, H.; Kim, T.W.; Shin, S.Y.; Park, M.J.; Yong, Y.; Kim, D.W.; Islam, T.; Lee, Y.H.; Jung, K.-Y.; Lim, Y. Design, synthesis and inhibitory activities of naringenin derivatives on human colon cancer cells. *Bioorg. Med. Chem. Lett.* **2003**, *23*, 232–238. [CrossRef]

13. Lee, S.; Lee, C.-H.; Moon, S.-S.; Kim, E.; Kim, C.-T.; Kim, B.-H.; Bok, S.-H.; Jeong, T.S. Naringenin derivatives as anti.atherogenic agents. *Bioorg. Med. Chem. Lett.* **2003**, *13*, 3901–3903. [CrossRef] [PubMed]

14. Copmans, D.; Orellana-Paucar, A.M.; Steurs, G.; Zhang, Y.; Ny, A.; Foubert, K.; Exarchou, V.; Siekierska, A.; Kim, Y.; de Borggraeve, W.; et al. Methylated flavonoids as anti-seizure agents: Naringenin 4′,7-dimethyl ether attenuates epileptic siezures in zebrafish and mouse models. *Neurochem. Int.* **2018**, *112*, 124–133. [CrossRef] [PubMed]

15. Brodowska, K.; Sykula, A.; Garribba, E.; Lodyga-Chruscinska, E.; Sójka, M. Naringenin Schiff base: Antioxidant activity, acid-base profile, and interactions with DNA. *Transit. Met. Chem.* **2016**, *41*, 179–189. [CrossRef]

16. Türkkan, B.; Özyürek, M.; Bener, M.; Güçlü, K.; Apak, R. Synthesis, characterization and antioxidant capacity of naringenin-oxime. *Spectrochim. Acta A Mol. Biomol. Spectrosc.* **2012**, *85*, 235–240. [CrossRef]

17. Potaniec, B.; Grabarczyk, M.; Stompor, M.; Szumny, A.; Zielinsky, P.; Zolnierczyk, A.K.; Aniol, M. Antioxidant activity and spectroscopic data of isoxanthohomol oxime and related compounds. *Spectrochim. Acta A Mol. Biomol. Spectrosc.* **2014**, *118*, 716–723. [CrossRef] [PubMed]

18. Kocyigit, A.; Koyuncu, I.; Taskin, A.; Dikilitas, M.; Bahadori, F.; Turkkan, B. Antigenotoxic and antioxidant potentials of newly derivatized compound naringenin-oxime relative to naringenin on human mononuclear cells. *Drug Chem. Toxicol.* **2016**, *39*, 66–73. [CrossRef] [PubMed]

19. Koyuncu, I.; Kocyigit, A.; Gonel, A.; Arslan, E.; Durgun, M. The protective effect of naringenin-oxime on cisplatin induced toxicity in rats. *Biochem. Res. Int.* **2017**, 9478958. [CrossRef] [PubMed]

20. Kocyigit, A.; Koyuncu, I.; Dikilitas, M.; Bahadori, F.; Turkkan, B. Cytotoxic, genotoxic and apoptotic effects of naringenin-oxime relative to naringenin on normal and cancer cell lines. *Asian Pac. J. Trop. Biomed.* **2016**, *6*, 872–880. [CrossRef]

21. Song, J.-Y.; Liu, Y.; Zhao, H.-Y.; Han, H.-T.; Li, Z.-F.; Guo, W.-H.; Chu, W.-Y.; Sun, Z.-Z. Efficient nickel(II) naringenin-oxime complex catalyzed Mizoroki-Heck cross-coupling reaction in the presence of hydrazine hydrate. *New J. Chem.* **2017**, *41*, 12288–12292. [CrossRef]

22. Kozłowska, J.; Grela, E.; Baczyńska, D.; Grabowiecka, A.; Anioł, M. Novel *O*-alkyl Derivatives of Naringenin and Their Oximes with Antimicrobial and Anticancer Activity. *Molecules* **2019**, *24*, 679. [CrossRef]

23. Liu, Z.; Wei, W.; Gan, C.; Huang, Y.; Liu, S.; Zhou, M.; Cui, J. Semisynthesis and cytotoxicity of *E*-Naringenin oximes from Naringin. *Chin. J. Org. Chem.* **2013**, *33*, 2551–2558. [CrossRef]

24. Hawkes, G.E.; Herwig, K.; Roberts, J.D. Nuclear magnetic resonance spectroscopy. Use of ^{13}C NMR spectra to establish configurations of oximes. *J. Org. Chem.* **1974**, *39*, 1017–1028. [CrossRef]

25. Molnár, J.; Szebeni, G.J.; Csupor-Löffler, B.; Hajdú, Z. Investigation of the antiproliferative properties of natural sesquiterpenes from *Artemisia asiatica* and *Onopordum acanthium* on HL-60 cells in vitro. *Int. J. Mol. Sci.* **2016**, *17*, 83. [CrossRef]

26. Zupkó, I.; Molnár, J.; Réthy, B.; Minorics, R.; Frank, É.; Wölfling, J.; Molnár, J.; Ocsovszki, I.; Topcu, Z.; Bitó, T.; et al. Anticancer and multidrug resistance-reversal effects of solanidine analogs synthetized from pregnadienolone acetate. *Molecules* **2014**, *19*, 2061–2076. [CrossRef]

27. Szabó, J.; Jerkovics, N.; Schneider, G.; Wölfling, J.; Bózsity, N.; Minorics, R.; Zupkó, I.; Mernyák, E. Synthesis and in vitro antiproliferative evaluation of C-13 epimers of triazolyl-ᴅ-Secoestrone alcohols: The first potent 13α-D-Secoestrone derivative. *Molecules* **2016**, *21*, 611. [CrossRef]

28. Réthy, B.; Hohmann, J.; Minorics, R.; Varga, A.; Ocsovszki, I.; Molnár, J.; Juhász, K.; Falkay, G.; Zupkó, I. Antitumour properties of acridone alkaloids on a murine lymphoma cell line. *Anticancer Res.* **2008**, *28*, 2737–2743.

29. Baji, Á.; Kovács, F.; Schneider, G.; Wöl, J.; Sinka, I. Investigation of pH and substituent effects on the distribution ratio of novel steroidal ring D- and A-fused arylpyrazole regioisomers and evaluation of their cell-growth inhibitory effects in vitro. *Steroids* **2017**, *126*, 35–49. [CrossRef] [PubMed]

30. Bózsity, N.; Minorics, R.; Szabó, J.; Mernyák, E.; Schneider, G.; Wöl, J.; Wang, H.; Wu, C.; Ocsovszki, I.; Zupkó, I. Mechanism of antiproliferative action of a new D-secoestrone-triazole derivative in cervical cancer cells and its effect on cancer cell motility. *J. Steroid Biochem. Mol. Biol.* **2017**, *165*, 247–257. [CrossRef] [PubMed]

31. Fukumoto, L.; Mazza, G. Assessing Antioxidant and Prooxidant Activities of Phenolic Compounds. *J. Agric. Food. Chem.* **2000**, *48*, 3597–3604. [CrossRef] [PubMed]

32. Mielnik, M.B.; Rzeszutek, A.; Triumf, E.C.; Egelandsdal, B. Antioxidant and other quality properties of reindeer muscle from two different Norwegian regions. *Meat Sci.* **2011**, *89*, 526–532. [CrossRef] [PubMed]